INTERDISCIPLINARY APPLIED MATHEMATICS

MATHEMATICAL BIOLOGY

Mathematical Biology

II: Spatial Models and Biomedical Applications

J.D. Murray

Third Edition

Springer

J.D. Murray

Mathematical Biology

II: Spatial Models and Biomedical Applications

Third Edition

With 298 Illustrations

Springer

J.D. Murray, FRS
Emeritus Professor
University of Oxford *and*
University of Washington
Box 352420
Department of Applied Mathematics
Seattle, WA 98195-2420
USA

Editors

S.S. Antman
Department of Mathematics
and Institute for Physical Science
and Technology
University of Maryland
College Park, MD 20742-4015
USA
ssa@math.umd.edu

J.E. Marsden
Control and Dynamical Systems
Mail Code 107-81
California Institute of Technology
Pasadena, CA 91125
USA
marsden@cds.caltech.edu

L. Sirovich
Division of Applied Mathematics
Brown University
Providence, RI 02912
USA
chico@camelot.mssm.edu

S. Wiggins
School of Mathematics
University of Bristol
Bristol BS8 1TW
UK
s.wiggins@bris.ac.uk

Cover illustration: © Alain Pons.

Mathematics Subject Classification (2000): 92B05, 92-01, 92C05, 92D30, 34Cxx

Library of Congress Cataloging-in-Publication Data
Murray, J.D. (James Dickson)
Mathematical biology. II: Spatial models and biomedical applications / J.D. Murray.—3rd ed.
p. cm.—(Interdisciplinary applied mathematics)
Rev. ed. of: Mathematical biology. 2nd ed. c1993.
Includes bibliographical references (p.).
ISBN 0-387-95228-4 (alk. paper)
1. Biology—Mathematical models. I. Murray, J.D. (James Dickson) Mathematical biology. II. Title. III. Series.
QH323.5 .M88 2001b
570′.1′5118—dc21 2001020447

ISBN 0-387-95228-4 Printed on acid-free paper.

Printed in the United States of America.

9 8 7 6 5 4 3 2 1 SPIN 10792366

www.springer-ny.com

Springer-Verlag New York Berlin Heidelberg
A member of BertelsmannSpringer Science+Business Media GmbH

Preface to the Third Edition

In the thirteen years since the first edition of this book appeared the growth of mathematical biology and the diversity of applications has been astonishing. Its establishment as a distinct discipline is no longer in question. One pragmatic indication is the increasing number of advertised positions in academia, medicine and industry around the world; another is the burgeoning membership of societies. People working in the field now number in the thousands. Mathematical modelling is being applied in every major discipline in the biomedical sciences. A very different application, and surprisingly successful, is in psychology such as modelling various human interactions, escalation to date rape and predicting divorce.

The field has become so large that, inevitably, specialised areas have developed which are, in effect, separate disciplines such as biofluid mechanics, theoretical ecology and so on. It is relevant therefore to ask why I felt there was a case for a new edition of a book called simply *Mathematical Biology*. It is unrealistic to think that a single book could cover even a significant part of each subdiscipline and this new edition certainly does not even try to do this. I feel, however, that there is still justification for a book which can demonstrate to the uninitiated some of the exciting problems that arise in biology and give some indication of the wide spectrum of topics that modelling can address.

In many areas the basics are more or less unchanged but the developments during the past thirteen years have made it impossible to give as comprehensive a picture of the current approaches in and the state of the field as was possible in the late 1980s. Even then important areas were not included such as stochastic modelling, biofluid mechanics and others. Accordingly in this new edition only some of the basic modelling concepts are discussed—such as in ecology and to a lesser extent epidemiology—but references are provided for further reading. In other areas recent advances are discussed together with some new applications of modelling such as in marital interaction (Volume I), growth of cancer tumours (Volume II), temperature-dependent sex determination (Volume I) and wolf territoriality (Volume II). There have been many new and fascinating developments that I would have liked to include but practical space limitations made it impossible and necessitated difficult choices. I have tried to give some idea of the diversity of new developments but the choice is inevitably prejudiced.

As to general approach, if anything it is even more practical in that more emphasis is given to the close connection many of the models have with experiment, clinical data and in estimating real parameter values. In several of the chapters it is not yet

possible to relate the mathematical models to specific experiments or even biological entities. Nevertheless such an approach has spawned numerous experiments based as much on the modelling approach as on the actual mechanism studied. Some of the more mathematical parts in which the biological connection was less immediate have been excised while others that have been kept have a mathematical and technical pedagogical aim but all within the context of their application to biomedical problems. I feel even more strongly about the philosophy of mathematical modelling espoused in the original preface as regards what constitutes good mathematical biology. One of the most exciting aspects regarding the new chapters has been their genuine interdisciplinary collaborative character. Mathematical or theoretical biology is unquestionably an interdisciplinary science *par excellence*.

The unifying aim of theoretical modelling and experimental investigation in the biomedical sciences is the elucidation of the underlying biological processes that result in a particular observed phenomenon, whether it is pattern formation in development, the dynamics of interacting populations in epidemiology, neuronal connectivity and information processing, the growth of tumours, marital interaction and so on. I must stress, however, that mathematical descriptions of biological phenomena are not biological explanations. The principal use of any theory is in its predictions and, even though different models might be able to create similar spatiotemporal behaviours, they are mainly distinguished by the different experiments they suggest and, of course, how closely they relate to the real biology. There are numerous examples in the book.

Why use mathematics to study something as intrinsically complicated and ill understood as development, angiogenesis, wound healing, interacting population dynamics, regulatory networks, marital interaction and so on? We suggest that mathematics, rather theoretical modelling, must be used if we ever hope to genuinely and realistically convert an understanding of the underlying mechanisms into a predictive science. Mathematics is required to bridge the gap between the level on which most of our knowledge is accumulating (in developmental biology it is cellular and below) and the macroscopic level of the patterns we see. In wound healing and scar formation, for example, a mathematical approach lets us explore the logic of the repair process. Even if the mechanisms were well understood (and they certainly are far from it at this stage) mathematics would be required to explore the consequences of manipulating the various parameters associated with any particular scenario. In the case of such things as wound healing and cancer growth—and now in angiogensesis with its relation to possible cancer therapy—the number of options that are fast becoming available to wound and cancer managers will become overwhelming unless we can find a way to simulate particular treatment protocols before applying them in practice. The latter has been already of use in understanding the efficacy of various treatment scenarios with brain tumours (glioblastomas) and new two step regimes for skin cancer.

The aim in all these applications is not to derive a mathematical model that takes into account every single process because, even if this were possible, the resulting model would yield little or no insight on the crucial interactions within the system. Rather the goal is to develop models which capture the essence of various interactions allowing their outcome to be more fully understood. As more data emerge from the biological system, the models become more sophisticated and the mathematics increasingly challenging.

In development (by way of example) it is true that we are a long way from being able to reliably simulate actual biological development, in spite of the plethora of models and theory that abound. Key processes are generally still poorly understood. Despite these limitations, I feel that exploring the logic of pattern formation is worthwhile, or rather essential, even in our present state of knowledge. It allows us to take a hypothetical mechanism and examine its consequences in the form of a mathematical model, make predictions and suggest experiments that would verify or invalidate the model; even the latter casts light on the biology. The very process of constructing a mathematical model can be useful in its own right. Not only must we commit to a particular mechanism, but we are also forced to consider what is truly essential to the process, the central players (variables) and mechanisms by which they evolve. We are thus involved in constructing frameworks on which we can hang our understanding. The model equations, the mathematical analysis and the numerical simulations that follow serve to reveal quantitatively as well as qualitatively the consequences of that logical structure.

This new edition is published in two volumes. Volume I is an introduction to the field; the mathematics mainly involves ordinary differential equations but with some basic partial differential equation models and is suitable for undergraduate and graduate courses at different levels. Volume II requires more knowledge of partial differential equations and is more suitable for graduate courses and reference.

I would like to acknowledge the encouragement and generosity of the many people who have written to me (including a prison inmate in New England) since the appearance of the first edition of this book, many of whom took the trouble to send me details of errors, misprints, suggestions for extending some of the models, suggesting collaborations and so on. Their input has resulted in many successful interdisciplinary research projects several of which are discussed in this new edition. I would like to thank my colleagues Mark Kot and Hong Qian, many of my former students, in particular Patricia Burgess, Julian Cook, Tracé Jackson, Mark Lewis, Philip Maini, Patrick Nelson, Jonathan Sherratt, Kristin Swanson and Rebecca Tyson for their advice or careful reading of parts of the manuscript. I would also like to thank my former secretary Erik Hinkle for the care, thoughtfulness and dedication with which he put much of the manuscript into LaTeX and his general help in tracking down numerous obscure references and material.

I am very grateful to Professor John Gottman of the Psychology Department at the University of Washington, a world leader in the clinical study of marital and family interactions, with whom I have had the good fortune to collaborate for nearly ten years. Without his infectious enthusiasm, strong belief in the use of mathematical modelling, perseverance in the face of my initial scepticism and his practical insight into human interactions I would never have become involved in developing with him a general theory of marital interaction. I would also like to acknowledge my debt to Professor Ellworth C. Alvord, Jr., Head of Neuropathology in the University of Washington with whom I have collaborated for the past seven years on the modelling of the growth and control of brain tumours. As to my general, and I hope practical, approach to modelling I am most indebted to Professor George F. Carrier who had the major influence on me when I went to Harvard on first coming to the U.S.A. in 1956. His astonishing insight and ability to extract the key elements from a complex problem and incorporate them into a realistic

and informative model is a talent I have tried to acquire throughout my career. Finally, although it is not possible to thank by name all of my past students, postdoctorals, numerous collaborators and colleagues around the world who have encouraged me in this field, I am certainly very much in their debt.

Looking back on my involvement with mathematics and the biomedical sciences over the past nearly thirty years my major regret is that I did not start working in the field years earlier.

Bainbridge Island, Washington *J.D. Murray*
January 2002

11. Growth and Control of Brain Tumours

Brief Historical Perspective on Brain Surgery

Surgery on the brain or skull has an incredibly long history and is arguably the most ancient of surgical interventions. The books of articles edited by Greenblatt (1997) and Walker (1951) make fascinating reading. There is an early description of how to treat head wounds in the Edwin Smith Surgical Papyrus of ancient Egypt (about 2500 BC) in which trepanning, or trephining, is described as a procedure. Trephining is the surgical removal of a piece of bone from the skull. Numerous skulls have been found showing healed craniotomies; the procedure was certainly far from always being fatal and the large number of such healed craniotomies suggests some success.

Verano and his colleagues (see Verano et al. 1999, 2000 and Arriaza et al. 1998 and other references there) discuss interesting examples, from archaeological finds, of trephination, and other major surgeries such as foot amputation, by the coastal cultures of Peru and the Incas. There is a remarkable photograph in Arriaza et al. (1998) of an Inca cranium (from the archaeological museum in Cuzco) showing four trephinations which were clearly well healed while the patient was alive. The trephinations on this skull are all of the order of 5 cm in diameter.

There are numerous pictures and woodcuts from the mediaeval period (see also the historical discussion on surgery and wound healing in Chapter 9) showing surgical operations on the head. The procedure for carrying out such trephining varies widely. Figure 11.1(a) is from a mediaeval manuscript showing how it might have been carried out while Figure 11.1(b) is from another mediaeval manuscript showing the end of a succesful completion of the surgery (albeit with a somewhat dubious and unhappy looking patient). Figure 11.1(c) is a caricature example of a late mediaeval operation, this time being carried out by a group of animal surgeons which indicates what people thought of surgeons at the time. As mentioned in the chapter on epidermal wound healing, Galen, who clearly carried out trephining, was very practical in his advice such as noting that the *'disadvantage of using a gouge is that the head is shaken vigorously by the hammer strokes.'*

Richard of Parma in his *Practica Chirugiae* (Practice of Surgery) of 1170 (see Valenstein 1997) writes: *'For mania or melancholy a cruciate incision is made in the top of the head and the cranium is penetrated to permit the noxious material to exhale to the outside. The patient is held in chains and the wound is treated, as above.'* The classic picture by the late 15th and early 16th century enigmatic Hieronymous Bosch called *The Cure of Folly* (or Madness) or *The Stone Operation* in the Prado Museum in Madrid

(a)

(b)

(c)

Figure 11.1. (**a**) Mediaeval illustration of the start of a skull operation. (**b**) This is from a late mediaeval manuscript showing post-surgery suturing. (**c**) Brain surgery being carried out by a number of animal 'surgeons.' It highlights the low opinion people had of surgeons in mediaeval times. (Courtesy of the Wellcome Trust Medical Library, London and reproduced with permission)

shows a man making an incision on the scalp of a seated man. The inscription (translated by Cinotto 1969) has been translated as *'Master, dig out the stones of folly, my name is "castrated dachshund."'* At the time a 'castrated dachshund' was frequently the name used for a simpleton. Madness was often believed to be caused by stones in the head. Art historians and others have discussed and disagreed about the interpretation of this painting for a very long time; some, for example, say it ridicules the itinerant mediaeval charlatans who went around 'curing' madness and other ailments by trephining while others say it is an allegory of human gullibility and stupidity which is so common in Bosch's paintings. The classic book *Anatomy of Melancholy* by Robert Burton (1652) includes *'tis not amiss to bore the skull with an instrument to let out the fuliginous*

vapours ... Guierius curted a nobleman in Savoy by boring alone, leaving the hole open a month together by means of which, after two years melancholy and madness he was delivered.'

The practice of trephining declined from the beginning of the 19th century when the surgical operation was moved into the hospitals because the mortality went up dramatically since such hospitals were infection paradises at the time. (Even now infection in hospitals is still a major killer, even if the prognosis of survival is much greater.)

Trephination by indigenous peoples has been used (and still is today) for a variety of problems, such as insanity, depression, behavioural disorders (lobotomies are still carried out by professional surgeons in many hospitals) to relieve the results of head injuries from blows to the head (such as depressed fractures) or falls from trees or simply from banging their head on a door lintel. Margetts (1967) and in particular the interesting article by Furnas et al. (1985) (see earlier references there) describe (with many photographs of actual operations) in fascinating medical detail craniotomies regularly performed by traditional craniotomists of the Kisii tribe in Kenya. The craniotomist (called an omobari) is highly respected and very skillful. They use a variety of herbs and drugs to aid healing and prevent infection. The operations are often carried out in the open. They use a series of instruments to scrape through the skull, roughly a 5×5 cm^2 patch, until a very thin layer is left. They then use a fine pick to puncture this last membrane thereby exposing the dura. Some, however, also use a drill or hacksaw. The aim of the treatment can be, for example, to remove bone splinters (resulting from a blow to the head) or to relieve depression or severe headaches. It appears that the mortality rate is low and patients seem satisfied with the results.

11.1 Medical Background

Cancerous tumours, or neoplasms, originate from the mutation of one or more cells which usually undergo rapid uncontrolled growth thereby impairing the functioning of normal tissue. There are many different cancers each with their own characteristics. In this chapter we shall only be concerned with brain tumours, and in particular gliomas or glioblastomas, which make up about half of all primary brain tumours diagnosed; they are particularly nasty tumours with a depressingly dismal prognosis for recovery. Gliomas are highly invasive and infiltrate the surrounding tissue. The impressive increased detection capabilities (but as we shall see, still woefully inadequate) in computerized tomography (CT) and magnetic resonance imaging (MRI) over the past 20 years have resulted in earlier detection of glioma tumours. Despite this progress, the benefits of early treatment have been minimal (see, for example, Silbergeld et al. 1991, Alvord and Shaw 1991, Kelley and Hunt 1994, Cook et al. 1995 and Burgess et al. 1997). For example, even with extensive surgical excision well beyond the grossly visible tumour boundary, regeneration near the edge of resection ultimately results in eventually leading to death (see, for example, Matsukado et al. 1961, Kreth et al. 1993, Woodward et al. 1996 and other references there). This failure of resection is analogous to trying to put out a forest fire from behind the advancing front. The action of the fire (tumour growth) is primarily at the periphery.

The brain basically consists of two types of tissue: grey matter and white matter. Grey matter is composed of neuronal and glial cell bodies that control brain activity while the cortex (like the 'bark') is a coat of grey matter that covers the brain. White matter fibre tracts are myelinated neuron axon bundles located throughout the inner regions of the brain. These fibres establish pathways between grey matter regions. The corpus callosum is a thick band of white matter fibres connecting the left and right cerebral hemispheres of the brain. Within each hemisphere, there are several white matter pathways connecting the cortex to the nuclei deep within the brain; see Figure 11.2. Figure 11.3 shows two photographs of a human brain showing grey and white matter distribution and the corpus collosum.

Gliomas are neoplasms of glial cells (neural cells capable of division) that usually occur in the upper cerebral hemisphere but which can be found throughout the brain (Alvord and Shaw 1991). Astrocytomas, originating from an abnormally multiplying astrocyte glial cell, are the most common gliomas. Depending on their aggressiveness (grade), astrocytomas are further divided into several subcategories. Astrocytomas are the least aggressive or lowest grade, anaplastic astrocytomas are the more aggressive or mid-grade and glioblastomas (multiforme) are the most aggressive or highest grade. Tumour grade indicates the level of malignancy and is based on the degree of anaplasia (or deformity in behaviour and form) seen in the cancerous cells under a microscope. Gliomas often contain several different grade cells with the highest or most malignant grade of cells determining the grade, even if most of the tumour is lower grade. There is still no general clinical agreement on the grading.

Generally, the higher-grade cancer cells are more capable of invading normal tissue and so are more malignant. However, even with their invasive abilities, gliomas very rarely metastasize outside the brain.

The prognosis for patients with neoplasms affecting the nervous system depends on many factors. A major element in the prognosis is the quantitative evaluation of the spatiotemporal infiltration of the tumour, taking into account the anatomic site of the tumour as well as the effectiveness of the various treatments.

Since we believe that the modelling developed in this chapter has a practical bearing on patient treatment it is necessary to give more detailed medical information which we believe is an important part of realistic medical modelling.

Difficulties in Treating Brain Tumours

An enormous amount of experimental and some theoretical work has been devoted to trying to understand why gliomas are so difficult to treat. Unlike many other tumours, gliomas can be highly diffuse. Experiments indicate that within 7 days of tumour implantation in a rat brain, glioma cells can be identified throughout the central nervous system (Silbergeld and Chicoine 1997). A locally dense tumour growth remains where the cancerous tissue was initially implanted but there are solitary tumour cells throughout the central nervous system (Silbergeld and Chicoine 1997 and Silbergeld, personal communication, 1998). Most glioma treatments are directed locally to the bulk mass when, in fact, the action of tumour growth and invasion is elsewhere.

There are various, regularly used, treatments for gliomas, mainly chemotherapy, radiation therapy and surgical intervention. Resection, the surgical removal of an accessible tumour, has a wretched history of success. Recurrence of tumour growth at the

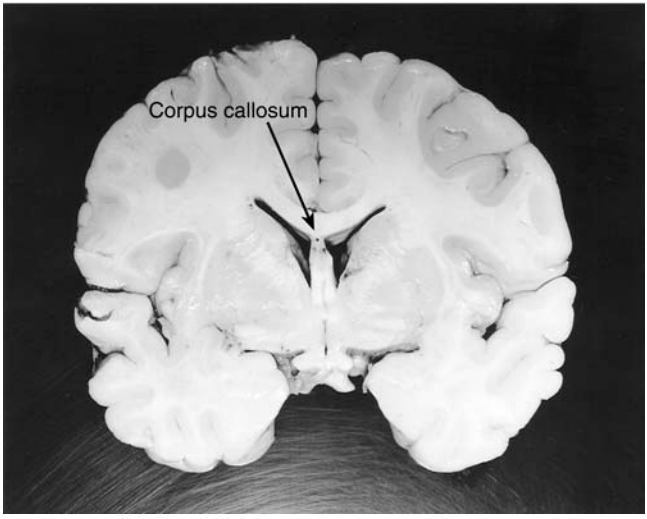

(a)

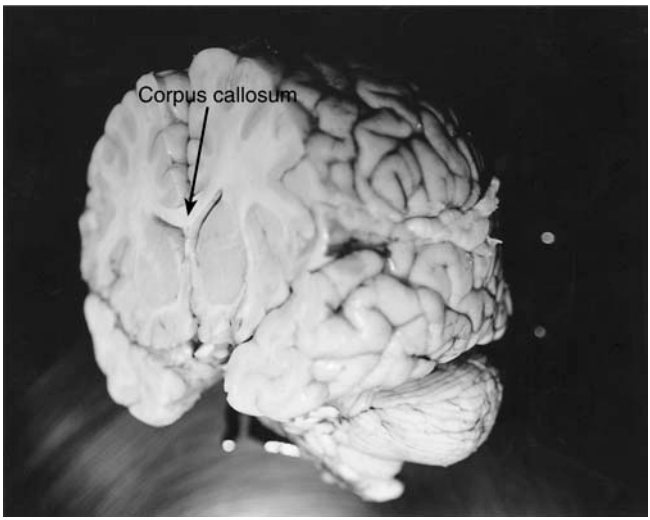

(b)

Figure 11.2. Two cross-sections of a human brain showing fibrous white matter and the corpus callosum which connects the left and right cerebral hemispheres. (Figure courtesy of Dr. E.C. Alvord, Jr.)

resection boundary is a well-documented phenomenon in glioma research (see, for example, Silbergeld and Chicoine 1997, Woodward et al. 1996, Kreth et al. 1993, Kelley and Hunt 1994 and other references there). Both experimentalists and theoreticians believe that the distantly invaded cells are responsible for tumour regeneration following surgery (Chicoine and Silbergeld 1995, Silbergeld and Chicoine 1997). Since the density of cancerous cells (remaining after resection) is highest at the resection boundary,

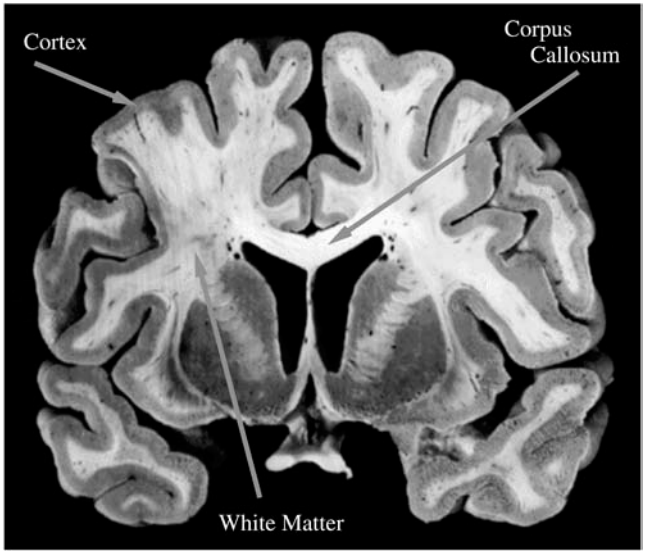

Figure 11.3. Cross-section of the human brain. The cortex consists of grey matter and is connected to other grey matter regions by white matter fibre bundles. The corpus callosum is a white matter tract connecting the left and right cerebral hemispheres. (Figure reproduced with the permission of Professor Paul Pietsch; derived from T.H. Williams, N. Gluhbegovic and J.Y. Jew Virtual Hospital Figure 5-30. http://www.vh.org/Providers/Textbooks/BrainAnatomy/BrainAnatomy.html)

regrowth seems most probable at this location. Alternatively, Silbergeld and Chicoine (1997) suggested, and are presently testing, the hypothesis that damaged brain tissue at the resection site releases cytokines that recruit the diffusely invaded tumour cells. Nevertheless, both explanations are consistent with the argument that the diffuse nature of gliomas is fundamentally responsible for tumour recurrence near the resection boundary. The difference is that the former is a physical model and the later is more biochemical. In this chapter we shall study a model (basically an incredibly simple one—even linear) for resection therapy and show why it generally fails. As we shall show, it increases life expectancy minimally; we compare the results and predictions with patient data.

Chemotherapy essentially uses specialized chemicals to poison the tumour cells. The brain is naturally defended from these and other types of chemicals by the intricate capillary structure of the blood–brain barrier. Water-soluble drugs, ions and proteins cannot permeate the blood–brain barrier but lipid-soluble agents can. Recently, agents have been devised to temporarily disrupt the blood–brain barrier. Many chemotherapeutic treatments are cell-cycle-dependent: the drugs are triggered by certain phases of the cell cycle. Silbergeld and Chicoine (1997) have observed that the motile cells distant from the bulk tumour do not appear to enter mitosis so cell-cycle specific drugs and standard radiation therapy have limited effectiveness. Not only that, gliomas are often heterogeneous tumours. Those drugs that do reach the cancerous cells are hindered by drug resistance commonly associated with cancer cell heterogeneity. While one cell type is responsive to treatment and dies off, other types are waiting to dominate. This

phenomenon requires a model which includes cell mutation to drug resistance cells, in other words a polyclonal model. Below we describe and analyze such a model for chemotherapy and again compare the results with patient data.

The biological complexity of gliomas makes treatment a difficult undertaking. For planning effective (or seemingly so) treatment strategies, information regarding the growth rates and invasion characteristics of tumours is crucial. The use of mathematical modelling can help to quantify the effects of resection, chemotherapy and radiation (it tries to kill the tumour cells with radiation) on the growth and diffusion of malignant gliomas. In this chapter we shed some light on certain aspects of brain tumour treatment with the aim of helping to determine better, or even optimal, therapeutic regimes for patients. A major goal is the development of interactive computer models with which the effects of various treatment strategies for specific tumours could be examined. We believe that the work described in this chapter goes some way in achieving this goal. Having said this, however, all of the treatments mentioned above have a very poor record of success. There is a pressing need for a totally different approach to the treatment of gliomas, several of which are currently being investigated.

11.2 Basic Mathematical Model of Glioma Growth and Invasion

Like all tumours, the biological and clinical aspects of gliomas are complex and the details of their spatiotemporal growth are still not well understood. In constructing models therefore we have to make some major assumptions. In doing so we have relied heavily on the medical input of Dr. E.C. Alvord (Professor of Neuropathology, University of Washington) with whom J.D. Murray has an ongoing collaboration which started in the early 1990s. The group has included many students and postdoctorals, all of whom are on one or another of the papers referred to below and in which more of the medical details are given. It is mainly their work and relevant medical studies on brain tumours that we discuss in detail here.

With the philosophy espoused in this book we start with as simple a model as is reasonable and build up from it. The simplest theoretical models involve only the total number of cells in the tumour, with growth of the tumour usually assumed to be exponential, Gompertzian, or logistic (Swan 1987, Marusic et al. 1994). Such models do not take into account the spatial arrangement of the cells at a specific anatomical location or the spatial spread of the cancerous cells. These spatial aspects are crucial in estimating tumour growth since they determine the invasiveness and the apparent border of the tumour. It is necessary to try and determine the extent of infiltration of the tumour in most treatment situations, such as estimating the likely benefit of surgical resection (Alvord 1991). Until the work described in this chapter, the absence of even a simple model explaining the growth and recurrence of human gliomas made it difficult to explain why results of treatment by surgical excision are so disappointing (Nazzarro and Neuwelt 1990, Kreth et al. 1993). One of the surprising aspects of the work we describe here is how a very simple (linear) deterministic model can provide meaningful and helpful clinical information with a direct bearing on patient care.

In this section we develop a mathematical model for the spatiotemporal dynamics of tumour growth. Importantly we can estimate the model parameters, including the

proliferation, or growth rate, and the diffusion coefficient of the cells from clinical data obtained from successive computerized tomography (CT) scans of patients and independent experimental work. This is described below in Section 11.10 on chemotherapy where we also describe what these CT scans show and how we use them.

Once we have established the feasibility of reconstructing some of the kinetic events in invasion from histological sections, it will be possible to investigate other gliomas with different characteristic growth patterns, geometries and the effects of various forms of therapy (surgery, chemo- and/or radiotherapy) using the same types of data from other patients. The growth patterns essentially define the gross and microscopic characteristics not only of the classical tumours of different degrees of malignancy but also of 'mixed-gliomas' and 'multi-centric gliomas' (Alvord 1992).

Previous mathematical modelling (Tracqui et al. 1995, Cruywagen et al. 1995, Cook et al. 1995, Woodward et al. 1996, Burgess et al. 1997) used a theoretical framework to describe the invasive nature of gliomas, both with and without treatment regimes, by isolating two characteristics: proliferation and diffusion. Here diffusion represents the active motility of glioma cells. These models showed that diffusion is more important in determining survival than the proliferation rate of the tumour. *In vivo* studies show that malignant glioma cells implanted in rats quickly invade the contralateral hemisphere of the brain dispersing via white matter tracts (Kelley and Hunt 1994, Silbergeld and Chicoine 1997). The diffusion of glioma cells in white matter is different from that in the grey matter and is included in a more realistic model.

The basic model considers the evolution of the glioma tumour cell population to be mainly governed by proliferation and diffusion. Tumour cells are assumed to grow exponentially. This is a reasonable reflection of the biology for the timescale with which we are concerned, namely, the time to the patient's death. Although necrotic core (a region of dead cells) formation is evident in some gliomas, only the highly proliferative, slowly diffusive tumours are significantly affected by necrosis; we do not include this but the model could be modified to include it. Also, a typical logisticlike growth would strictly be more accurate but we are most interested in understanding the diffusive nature of the tumour behaviour and the medical timescale considered. Logistic growth can be trivially incorporated. (In the case of breast cancer Hart et al. 1998 and Shochat et al. 1999 have shown that exponential growth is not a valid approximation.) Silbergeld and Chicoine (1997) suggested that diffusion is a good approximation for the tumour cell motility. A very good review of glioma invasion is given by Giese and Westphal (1996). We show later that diffusion reasonably models the cell spreading dynamics observed *in vitro*.

Let $\bar{c}(\bar{\mathbf{x}}, \bar{t})$ be the number of cells at a position $\bar{\mathbf{x}}$ and time $\bar{t}$. We take the basic model, in dimensional form, as a conservation equation

$$\frac{\partial \bar{c}}{\partial \bar{t}} = \bar{\nabla} \cdot \mathbf{J} + \rho \bar{c}, \tag{11.1}$$

where ρ (time^{-1}) represents the net rate of growth of cells including proliferation and death (or loss). The diffusional flux of cells, $\mathbf{J}$, we take as proportional to the gradient of the cell density:

$$\mathbf{J} = \bar{D} \bar{\nabla} \bar{c}, \tag{11.2}$$

where $\bar{D}$ (distance^2/time) is the diffusion coefficient of cells in brain tissue. The theoretical models, referred to above, considered the brain tissue to be homogeneous so the diffusion and growth rates of the tumour cells are taken to be constant throughout the brain. This is not the case, of course, when considering tumour invasion into white matter from grey. With constant diffusion the governing equation (11.1) with (11.2) is then

$$\frac{\partial \bar{c}}{\partial \bar{t}} = \bar{D}\bar{\nabla}^2\bar{c} + \rho\bar{c}. \tag{11.3}$$

As we shall see this model gives reasonable agreement with the CT scans on which the model is based and has given surprisingly good results in predicting survival times under various treatment scenarios (Tracqui et al. 1995, Cruywagen et al. 1995, Cook et al. 1995, Woodward et al. 1996, Burgess et al. 1997). We give a full discussion of some of these models and results below. Although the models gave surprisingly (in view of the gross simplifying assumptions) good results, they contain several basic simplifications which can now be reconsidered, as was done by Swanson (1999) and Swanson et al. (2000). For example, given a source of glioma cells at a given location, most of the previous models, for numerical simplicity (and ignoring anatomic boundaries), considered the 'front' of detectable cells propagates symmetrically out from the source. They all knew, of course, that clinical and experimental observation indicate that, in fact, symmetry in growth of the tumour is not the case. The first model we discuss here deals with this aspect as well as tissue heterogeneity.

White matter serves as a route of invasion between grey matter areas for glioma cells. The diffusion coefficient (motility) for glioma cells is larger in the white matter than in the grey matter. *In vivo* studies show that malignant glioma cells implanted in rats quickly invade the contralateral hemisphere of the brain dispersing via white matter tracts (Chicoine and Silbergeld 1995, Silbergeld and Chicoine 1997, Kelley and Hunt 1994). The model we study now incorporates the effects of the heterogeneous tissue on the cell diffusion and tumour growth rates to emulate more accurately the clinically and experimentally observed asymmetries of the gross visible tumour boundaries.

Model with Spatial Heterogeneity

We can account for spatial heterogeneity in our model by taking the diffusion $\bar{D}$ to be a function of the spatial variable, $\bar{\mathbf{x}}$, thereby differentiating regions of grey and white matter. This gives, in place of (11.3),

$$\frac{\partial \bar{c}}{\partial \bar{t}} = \bar{\nabla} \cdot (\bar{D}(\bar{\mathbf{x}})\bar{\nabla}\bar{c}) + \rho\bar{c}. \tag{11.4}$$

We take zero flux boundary conditions on the anatomic boundaries of the brain and the ventricles. So, if B is the brain domain on which the equation (11.4) is to be solved, the boundary conditions are

$$\mathbf{n} \cdot \bar{D}(\bar{\mathbf{x}})\bar{\nabla}\bar{c} = 0 \quad \text{for } \mathbf{x} \text{ on } \partial B, \tag{11.5}$$

where $\mathbf{n}$ is the unit normal to the boundary ∂B of B. With the geometric complexity of an anatomically accurate brain (which we shall in fact use) it is clearly a very difficult analytical problem and a nontrivial numerical problem, even in two dimensions. We studied this problem in both two and three dimensions with anatomically accurate white and grey matter distribution obtained from EMMA (Extensible MATLAB Medical Analysis). This is a programme package developed by Collins et al. (1998) at the McConnel Brain Imaging Centre (Montreal Neurological Institute) to aid the analysis of medical imaging. Figure 11.4 shows an example of the white and grey matter distribution in a horizontal slice of the brain produced by EMMA.

In two dimensions, Swanson (1999) mapped out the regions of white and grey matter to simulate the clinical data from the CT scans used as the basis for the original two-dimensional model (11.3). Her initial goal was to simulate and produce a more accurate qualitative reproduction of these CT scan images than the original models which considered only homogeneous brain tissue. As mentioned, even with this simplification the results compared well with various gross medical quantities and patient data. We are particularly interested in the effects of grey and white matter distributions on glioma growth and invasion.

We first use the simplified anatomical domain of the rat brain. Numerical simulation and analytic results of this simpler case will be compared with experimental data procured and analyzed in the Neuropathology Laboratory at the University of Washington Medical School by (our collaborators) Dr. Ellsworth Alvord, Jr. (Head of Neuropathology) and Dr. Daniel Silbergeld (Neurological Surgery). We shall then consider, in detail, the model on an anatomically accurate human domain in both two and three dimensions.

We first nondimensionalise the spatially heterogeneous model, which as usual, also decreases the number of effective parameters in the system, and get some idea of the relative importance of various terms (without regard to units). To give some concept of the numbers involved there can be 10^{11} cancerous cells in a small tumour while the diffusion coefficient can be of the order 10^{-4} cm^2/day. Parameter estimates are given later in various tables.

We consider the diffusion coefficients to be constant, but different, in each of the two tissues, the white matter and the grey matter. So, we have to solve

$$\frac{\partial \bar{c}}{\partial \bar{t}} = \bar{\nabla} \cdot (\bar{D}(\bar{\mathbf{x}}) \bar{\nabla} \bar{c}) + \rho \bar{c}, \tag{11.6}$$

where

$$\bar{D}(\bar{\mathbf{x}}) = \begin{cases} D_w & \text{for } \bar{\mathbf{x}} \text{ in white matter} \\ D_g & \text{for } \bar{\mathbf{x}} \text{ in grey matter} \end{cases} \tag{11.7}$$

subject to the zero flux boundary conditions

$$\mathbf{n} \cdot \bar{D}(\bar{\mathbf{x}}) \bar{\nabla} \bar{c} = 0 \quad \text{for } \mathbf{x} \text{ on } \partial B \tag{11.8}$$

and initial condition $\bar{c}(\bar{\mathbf{x}}, 0) = \bar{f}(\bar{\mathbf{x}})$: we come back to the appropriate form of $\bar{f}(\bar{\mathbf{x}})$ below.

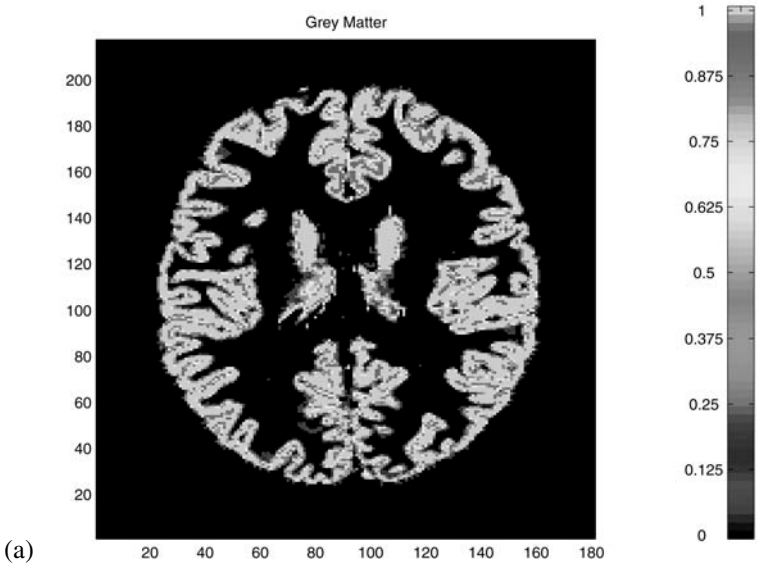

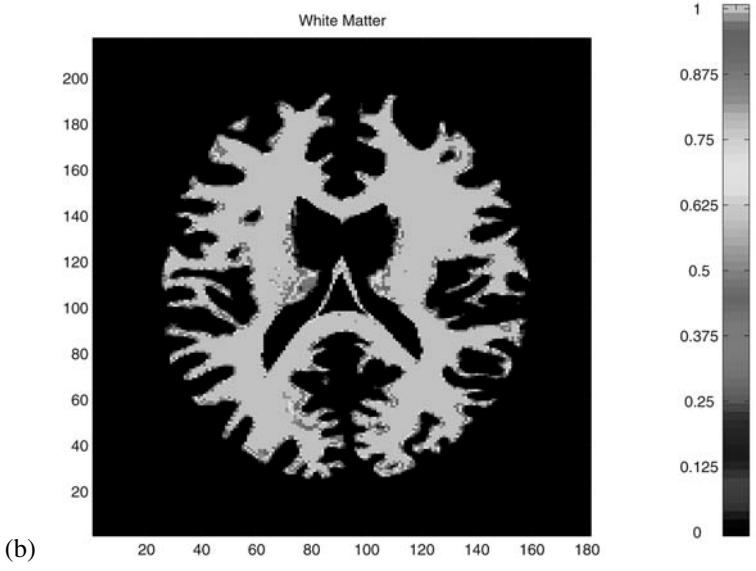

Figure 11.4. Grey and white matter distributions in a horizontal slice of the brain. The figure was generated using EMMA (Extensible MATLAB Medical Analysis) developed by Collins et al. (1998). (See the comment in parentheses in Figure 11.10 below.)

Introduce the nondimensional variables

$$\mathbf{x} = \sqrt{\frac{\rho}{D_w}}\,\bar{\mathbf{x}}, \quad t = \rho\bar{t}, \quad c(\mathbf{x}, t) = \frac{D_w}{\rho N_0}\bar{c}\left(\sqrt{\frac{\rho}{D_w}}\,\bar{\mathbf{x}}, \rho\bar{t}\right), \tag{11.9}$$

where $N_0 = \int \bar{f}(\bar{x})d\bar{x}$ represents the initial number of tumour cells in the brain at model time $\bar{t} = 0$. With these (11.6) becomes

$$\frac{\partial c}{\partial t} = \nabla \cdot (D(\mathbf{x})\nabla c) + c, \tag{11.10}$$

where

$$D(\mathbf{x}) = \begin{cases} 1 & \text{for } \mathbf{x} \text{ in white matter} \\ \gamma = \frac{D_g}{D_w} & \text{for } \mathbf{x} \text{ in grey matter} \end{cases} \tag{11.11}$$

with $c(\mathbf{x}, 0) = f(\mathbf{x}) = (D_w/\rho N_0)\bar{f}(\sqrt{(\rho/D_w)}\,\bar{\mathbf{x}})$ and $\mathbf{n} \cdot D(\mathbf{x})\nabla c = 0$ for $\mathbf{x}$ on ∂B. With this nondimensionalisation, diffusion is on the spatial scale of diffusion in white matter with time measured on the timescale of the tumour growth.

Let us now consider the form of the initial condition and appropriate forms for $f(\mathbf{x})$. Theoretically, the tumour started out as one cancerous cell, but the time of appearance of this original cell and the type of growth and the spread of the early cancer cells are unknown. We assume that, at the time of the first scan, the diffusion process has already broken any previous, possibly uniform, distribution of the cells. So, the cells are normally distributed with a maximum cell density, a, at the centre, $\mathbf{x}_0$, of the tumour; that is,

$$c(\mathbf{x}, 0) = a \exp\left(\frac{-|\,\mathbf{x} - \mathbf{x}_0\,|^2}{b}\right), \tag{11.12}$$

where b is a measure of the spread of tumour cells.

Initial Analytical Estimate of Survival Time

Clinically, tumour cells can not be detected at very low densities. On a CT scan, the profile of the tumour is defined by some nonzero level of resolution corresponding to a cellular density c^* (roughly 40, 000 cells/cm^2). Below this threshold, cancer cells are not detected by the imaging technique. A typical serial CT scan is in essence a series of pictures at several different levels of the brain where the tumour is located. From these an approximate three-dimensional shape is constructed. Figure 11.5 is an idealized scan of a tumour with three levels. With these we can approximate the size of the tumour and an equivalent spherical radius; see Section 11.10 where patient scans are used directly to estimate parameters to determine tumour size and growth.

In the case of a constant growth rate ρ and homogeneous diffusion $\bar{D}(\bar{\mathbf{x}}) = D$, equation (11.3) in two spatial dimensions with an initial delta function source of N_0

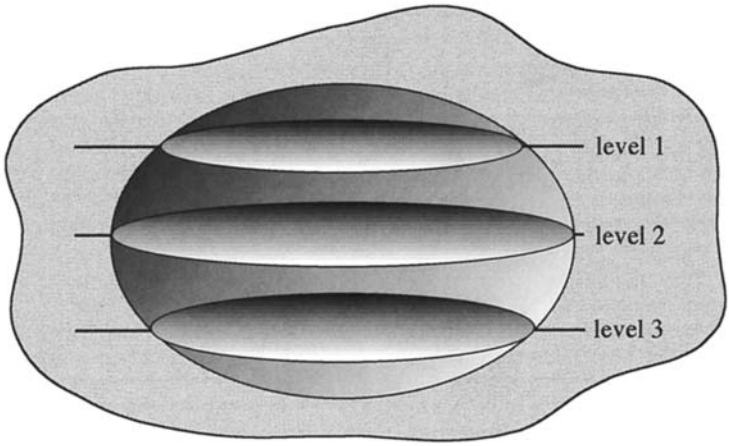

Figure 11.5. Idealized 3-level computerized tomography (CT) scan. With the three areas of detected cancer cells we can reconsruct an approximate tumour shape and volume. An example of an actual scan is shown in Figure 11.12.

tumour cells at $\bar{\mathbf{x}} = 0$ has the solution

$$\bar{c}(\bar{\mathbf{x}}, \bar{t}) = \frac{N_0}{4\pi D\bar{t}} \exp\left(\rho\bar{t} - \frac{\bar{r}^2}{4D\bar{t}}\right), \tag{11.13}$$

where $\bar{r}$ is the axially symmetric radial coordinate. If the detectable threshold density is $\bar{c}^*$ then the radius $\bar{r}^*$ of the tumour profile, given by (11.13) with $\bar{c}(\bar{\mathbf{x}}, \bar{t}) = \bar{c}^*$ is

$$\bar{r}^* = 2\sqrt{D\rho}\,\bar{t}\sqrt{1 - \frac{1}{\rho\bar{t}} \ln\left(4\pi D\bar{t}\frac{\bar{c}^*}{N_0}\right)} \sim 2\sqrt{D\rho}\,\bar{t} \quad \text{for } t \text{ large.} \tag{11.14}$$

The last expression is, of course, just the asymptotic form of the radial travelling wave of the axisymmetric Fisher–Kolmogoroff equation; it has velocity $2\sqrt{D\rho}$ (refer to Chapter 13, Volume I). So, if the tumour is identified when it has a radius $\bar{r}_{\text{detect}}$ and the tumour is fatal when it has a radius $\bar{r}_{\text{lethal}}$ we can approximate the untreated survival time by

$$\begin{aligned} \text{survival time} &= \bar{t}_{\text{lethal}} - \bar{t}_{\text{detect}} \\ &\approx \frac{1}{\sqrt{D\rho}} \left(\bar{r}_{\text{lethal}} - \bar{r}_{\text{detect}}\right). \end{aligned}$$

This shows that D and ρ are both important parameters in determining survival time: increasing either ρ or D will decrease survival time. The average radius (or rather equivalent radius) at which a tumour is identified is 1.5 cm and lethal is 3.0 cm (Burgess et al. 1997). The estimates for the detectable and lethal radii are only average values ob-

served clinically (Blankenberg et al. 1995); the range is quite large. With these radii, the untreated survival time is given approximately by $3/(2\sqrt{D\rho}\,)$. For a high grade tumour (parameter values are given in Section 11.5, Table 11.5 below), the untreated survival time suggested by the model is approximately 200 days. This is consistent with the observed 6 to 12 month median survival time for treated glioblastoma (Alvord 1991).

In terms of the nondimensional variables defined in (11.9)

$$r^* = 2t\sqrt{1 - \frac{1}{t}\ln \psi t}, \quad \psi = 4\pi \frac{D\bar{c}^*}{\rho N_0}. \tag{11.15}$$

Depending on the parameter value ψ, the observed radius of the tumour either increases monotonically with time or there is a delay between tumour initiation and visible progression; this time lapse is sometimes referred to as the establishment phase. Basically it is the time it takes the tumour to get established before it starts to spread.

The length of the establishment phase t_e can be calculated by simply setting $r^* = 0$ and $t = t_e$ in (11.15) which gives

$$t_e = \ln \psi t_e. \tag{11.16}$$

An establishment phase only exists for $\psi > 1$. We can see this immediately if we plot the curve $\psi = e^{t_e}/t_e$, note that the minimum is at $t_e = e$ and so a solution exists only for for $\psi > e$. This defines a relationship between all the parameters and can be useful in relating experimental observations and model parameters. From (11.16) the length of the establishment phase increases with ψ and, since $\psi \propto D/\rho$, it increases as D/ρ increases.

For a fixed ψ, the nondimensional detectable tumour radius r^* is given by a single curve. So, we can imagine a high grade tumour (that is, high ρ, high D) and a low grade tumour (low ρ, low D) such that the ratio D/ρ (and thus ψ) is fixed. The detectable tumour radii r^* increase in the same manner for both tumours but it takes the low grade tumour longer to reach a lethal size. Although the spatial invasion characteristics are the same for a fixed ψ, the timescale on which they occur can be very different.

Spatial dispersal in a heterogeneous environment has mainly been studied in an ecological context. For example, Cantrell and Cosner (1991) modelled the dynamics of a population inhabiting a heterogeneous environment with a diffusive logistic equation with spatially varying growth rates. They were interested in the effect of the spatial arrangement of favorable and unfavorable patches on the overall suitability of the environment. Cruywagen et al. (1996) modelled the risk of spread of a genetically engineered organism using a reaction diffusion model on a spatially heterogeneous environment. Conditions for invasion of the organism were determined for the case of spatially periodic diffusion rates and carrying capacity. Their work is discussed in Chapter 1. Shigesada and Kawasaki (1997) in their book on biological invasions discuss dispersal with a piecewise-constant spatially varying diffusion coefficient. The environment consists of an arrangement of favorable and unfavorable patches. With diffusion and logistic growth spatially periodic, they show the existence of traveling periodic wave solutions.

With respect to the spatial spread of brain tumours in a heterogeneous domain, Swanson (1999) carried out a one-dimensional analysis for the model equation (11.10)

with (11.11) in which the spatial domain consisted of a small $O(\epsilon)$ domain of white matter embedded in an infinite domain of grey matter. The boundary conditions consist of continuity of the cell density and the cell flux at the boundaries between the grey and white regions. From an asymptotic point of view, with $\epsilon \ll 1$, since the diffusion coefficient in the white region is larger than that in the grey regions intuitively we would expect that the cell density is approximately constant in the white region as was confirmed analytically.

11.3 Tumour Spread *In Vitro*: Parameter Estimation

In vitro experiments are frequently used to help characterize *in vivo* behaviour. Necessarily, several parameter estimates come from such *in vitro* experiments. Underlying the parameter estimation from experimental data is the general assumption that our modelling approach and the model apply to these experiments. In this section, we consider two such experiments to determine parameter estimates. We discuss this in some detail since parameter estimation is particularly important when making predictions as to possible patient treatment.

Normal glial cells have a very low motility rate (Silbergeld and Chicoine 1997) but glioma cells can exhibit abnormally high motility rates (Chicoine and Silbergeld 1995, Giese et al. 1996a,b,c, Giese and Westphal 1996, Pilkington 1997a,b, Silbergeld and Chicoine 1997, Amberger et al. 1998, Giese et al. 1998). Using time-lapse video microscopy and other techniques, Chicoine and Silbergeld (1995) quantified brain tumour cell motility and invasion capabilities *in vivo* and *in vitro* and their results suggest an average linear velocity of 12.5 μm/hr for human glioma cells *in vitro* and a minimum linear velocity of 4.8 μm/hr *in vivo*.

In Vitro Experiments of Chicoine and Silbergeld (1995): Cell Motility

Chicoine and Silbergeld (1995) developed a tumour cell motility assay known as the 'radial dish assay.' Basically 2×10^4 cells are plated in a central 2-cm diameter disk of an 8-cm diameter petri dish. Cell mitosis is inhibited and daily microscopy of the dish shows the spatial spread of the cell population. We can use the above model as it applies to this experiment to estimate the diffusion coefficient of the glioma tumour cells *in vitro*.

In this situation there is no growth so $\rho = 0$ and no heterogeneity in diffusion so $\bar{D}(\bar{x}) = D$. The dimensional model (11.3) (with radial symmetry) is then

$$\frac{\partial \bar{c}}{\partial \bar{t}} = D\bar{\nabla}^2\bar{c} \tag{11.17}$$

with zero flux boundary conditions

$$\bar{\mathbf{n}} \cdot \bar{\nabla}\bar{c}(\bar{r}, \bar{t}) = 0 \quad \text{for } \bar{r} = R_0, \tag{11.18}$$

where R_0 is the radius of the petri dish; in the assay $R_0 = 4$ cm. Initially cells are uniformly distributed in a central circular area of radius R:

$$\bar{c}(\bar{r}, 0) = \bar{c}_0 H(R - \bar{r}), \tag{11.19}$$

where H denotes the Heaviside function and $R = 1$ cm in the Chicoine et al. (1995) experiments. Since mitosis is blocked, there is no growth and a total of $N = \bar{c}_0 \pi R^2$ cells are in the petri dish throughout the experiment.

If we now nondimensionalise the model by setting

$$\mathbf{x} = \frac{\bar{\mathbf{x}}}{R_0}, \quad t = \frac{D}{R_0^2}\bar{t}, \quad c(\mathbf{x}, t) = \frac{\bar{c}\left(\frac{\bar{\mathbf{x}}}{R_0}, \frac{D}{R_0^2}\bar{t}\right)}{\bar{c}_0}, \tag{11.20}$$

where $N = \bar{c}_0 \pi R^2$ is the initial number of tumour cells at time $t = 0$ the nondimensional model, which, with radial symmetry involves only the radial coordinate r, becomes

$$\begin{aligned} \frac{\partial c}{\partial t} &= \frac{\partial^2 c}{\partial r^2} + \frac{1}{r}\frac{\partial c}{\partial r} \quad \text{for } 0 < r < 1 \\ c(r, 0) = H(\lambda - r), &\quad \frac{\partial c}{\partial r} = 0 \quad \text{at } r = 1, \end{aligned} \tag{11.21}$$

where $\lambda = R/R_0$; in the case of the radial dish assay experiments, $\lambda = 1/4$.

Asymptotic Approximation for the Cell Density $c(r, \theta, t)$

If we can assume that the petri dish is sufficiently large, $R_0 \gg R$, we can approximate the solution by (11.13) with $\rho = 0$, the solution of the simple diffusion equation on an infinite domain. However, $\lambda = 1/4$ is not small and so we have to use a more accurate approximation.

The solution of (11.21) is a classical one involving Bessel functions and is obtained by standard methods; see, for example, Kevorkian (1999) or Carslaw and Jaeger (1959). It can be derived by superposition of the basic solution for a ring at radius r_0 integrated from 0 to λ.

Since we are primarily interested in large t all we need is the asymptotic approximation to the solution. The solution for a ring of cells at r_0 is given by

$$c_{\text{ring}}(r, t; r_0) = \frac{1}{4\pi t} \exp\left(-\frac{r^2 + r_0^2}{4t}\right) I_0\left(\frac{r r_0}{2t}\right), \tag{11.22}$$

where I_0 is the modified Bessel function. Asymptotically, for $r r_0/2t$ small, this solution is given approximately by

$$c_{\text{ring}}(r, t; r_0) \sim \frac{1}{4\pi t} \exp\left(-\frac{r^2 + r_0^2}{4t}\right)\left[1 + \frac{1}{4}\left(\frac{r r_0}{2t}\right)^2 + O\left(\left(\frac{r r_0}{2t}\right)^4\right)\right]. \tag{11.23}$$

When $r_0 = 0$ this gives, of course, the exact solution for a point source of cells at the origin.

For a disk of cells of radius R we have

$$c(r,0) = H(\lambda - r) = 2\pi \int_0^{\lambda} c_{\text{ring}}(r,0;r_0) r_0 \, dr_0.$$

Combining this with the approximation (11.23), the solution of the full problem (11.21) with disk initial conditions is then

$$\begin{aligned} c(r,t) &= 2\pi \int_0^{\lambda} c_{\text{ring}}(r,t;r_0) r_0 \, dr_0 \\ &\sim e^{-\frac{r^2}{4t}} \left(1 - e^{-\frac{\lambda^2}{4t}}\right) + \frac{r^2}{4t} e^{-\frac{r^2}{4t}} \left[1 - \left(1 + \frac{\lambda^2}{4t}\right) e^{-\frac{\lambda^2}{4t}}\right] + \cdots \end{aligned} \tag{11.24}$$

for $\nu = r\lambda/2t$ small. In the case of the Chicoine and Sibergeld (1995) experiments $\nu = r/8t$.

We now use the approximate solution (11.24) to obtain an *in vitro* estimate for the diffusion coefficient for the glioma cells. We expect the estimate to be most accurate for small r and $t \sim O(1)$ or larger. Figure 11.6(a) is a plot of the experimental measurements of cell densities in the radial dish assay from Chicoine and Silbergeld (1995) with the (dimensional) form of the asymptotic solution (11.24) for $D = 0.002$ cm^2/hr at the different experimental times. Swanson (1999) solved the full problem (11.22) numerically for $D = 0.002$ cm^2/hr with the same experimental data from Figure 11.6(a) and this is shown in Figure 11.6(b). Comparing the two figures, the asymptotic approximation (11.24) is quite accurate for determining parameter estimates.

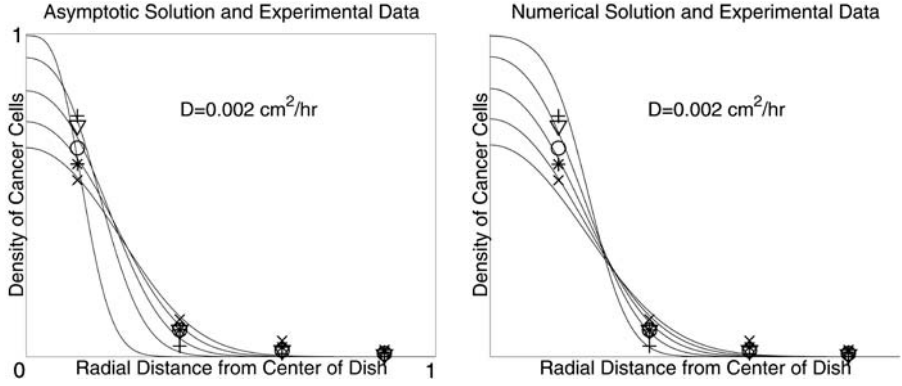

Figure 11.6. Experimental *in vitro* cell density results from Chicoine and Silbergeld (1995) as compared with the (**a**) asymptotic approximation from (11.24) and (**b**) the numerical solution of (11.22) (from Swanson 1999). The cell densities were observed for mixed glioma cells in the radial dish assay experiment. The asymptotic approximation is strictly only valid for moderate t and small r (that is, $r\lambda/2t$ small). The different curves correspond to experimental observation times $t = 24, 48, 72, 96, 120$ hours.

Asymptotic Approximation for the Average Distance, $\langle r\rangle$, of Cells from the Initial Inoculum

Chicoine and Silbergeld (1995) also calculated the average distance from the origin, $\langle r\rangle$, for the glioma cells in the radial dish assay method. To determine $\langle r\rangle$ we have to integrate the solution for all r. The asymptotic solution (11.24) is only strictly valid for $r\lambda/2t$ small which is not small for arbitrarily large r. So, we really have to calculate $\langle r\rangle$ in full.

If $c(r,t)$ is the distribution of the cells at time t, then the mean radial distance of cells from the origin $\langle r\rangle$ is given by:

$$\langle r\rangle = \frac{\int_0^\infty r^2 c(r,t)\,dr}{\int_0^\infty r c(r,t)\,dr} = \int_0^\infty r^2 c(r,t)\,dr, \tag{11.25}$$

where $c(r,t)$ is given by the integral in (11.24). The answer is given in terms of an integral which we approximate for large and small t. It involves some algebra and a straightforward application of Laplace's method for evaluating integrals involving small and large parameters (see, for example, Murray 1984 for a pedagogical discussion). For small t with $A = 1/4t$ we obtain

$$\begin{aligned}\langle r\rangle &\sim \frac{3+2A\lambda^2}{6A\lambda}\left(1+\operatorname{erf}(\sqrt{A}\,\lambda)\right) - \frac{5}{6\lambda^2\sqrt{A^3\pi}} + \frac{5+2A\lambda^2}{6\sqrt{\pi}\,A\lambda^2}e^{-A\lambda^2}\\ &= \frac{6t+\lambda^2}{3\lambda}\left[1+\operatorname{erf}\left(\frac{\lambda}{2\sqrt{t}}\right)\right] - \frac{20}{3\lambda^2}\sqrt{\frac{t^3}{\pi}} + \frac{10t+\lambda^2}{3\sqrt{\pi}\,\lambda^2}e^{-\frac{\lambda^2}{4t}}\\ &\sim \frac{2\lambda}{3} + \frac{4t}{\lambda} + \cdots \quad \text{as } A = \frac{1}{4t} \to \infty.\end{aligned} \tag{11.26}$$

As $t \to 0$ ($A \to \infty$), $\langle r\rangle$ approaches $2\lambda/3$ which corresponds to the exact mean radial distance associated with the (nondimensional) initial distribution of cells.

For large t (small A), the mean displacement is given by

$$\langle r\rangle = \sqrt{\pi t}\left(1 + \frac{\lambda^2}{16t} - \frac{\lambda^4}{768t^2} + \cdots\right). \tag{11.27}$$

For t large, the mean radius converges to the case of a point source of cells at the origin: $\langle r\rangle = \sqrt{\pi t}$ (in dimensional form, $\langle \bar{r}\rangle = \sqrt{\pi D\bar{t}}$). What it means is that after a long time diffusion will have spread the population out sufficiently so that the original distribution can not be identified. However, for large time, the effects of the boundaries of the petri dish become important. Since the cells in the petri dish are not allowed to grow during the Chicoine and Silbergeld (1995) experiments, as $t \to \infty$, the cell density approaches a uniform steady state $c \to \lambda^2$ (in dimensional form, $\bar{c} \to \bar{c}_0\lambda^2$). So a more accutate asymptotic estimate for the large time behaviour should use this steady state to compute the mean displacement:

$$\langle r\rangle = 2\pi \int_0^\infty r^2 c(r,t)\,dr \to 2\pi \int_0^1 \lambda^2 r^2\,dr = \frac{2\pi}{3}\lambda^2, \tag{11.28}$$

which is the long time limit for the petri dish experiments. When compared with the experimental results neither of these approximations is very good although the small t approximation is better.

Chicoine and Silbergeld (1995) actually calculated a 'mean radius' in a slightly different way to what we have done here. Their calculation neglected the contribution of the cells within the initial ring of radius R. This corresponds to simply replacing the lower limit 0 in the integral in (11.25) with λ. If we denote this new 'mean radius' by $\langle r^*\rangle$ it satisfies

$$\langle r^*\rangle = \frac{\int_\lambda^\infty r(r-\lambda)c(r,t)\,dr}{\int_\lambda^\infty rc(r,t)\,dr} = \frac{2\pi}{1-\lambda^2}\int_\lambda^\infty r(r-\lambda)c(r,t)\,dr. \tag{11.29}$$

Swanson (1999) has shown, using similar approximation methods to those above for $\langle r\rangle$,

$$\langle r^*\rangle \sim \frac{2\pi t^2}{1-\lambda^2} + \frac{40}{3(1-\lambda^2)}\sqrt{\pi t^3} + \cdots \qquad \text{for small } t \text{ (large } A\text{)}. \tag{11.30}$$

Remember that $R = 1$ cm which in the experiments gives $\lambda = 1/4$.

The glioblastoma cells are observed to reach the edge of the petri dish by 96 hours thus defining the overestimation of the asymptotic result for large t values in Figure 11.7(c).

In Figure 11.7 we plot the mean radius $\langle r^*\rangle$ computed from the experimental observations with the asymptotic expression (11.30) which is strictly only valid for small t. This figure suggests estimates of 1.6×10^{-4} cm^2/hr, 2×10^{-3} cm^2/hr and 3×10^{-3} cm^2/hr for the diffusion coefficients for anaplastic astrocytoma, mixed glioma, and glioblastoma multiforme cells, respectively. Therefore, with increasing malignancy, the cell motility increases. In fact, these results suggest that there is approximately a twofold difference between the motility of mid-grade anaplastic astrocytoma cells and high grade glioblastoma cells *in vitro*.

In Figure 11.7 we see that for glioblastoma cells the asymptotic expansion (11.26) overestimates the mean radius for $\bar{t} > 96$ hours. This is as we should expect because Chicoine and Silbergeld (1995) observed that the glioblastoma cells move so quickly they are capable of reaching the edge of the dish in 96 hours and so boundary effects become important. The anaplastic astrocytoma and mixed glioma cells are not capable of reaching the petri dish edge until later times.

From the calculations of $\langle r\rangle$, there is a steady state limit for the tumour cell population in the petri dish, namely, $c \to \lambda^2$ for large time. We can calculate the effect this steady state has on the limiting value of $\langle r^*\rangle$:

$$\langle r^*\rangle \to \frac{\int_\lambda^1 r(r-\lambda)\lambda^2\,dr}{\int_\lambda^1 \lambda^2 r\,dr} = \frac{2-3\lambda+\lambda^3}{3(1-\lambda^2)} \tag{11.31}$$

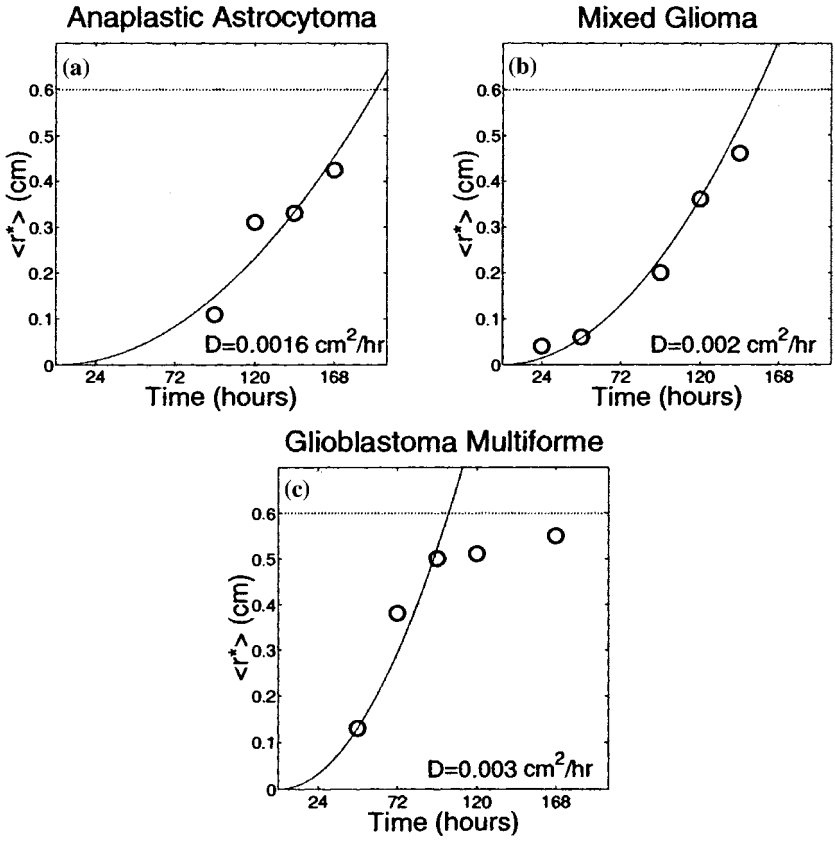

Figure 11.7. Asymptotic approximation for the mean radius $\langle r^* \rangle$ from (11.30) versus time for (**a**) anaplastic astrocytoma ($D = 1.6 \times 10^{-3}$ cm^2/hr), (**b**) mixed glioma ($D = 2 \times 10^{-3}$ cm^2/hr) and (**c**) glioblastoma multiforme ($D = 3 \times 10^{-3}$ cm^2/hr) cells. The uniform steady state solution defines the long time limit (dotted line) of $\langle r^* \rangle$ given by (11.31). (From Swanson 1999)

as $t \to \infty$. This limiting value is included in Figure 11.7 and defines the overestimation of $\langle r^* \rangle$ by the asymptotic approximation (11.30) for glioblastoma multiforme cells in Figure 11.7(c).

In Vitro Experiments of Giese et al. (1996a,b,c): Cell Motility and Proliferation

As we have mentioned, glioma cell motility in white matter is higher than that in grey matter. Giese et al. (1996b) carried out *in vitro* experiments to characterize the increased motility of glioma cells on myelin, a key component of white matter. These experiments were similar to those of Chicoine and Silbergeld (1995) but on a shorter timescale, namely, 40 to 100 hours, with the main difference being that Giese et al. (1996b) allowed the cells to proliferate during the experiment. They also tabulated the increase in radius of the visible front of tumour cells. In addition, the initial inoculum of cells covered a smaller region than in the Chicoine and Silbergeld (1995) experiments. So, we expect

the experiment to be modelled more appropriately by

$$\frac{\partial \bar{c}}{\partial \bar{t}} = \bar{D}\bar{\nabla}^2\bar{c} + \rho\bar{c} \quad \text{for } \bar{r} \leq R_0, \tag{11.32}$$

where R_0 is the radius of the dish in which the cells are allowed to migrate, the Laplacian is axisymmetric and there are zero flux boundary conditions

$$\mathbf{n} \cdot \bar{\nabla}\bar{c}(\bar{r}, \bar{t}) = 0 \quad \text{for } \bar{r} = R_0, \tag{11.33}$$

with $\mathbf{n}$ the outward pointing normal at the edge of dish. Initially, there is a point source of N cells at the origin:

$$\bar{c}(\bar{r}, 0) = N\delta(\bar{r}). \tag{11.34}$$

For sufficiently large R_0, the solution is approximately (11.13); that is,

$$\bar{c}(\bar{r}, \bar{t}) \sim \frac{N}{4\pi D\bar{t}} \exp\left(\rho\bar{t} - \frac{\bar{r}^2}{4D\bar{t}}\right). \tag{11.35}$$

To estimate diffusion coefficients from the experimental data we use the Fisher–Kolmogoroff approximation. In the case of the Fisher–Kolmogoroff equation in one space dimension studied in some detail in Chapter 13, Volume I we saw that the travelling wavespeed is given by $v = 2\sqrt{\rho D}$ where D and ρ are the diffusion coefficient and the linear growth rate respectively. So, a population governed by growth and diffusion alone expands at a rate of $2\sqrt{\rho D}$ after a large time. In the two-dimensional case defined by (11.32)–(11.34) the tumour cell concentration is given by (11.35) if the boundary R_0 is far enough away to approximate an infinite domain. Since experimentally we can track the profile of tumour cells above some detection level c^*, substituting this into the last equation, and solving for D, gives

$$\begin{aligned} D &= \frac{\bar{r}^2}{4\bar{t}}\left[\rho\bar{t} - \ln\left(4c^*\pi D\bar{t}/N\right)\right]^{-1} \\ &\approx \frac{\bar{r}^2}{4\rho\bar{t}^2} \quad \text{for large } \bar{t} \text{ since } \rho\bar{t} \gg \ln\bar{t}. \end{aligned}$$

Let $v = \bar{r}/\bar{t}$ be the velocity of the profile front; then

$$D \approx \frac{v^2}{4\rho}. \tag{11.36}$$

We therefore associate the diffusion coefficients in white and grey matter by $D_w = v_w^2/4\rho$ and $D_g = v_g^2/4\rho$ with the experimentally observed linear velocities v_w and v_g, respectively. To deduce estimates for the diffusion coefficients we need to determine the growth rate of the tumour cells. We now use this approximation (11.36) with the experimental results.

We should introduce here a note of caution. With this derivation, the Fisher–Kolmogoroff estimate implies that a very low growth rate with a large linear velocity gives very high estimates for the diffusion rate for the tumour cells in both grey and white matter. Since the proliferation and motility rates are generally (positively) correlated with malignancy as we show below, the tumour cell populations with high linear velocities could have a high (or at least not small) growth rate. Of course, certain midgrade tumours with small ρ and large D could spawn subpopulations with even larger D's with ρ only increasing marginally, if at all.

Giese et al. (1996b) determined the range expansion of the population over time on myelin. That is, given some threshold of detection c^*, the radius of the detectable tumour cell region was recorded as a function of time. From (11.14) the detectable radius r^* of the tumour cell population is given by

$$r^* \sim 2\sqrt{D\rho}\, t \tag{11.37}$$

for large t. Figure 11.8 is a linear least squares fit of the Giese et al. (1996b) experimental observations of the detectable radius versus time for three glioblastoma cell lines (G-112, G-140, G-168). The slope of the line is taken to be equal to $2\sqrt{\rho D}$. So, with an estimate for the growth rate ρ we can deduce a value for the diffusion coefficient, D, from these linear least squares fits to the data.

In Table 11.1 we give the slopes of the linear fits shown in Figure 11.8. By assuming ρ does not vary when the cells are migrating on the control extracellular matrix material (ECM) or on the myelin, we can use the slopes in Table 11.1 to deduce a relationship between the diffusion coefficient on ECM and myelin. Denote by D_{ECM} and v_{ECM} the diffusion coefficient and linear velocity of the cells on ECM, respectively. Similarly, denote by D_m and v_m the diffusion coefficient and linear velocity of the cells on myelin, respectively. The linear velocities then satisfy

$$v_{\text{ECM}} = 2\sqrt{\rho D_{\text{ECM}}}, \quad v_m = 2\sqrt{\rho D_m} \Rightarrow \frac{D_m}{D_{\text{ECM}}} = \left(\frac{v_m}{v_{\text{ECM}}}\right)^2. \tag{11.38}$$

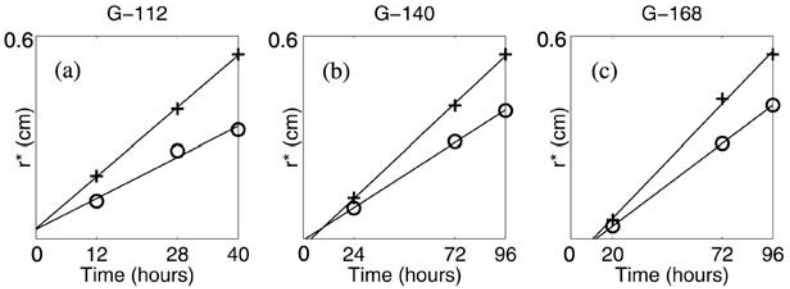

Figure 11.8. Model prediction of the detectable radius r^* for the experimental observations of Giese et al. (1996b) for three different glioblastoma cell lines: (**a**) G-112, (**b**) G-140, (**c**) G-168 on the control substrate; o denotes extracellular matrix (ECM) and + denotes white matter myelin. (From Swanson 1999)

Table 11.1. Velocity v of detectable tumour radius as defined by the slope of linear least squares fit to the Giese et al. (1996a) data shown in Figure 11.8. This suggests there is a 2 to 3 fold difference between the diffusion coefficient on ECM and myelin for these experimental conditions.

Cell Line	Velocity on Myelin (cm/hr)	Velocity on ECM (cm/hr)	Ratio of Diffusion Coefficients in Myelin and ECM
	v_m	v_{ECM}	D_m/D_{ECM}
G-112	2.6×10^{-3}	1.5×10^{-3}	3.00
G-140	1.9×10^{-3}	1.3×10^{-3}	2.14
G-168	3.5×10^{-3}	2.5×10^{-3}	1.96

From the velocity values given in Table 11.1 we deduce that the ratio of the diffusion coefficient on myelin to that on ECM diffusion coefficient is approximately 2. If we associate D_{ECM} with the diffusion coefficient in grey matter then we can suggest that the diffusion coefficient in white matter is twice that in grey matter. Clearly, *in vitro* experimental conditions are different to those observed *in vivo* but from this result we expect at least a twofold difference between the diffusion coefficient in grey and white matters.

As with all experimental results, there is the question as to whether the behaviour observed in the petri dish is analogous to that *in vivo*. To deal with this problem a range of experimental conditions is often considered. In Table 11.2 we give the results of another series of experiments by Giese et al. (1996b). Each row of Table 11.2 corresponds to slightly different experimental conditions defined by the amount of fetal calf serum supplied to the cells. With increasing concentrations of serum (Experiments $1 \rightarrow 4$), the growth rate of the tumour cells increases with serum concentration but the motility reaches a maximum and then decreases. From the various experimental conditions we now use the approximation for the rate of expansion given by the Fisher–Kolmogoroff approximation for the wavespeed for large t, namely, $2\sqrt{\rho D}$ (essentially the derivative with respect to t of (11.37)) to deduce the diffusion coefficient for the glioblastoma cells from $D = v^2/4\rho$.

Table 11.2. Giese et al. (1996b) experimental observations of the detectable tumour radius velocity v_{ECM} in ECM and the growth rate ρ. From v_{ECM} and ρ, the diffusion coefficient is deduced using the Fisher–Kolmogoroff approximation $D = v^2/4\rho$. Each row corresponds to slightly different experimental conditions (defined by the amount of fetal calf serum supplied to the cells).

Experiment Number	Velocity on ECM v_{ECM} (cm/hr)	Growth Rate ρ (1/day)	Diffusion Coefficient D_{ECM} (cm^2/hr)
1	6×10^{-4}	.075	3×10^{-5}
2	1.2×10^{-3}	.1	9×10^{-5}
3	1.55×10^{-3}	.2	7×10^{-5}
4	1.15×10^{-3}	.575	10^{-5}

Table 11.3. *In vitro* parameter estimates for mid-grade (anaplastic astrocytoma) to high-grade (glioblastoma multiforme) gliomas. (From Swanson 1999)

Parameter	Symbol	Range of Values	Units
Linear velocity on ECM	v_{ECM}	$0.6 - 2.1 \times 10^{-3}$	cm/hr
Linear velocity on myelin	v_m	$1.8 - 3.0 \times 10^{-3}$	cm/hr
Diffusion coefficient on ECM	D_{ECM}	$1.0 - 9.0 \times 10^{-5}$	cm^2/hr
Diffusion coefficient on myelin	D_m	$> 0.2 - 2.0 \times 10^{-4}$	cm^2/hr
Net growth rate	ρ	$0.075 - 0.575$	day^{-1}

We now incorporate all of the above results to determine parameter estimates for glioma cells *in vitro*. Table 11.3 summarizes the various estimates we have obtained for the *in vitro* experimental conditions discussed above.

11.4 Tumour Invasion in the Rat Brain

Rats are commonly used to study the *in vivo* dynamics of tumour spread. With gliomas, typically a tumour is implanted in the cortex of the rat brain and allowed to grow and spread. At some later time, the rat is sacrificed and the tumour dynamics are approximated. Experimental studies of gliomas in rats provide estimates for the minimum linear velocity of tumour cells. Although glioma cells do not travel a linear path, if cells are identified at some distance from the original implantation location at sacrifice, the cells must have traveled at some minimum linear velocity to reach that distance. We can take this linear velocity to correpond to the velocity of the detectable radius of the tumour where the threshold concentration for detection is very low. The model equation describing tumour cell dynamics *in vivo* in rats is the spatially heterogeneous model derived in Section 11.2 and given by equation (11.4) in dimensional form.

In Vivo Parameter Estimation for the Rat Brain

Using time-lapse video microscopy and other techniques, Chicoine and Silbergeld (1995) and Silbergeld and Chicoine (1997) quantified brain tumour cell motility and invasion capabilities *in vivo* in rats. Their results suggest a minimum linear velocity of 4.8 μm/hr *in vivo* in rats.

We are particularly interested in the variation in parameter values in white and grey matter regions. A mean linear velocity of 36 μm/hr and 70 μm/hr in grey (v_g) and white (v_w) matter, respectively, has been suggested (D.L. Silbergeld, personal communication 1998). These values are higher than the estimates given in the last section but represent the evolution of new experimental techniques for assessing motility. This highlights an ongoing problem in determining definitive parameter estimates. Even with the best possible theoretical techniques we have to rely on the ever-changing best experimental techniques and so parameter estimates inevitably change.

Glioma cells do not travel a linear path which is why we model glioma motility by a random walk. To relate linear velocity v, proliferation ρ and a random walk diffusion

Table 11.4. Parameter estimates for the rat model using the Fisher–Kolmogoroff approximation (11.36) with the linear velocities from D.L. Silbergeld (personal communication 1998) and the doubling time from Alvord and Shaw (1991).

Parameter	Symbol	Range of Values	Units
Linear velocity in grey matter	v_g	36 ± 12	μm/hr
Linear velocity in white matter	v_w	70 ± 15	μm/hr
Diffusion coefficient in grey matter	D_g	$.008 - 3.3$	cm^2/day
Diffusion coefficient in white matter	D_w	$.032 - 12.0$	cm^2/day
Tumour doubling time	t_d	$\frac{1}{4} - 12$	months
Net growth rate	ρ	$0.001 - 0.1$	day^{-1}

D we again use the Fisher–Kolmogoroff approximation $D \approx v^2/4\rho$ from (11.36) as was also used by Burgess et al. (1997). We again associate the diffusion coefficients in white and grey matter by $D_w = v_w^2/4\rho$ and $D_g = v_g^2/4\rho$ with the experimentally observed linear velocities v_w and v_g, respectively. To deduce estimates for the diffusion coefficients we need to determine the growth rate of the tumour cells. Alvord and Shaw (1991) cite doubling times of one week to one month for gliomas *in vivo*. The resulting parameter estimates for rats *in vivo* are presented in Table 11.4. With these, using the Fisher–Kolmogoroff estimate (as described in the last section) with a very low growth rate and with a large linear velocity gives very high estimates for the diffusion rate for the tumour cells in both grey and white matter. Since the proliferation and motility rates are generally (positively) correlated with malignancy as we see from the above, the tumour cell populations with high linear velocities could have a high (or at least not small) growth rate. So, the very large diffusion coefficients given in Table 11.4 may not be that accurate.

Numerical Simulations of Tumour Invasion in the Rat Brain

In earlier studies of untreated tumour invasion (Burgess et al. 1997) the brain was considered homogeneous. Swanson (1999) investigated the increased invasion capabilities associated with the introduction of heterogeneity as a consequence of the white and grey matter. We first focused on the simple rat brain topology illustrated in Figure 11.9. For illustrative purposes she assumed a diffusion coefficient in white matter of approximately 10 times that in grey matter. From the parameter estimates in Table 11.4, experimental results indicate a diffusion coefficient in white matter from 2 to 100 times greater than the diffusion coefficient in grey matter.

It is generally accepted that the corpus callosum is a common pathway for invasion of tumour cells to the contralateral hemisphere. In the coronal plane of the simpler rat brain topology in Figure 11.9, the corpus callosum is a compact arch of white matter fibres connecting the left and right cerebral hemispheres. In the simulations we approximate the corpus callosum of the rat brain by the regular area enclosed by the curve in Figure 11.10 that looks like a pair of horns.

In the preliminary simulations the corpus callosum is connected to the grey matter cortex by white matter fibres radiating from the corpus callosum, represented by the

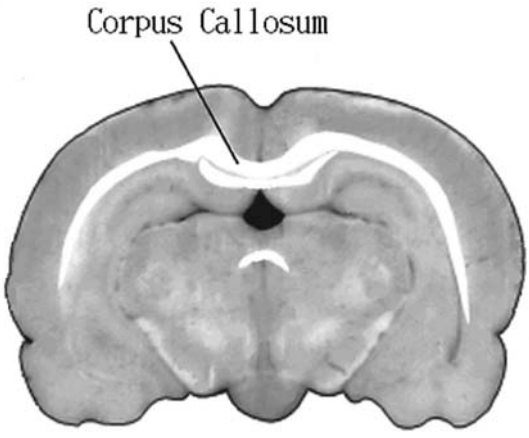

Figure 11.9. Geometry of a coronal slice of a rat brain. White matter appears white and grey matter appears dark grey. The corpus callosum is the arch of white matter connecting the left and right cerebral hemispheres. The width of the brain is about 1.5 mm. (Redrawn from Toga et al. 1995)

boomerang shape, as shown in Figure 11.10(a)–(d). Remember that the corpus callosum is an extensive bundle of white matter fibre. These fibre tracts running from the corpus callosum to the cortex are much narrower than the corpus callosum. They are represented as straight lines extending from the corpus callosum. In the human brain some of these (curvilinear) tracts connecting the cortex to the corpus callosum are identified by a thin trail of cancer cells. Swanson (1999) simulated the model system defined by (11.10) and (11.11) with zero flux boundary conditions and continuity and conservation conditions discussed in Section 11.2 to demonstrate how the tumour invasion is facili-

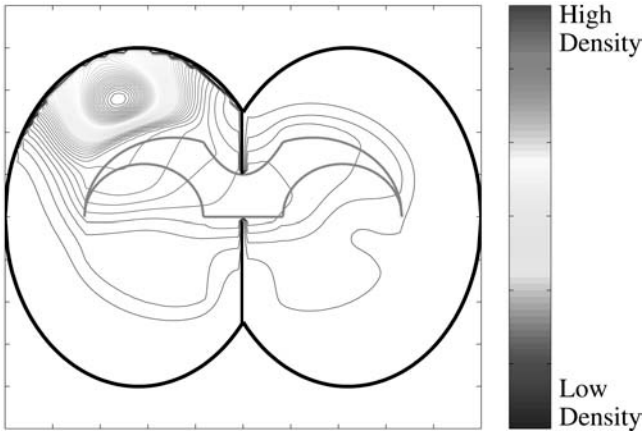

Figure 11.10. A small tumour was introduced and allowed to diffuse according to the model. There is clear enhanced invasion via white matter tracts; the corpus calossum fairly quickly fills with cancer cells. The model parameters are: $D_g = 1.3 \times 10^{-3}$ cm^2 day^{-1}, $D_w = 10D_g$, $\rho = 1.2 \times 10^{-2}$ day^{-1}. (From Swanson 1999) (The scale is a black and white copy of the original colour scale (blue at low density via yellow to red at high density). The interpretation is an increase in density from the outer lines towards the tumour origin.)

tated by these thin fibrous tracts and the corpus callosum. These fibres help to facilitate the invasion by the tumour cells to more distant regions more quickly. The review article by Giese and Westphal (1996) shows some examples where the tumour spread has been facilitated by the corpus collosum in the human brain.

The simulations in Figure 11.10, in which a small tumour was introduced and allowed to diffuse and grow according to the model, show a dramatic increase in invasion capability by the presence of white matter to invade more distant locations. In a relatively short time tumour cells essentially fill the corpus callosum as is observed experimentally and also clinically in the human brain (see Giese and Westphal 1996).

It is commonly noted in experiments that tumour cells migrate across the corpus callosum laterally. It is because of this lateral invasion, that it is thought that gliomas cells move preferentially along the fibres of the white matter corpus callosum (see, for example, Giese and Westphal 1996). The simulations in Figure 11.10 show that anisotropy in the diffusion is *not* necessary to result in a bulk lateral movement of the tumour margin across the corpus calossum. It can be argued that the different diffusivi-

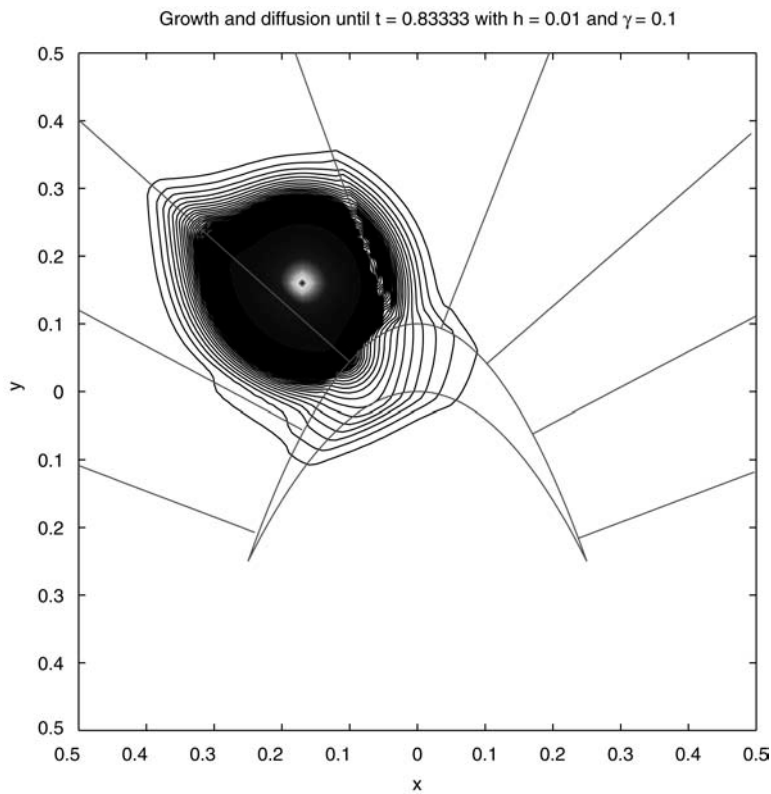

(a)

Figure 11.11. Simulation of the model on the rat brain with the white matter corpus callosum present. Parameter values are: $D_g = 1.3 \times 10^{-3}$ cm^2 day^{-1}, $D_w = 10D_g$, $\rho = 1.2 \times 10^{-2}$ day^{-1} at times (**a**) $t \approx 0.83$, (**b**) $t \approx 1.67$, (**c**) $t \approx 2.5$, (**d**) $t \approx 3.3$. (From Swanson 1999)

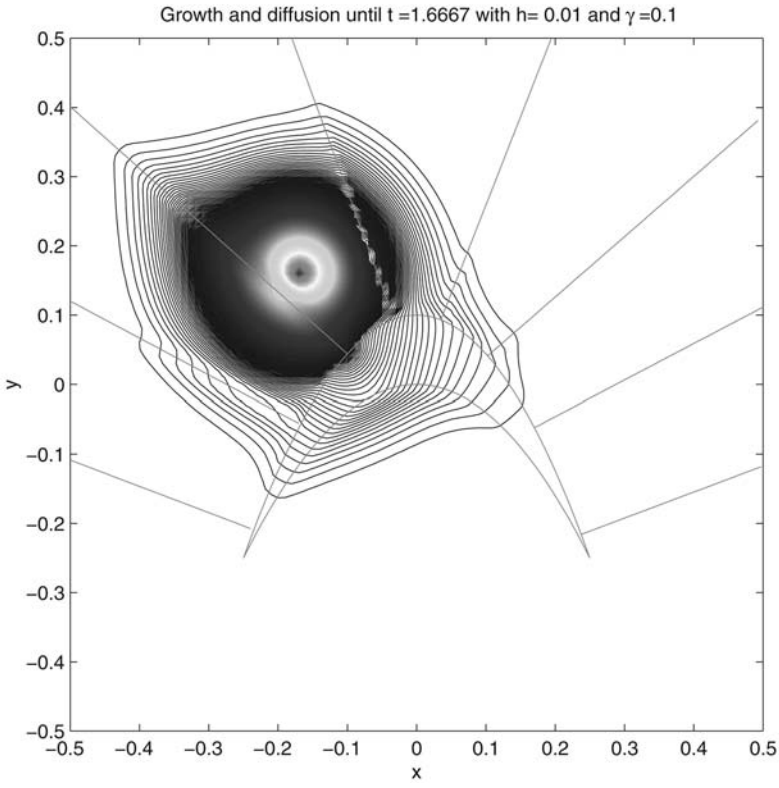

(b)

Figure 11.11. (continued) (See the comment in parentheses in Figure 11.10.)

ties in the grey and white matter are a kind of anisotropy. This lateral invasion is accentuated by the physical structure of the brain in the region of the corpus callosum—the ventricles below and the fissure of the cortex above the corpus callosum help to facilitate the lateral invasion.

Figure 11.11 is a simulation of the rat brain with anatomical boundaries, along with spatially heterogeneous grey and white matter distributions as given in Figure 11.9. Because of the restriction of the rat brain cortex, there is an accumulation of tumour cells near the boundaries. In addition, since the corpus callosum is situated between the ventricles and the cortex we expect to see a marked increase in the invasion of cells across the corpus callosum to the contralateral hemisphere.

11.5 Tumour Invasion in the Human Brain

The simple geometry of the rat brain is a good model for fetal human brain topology where the cortex is smooth. The complex geometries of the adult human brain only accentuate the effects we have seen in the rat brain geometry. We expect increased bound-

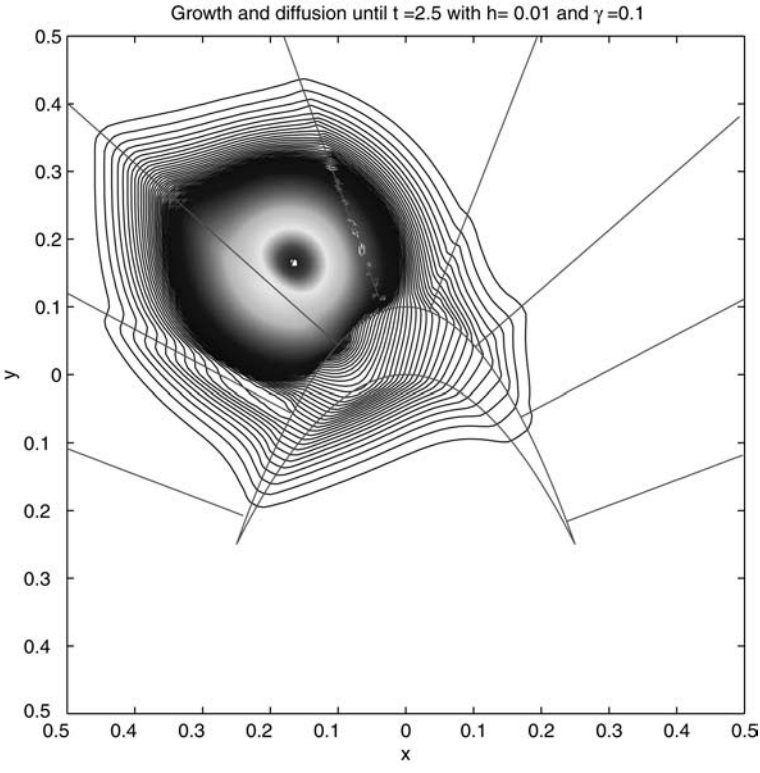

(c)

Figure 11.11. (continued) (See the comment in parentheses in Figure 11.10.)

ary effects and more complex patterns of invasion due to the heterogeneous distribution of grey and white matter. We now discuss the model application to the human brain geometry and investigate the implications of heterogeneous diffusion on the spread of an introduced virtual tumour.

A major development which let us apply our model of tumour invasion to the human brain was provided by the BrainWeb database[1] (Collins et al. 1998) and EMMA, mentioned above. Briefly, EMMA (Extensible MATLAB Medical Analysis) is a tool for manipulating medical images. The Brain Web database was created using an MRI simulator and defines the locations and distribution of grey and white matter in the brain in three spatial dimensions on a $181 \times 217 \times 181$ grid. It was created to visualize frozen images in MATLAB so that they could be manipulated and studied. In this section, we describe some of the numerical simulations of the model system (11.10) and (11.11) presented by Swanson et al. (2000). The results are for two-dimensional slices of the brain for ease of representation. Three-dimensional studies have been carried out and some of these will be discussed below.

[1] http://www.bic.mcgill.ca/brainweb.

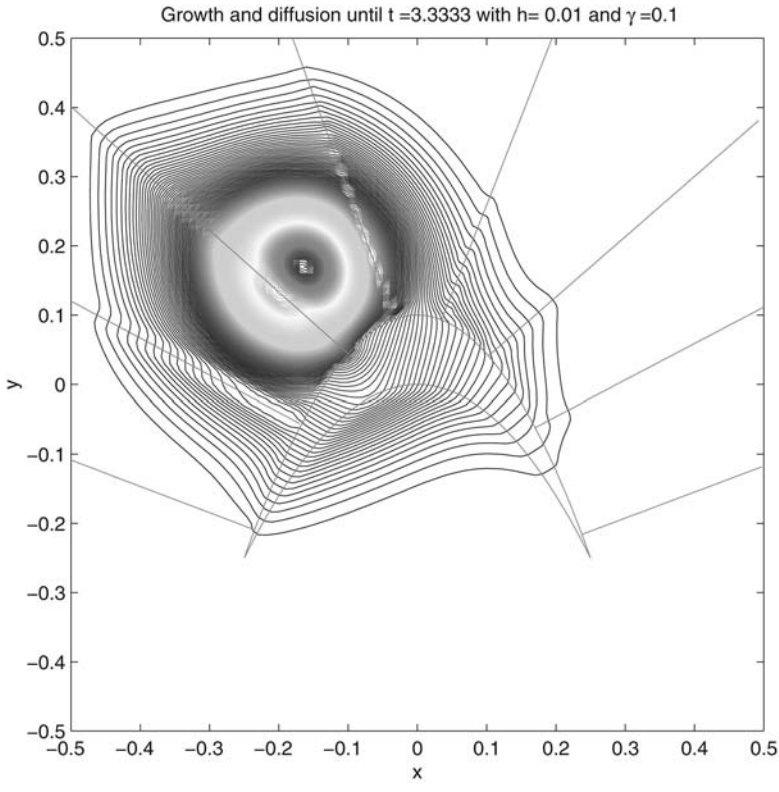

(d)

Figure 11.11. (continued) (See the comment in parentheses in Figure 11.10.)

Parameter Estimates

Parameter estimates are obtained from data on mid to high grade astrocytomas (glioblastoma multiforme). High grade astrocytomas account for $\sim$ 50% of all astrocytomas, which in turn make up $\sim$ 50% of all primary brain tumours (Alvord and Shaw 1991).

We use the Alvord and Shaw (1991) estimate of one week to 12 months as the doubling times for gliomas. So, for cell proliferation of a high grade astrocytoma, we take a growth rate of $\rho = 0.012$/day which corresponds to a 60-day doubling time.

In the last section, we discussed the marked motility of glioma cells *in vitro* and *in vivo* in rats and used experimental data of Chicoine and Silbergeld (1995) and Silbergeld and Chicoine (1997) to estimate the parameters in the model.

For the human brain model, we are interested in the variation in parameter values in white and grey matter regions. Practically, the data describing the tumour growth and invasion for a patient are obtained from medical images such as CT scans and MRI (magnetic resonance imaging). As mentioned these scans approximately define the profile of the *detectable* portion of the tumour. While Figure 11.5 is the idealized form of a CT scan an actual scan is very much less clear. This study originally began with analysis

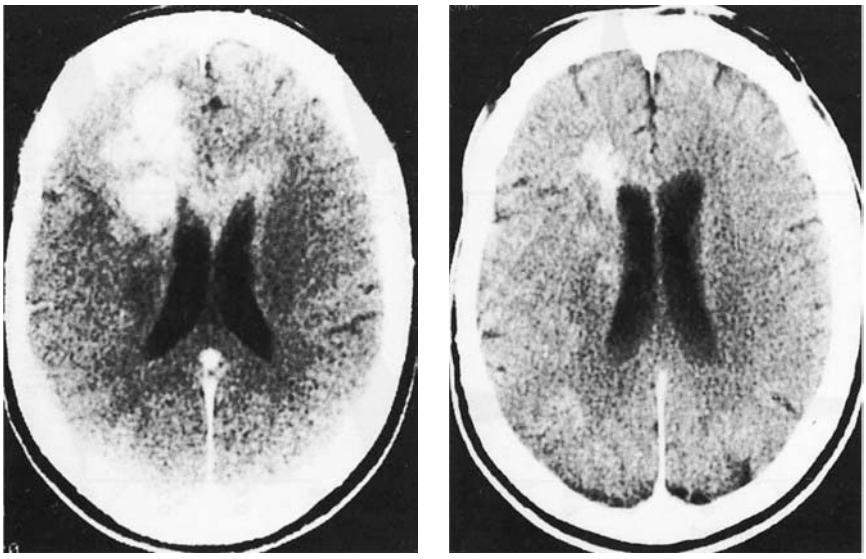

(a) (b)

Figure 11.12. CT scans during the terminal year of a patient with anaplastic astrocytoma who was undergoing chemotherapy and radiation treatment. The image on left was taken approximately 180 days after the image on the right. (Figures from Tracqui et al. 1995)

of serial CT scans during the terminal year of a patient with anaplastic astrocytoma. The patient underwent various chemotherapy and radiation treatments which we discuss in detail in Section 11.10; an example of one of these scans is shown in Figure 11.12.

As in the previous section, we use the Fisher–Kolmogoroff approximation to approximate D in terms of the linear velocity v and proliferation ρ. We then have $D_w = v_w^2/4\rho$ and $D_g = v_g^2/4\rho$ with the experimentally observed linear velocities v_w and v_g, respectively. We now have to determine v_w and v_g for a given patient. The most accessible information regarding tumour infiltration for a human patient is given by CT, MRI or other imaging scans. We use the CT scans used in the development of the original model (see Figure 11.12) to determine the velocities of the tumour front in grey and white matter. Within the right hemisphere the margin of detectable tumour moved about 1.5 cm in 180 days (Tracqui et al. 1995, Woodward et al. 1996), that is, an average speed of $v = 8.0 \times 10^{-3}$ cm/day. For the growth rate $\rho = 0.012$/day, the Fisher–Kolmogoroff approximation then gives the diffusion coefficient $D = v^2/4\rho = 1.3 \times 10^{-3}$ cm^2/day. Due to the proximity of the invasion to the deep cerebral nuclei (grey matter in the right hemisphere), we associate this value with grey matter diffusion so $v_g \approx 8.0 \times 10^{-3}$ cm/day (Tracqui et al. 1995) and $D_g \approx 1.3 \times 10^{-3}$ cm^2/day. From the CT scans, the speed of advance of the tumour margin across the corpus callosum (white matter) was two to three times as fast as that in (predominately) grey matter so we estimate $v_w > 2v_g \approx 1.6 \times 10^{-2}$ cm/day and $D_w > 4D_g \approx 4.2 \times 10^{-3}$ cm^2/day. In our simulations, we generally assumed a five-fold difference in the diffusion coefficient in grey and white matter $D_w = 5D_g$.

Table 11.5. Parameter estimates from patient data for a high-grade human glioma. (From Swanson 1999)

Parameter	Symbol	Range of Values
Linear velocity in grey matter	v_g	8.0×10^{-3} cm/day
Linear velocity in white matter	v_w	$> 1.6 \times 10^{-2}$ cm/day
Diffusion coefficient in grey matter	D_g	1.3×10^{-3} cm^2/day
Diffusion coefficient in white matter	D_w	$> 4.2 \times 10^{-3}$ cm^2/day
Tumour doubling time	t_d	2 months
Net growth rate	ρ	1.2×10^{-2} day^{-1}

We can also estimate the diffusion coefficient from the linear velocity of individual glioma cells by using the root-mean-square distance (in two dimensions) from the origin,

$$\langle \bar{r}^2 \rangle = 4D\bar{t}.$$

Since growth is not included in this definition, the value of D, calculated from this formula using our experimental data regarding the progression of the tumour profile, would be an overestimate of the actual diffusion coefficient. Although only valid for large $\bar{t}$, the Fisher–Kolmogoroff estimate is probably a better approximation for the glioma diffusion coefficients. Parameter estimates (patient generated) for a high grade glioma are listed in Table 11.5.

Numerical Simulations of the Model System: Invasion of Virtual Tumours

Solving the model equations on an anatomically accurate domain is a fairly complicated numerical undertaking. For our simulations (Swanson 1999, Swanson et al. 2000) we allow a 10-fold variation in ρ and D to simulate different tumour grades: high grade (high ρ and high D), intermediate grade (high ρ and low D or low ρ and high D) and low grade (low ρ and low D). Woodward et al. (1996) found that this range accords very well with the various types of glioma tumour growth and invasion. The numerical simulation procedure lets us track the invasion of virtual tumours of any initial size and distribution from any site.

Figure 11.13 shows a coronal section of the human brain obtained with EMMA as the domain for our model simulations. In the figure, white and grey matter appear white and grey. The three tumour sites we specifically consider are labeled in Figure 11.13: Position 1 represents an inferior fronto-parietal tumour, Position 2 corresponds to a superior fronto-parietal tumour and Position 3 a temporal lobe tumour. At each of these locations we consider the 4 tumour grades representing 10-fold variations in the growth rate ρ and the diffusion coefficient D: High Grade (high ρ, high D), Intermediate Grade (high ρ, low D or low ρ, high D) and Low Grade (low ρ, low D).

Tumour Invasion as a Function of Initial Tumour Location

Due to the heterogeneity of the brain tissue composition and geometry of the cortex, which is very clear in Figure 11.13, the dynamics of invasion can be very different

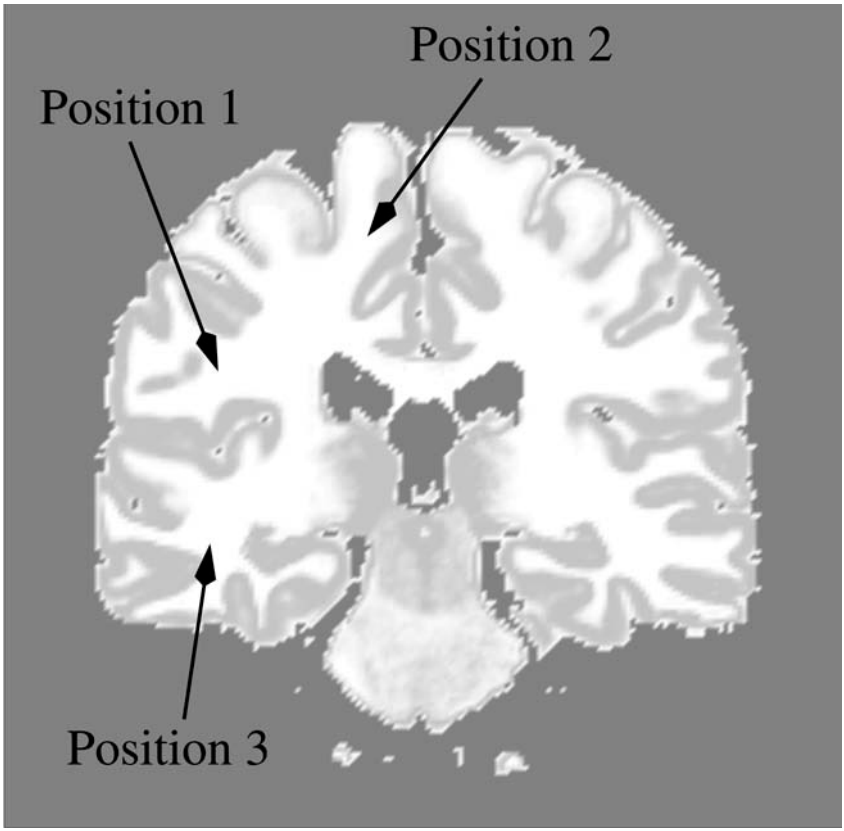

Figure 11.13. Computational domain with tumour locations. Grey and white matter appear grey and white. Position 1 is the area location of an inferior fronto-parietal tumour, Position 2 is the location for a superior fronto-parietal tumour, while Position 3 is for a temporal lobe tumour.

depending on the location of the bulk tumour. For a given tumour grade, that is, fixed ρ and D, the extent of tumour invasion is different at each tumour position as seen in Figures 11.14–11.16, and depends on the local distribution of grey and white matter and the proximity to anatomical boundaries.

Figure 11.15 represents simulations of a high grade (high ρ, high D) tumour at Position 2 (defined in Figure 11.13) within the brain. Figure 11.15(a) represents the portion of the detectable tumour on enhanced CT at diagnosis. Here we assume that diagnosis occurs when the detectable tumour, that is, the portion of tumour with density above the threshold of detection, covers an area equivalent to a circle of diameter 3 cm. Although the tumour looks fairly localized, by increasing our detection abilities by a factor of 20 (mathematically we can set the threshold at any positive value), which corresponds to 500 cells/cm^2, we see in Figure 11.15(c) that the tumour has dramatically invaded throughout the right cerebral lobe and across the corpus callosum to the contralateral hemisphere. After 140 days, Figure 11.15(b) represents the portion of the tumour detectable on enhanced CT at the time of death. Here death is assumed to occur when the

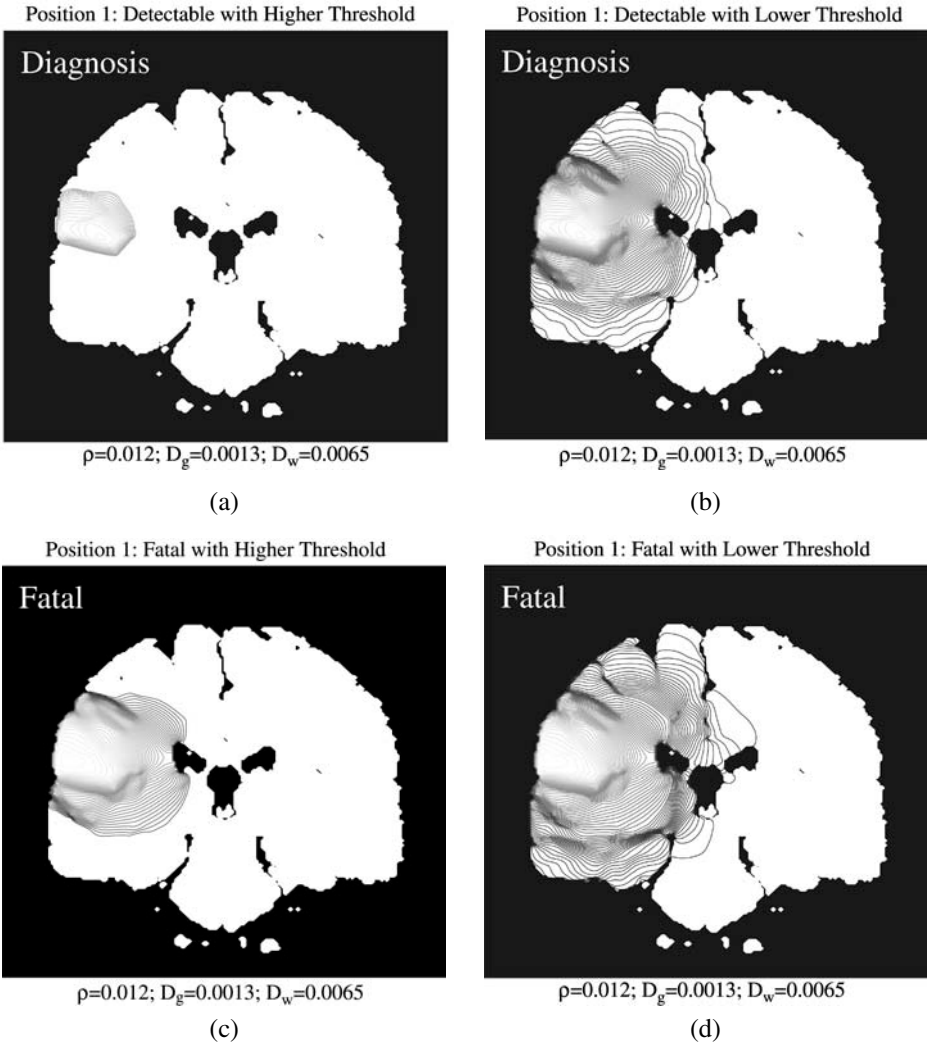

Figure 11.14. Simulation of tumour invasion of a High Grade Glioma in Position 1 in the inferior cerebral hemisphere: (**a**) and (**b**) at diagnosis; (**c**) and (**d**) at death; (**a**) and (**c**) as seen on the CT scan; (**b**) and (**d**) as calculated out to 5% of the threshold (boundary) cell concentration defined by CT. (From Swanson et al. 2000) (See the comment in parentheses in Figure 11.10.)

detectable tumour (again the portion of tumour with density above the threshold of detection) covers an area equivalent to a circle of diameter 6 cm. By increasing detection capabilities to correspond to a resolution of 500 tumour cells/cm^2, Figures 11.15(b) and (d) clearly show the augmented invasion not apparent with the present technology of enhanced CT. Note that Figures 11.15(b) and (d) do not represent the full extent of tumour invasion but rather an increase in detection ability associated with a theoretical imaging technique.

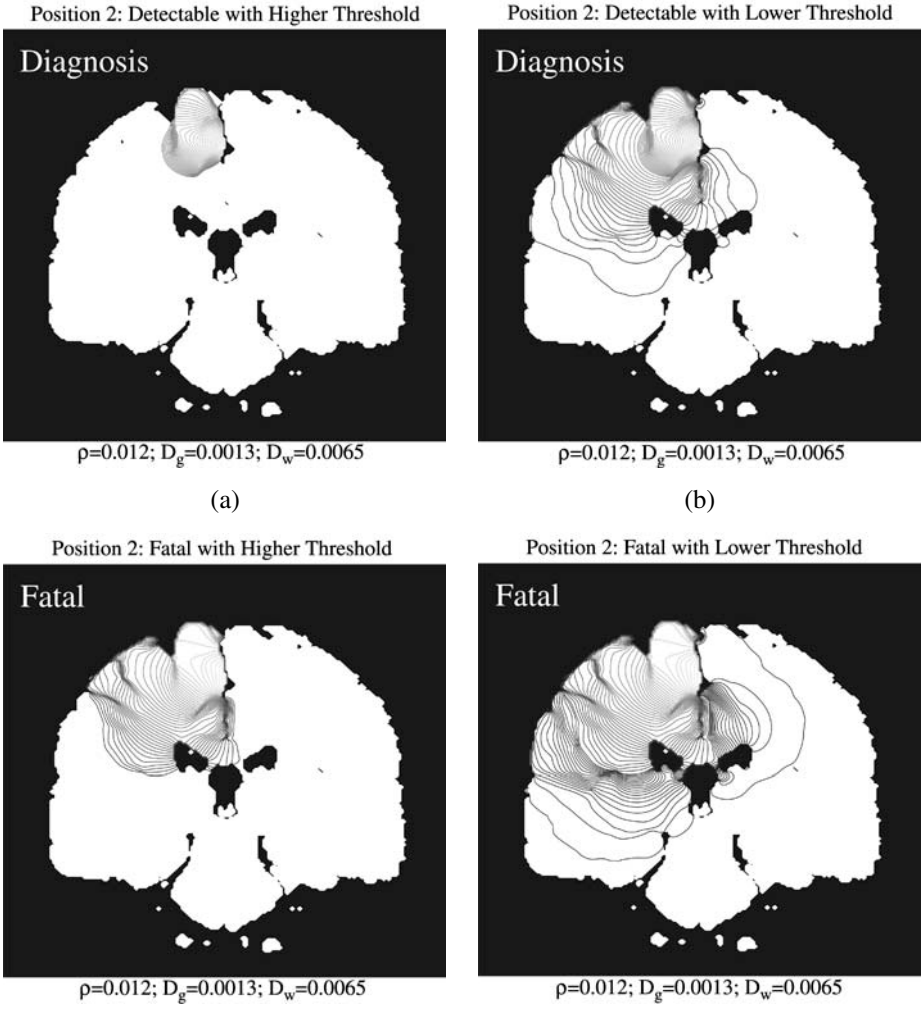

Figure 11.15. Simulation of tumour invasion of a High Grade Glioma in Position 2 in the superior cerebral hemisphere: (**a**) and (**b**) at diagnosis; (**c**) and (**d**) at death; (**a**) and (**c**) as seen on the CT scan; (**b**) and (**d**) as calculated out to 5% of the threshold (boundary) cell concentration defined by the CT scan. (From Swanson et al. 2000) (See the comment in parentheses in Figure 11.10.)

Swanson (1999) also compared the simulated tumour invasion in the case of a high grade tumour initially at Position 3 in Figure 11.13 with clinically observed invasion from microscopic postmortem analysis of the entire brain by Burger et al. (1988) and found shapes similar to the subthreshold-CT invasion depicted by the high grade tumour simulated invasion shown in Figures 11.16(b) and (d).

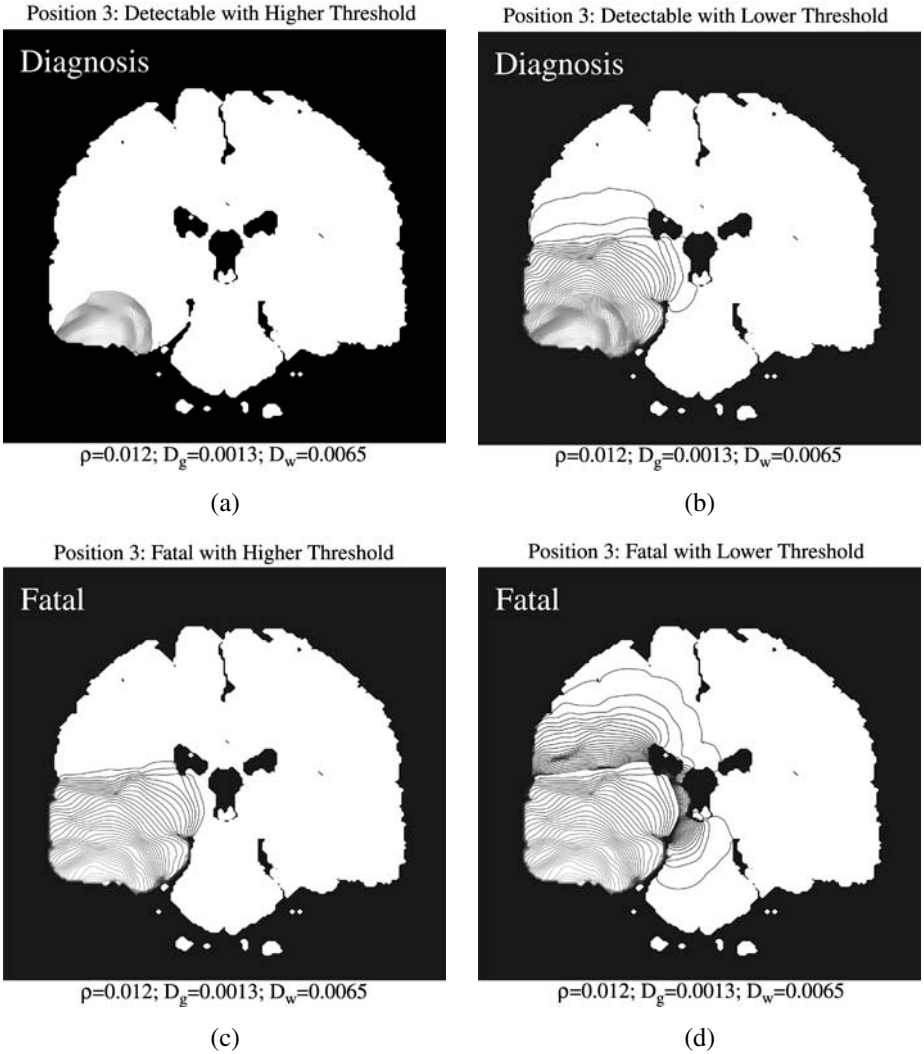

Figure 11.16. Simulation of tumour invasion of a High Grade Glioma in Position 3 in the temporal lobe: (**a**) and (**b**) at diagnosis; (**c**) and (**d**) at death; (**a**) and (**c**) as seen on the CT scan; (**b**) and (**d**) as calculated out to 5% of the threshold (boundary) cell concentration defined by the CT scan. (From Swanson et al. 2000) (See the comment in parentheses in Figure 11.10.)

Untreated Survival Time as a Function of Tumour Location

Table 11.6 quantifies the effect of tumour position on survival time for the 4 hypothetical tumour grades representing 10-fold variations in the growth rate, ρ, and diffusion coefficient, D_g and D_w, parameters.

In Table 11.6, the time to diagnosis is defined to be when the detectable tumour covers an area of $\pi(1.5)^2$ cm^2, that is, equivalent to a circular tumour of radius 1.5 cm. The time of death is assumed to be when the detectable tumour covers an area of $\pi(3)^2$ cm^2, which is equivalent to a circular tumour of radius 3.0 cm. The clinically definable sur-

Table 11.6. Survival periods for various grades of gliomas at different sites in the human brain given in Figure 11.13. The diffusion coefficient in white matter, D_w, is 5 times the diffusion coefficient in grey matter, D_g, for each tumour grade. (From Swanson 1999)

	Growth Rate ρ (1/day)	Diffusion Coefficient Grey Matter D_g (cm^2/day)	Survival Period t_S (day) Position		
Grade			1	2	3
High (HH)	1.2×10^{-2}	1.3×10^{-3}	109.7	137.5	172.7
Intermediate (HL)	1.2×10^{-2}	1.3×10^{-4}	398.2	494.9	581.9
Intermediate (LH)	1.2×10^{-3}	1.3×10^{-3}	55.5	259.3	347.2
Low (LL)	1.2×10^{-3}	1.3×10^{-4}	1097.2	1375.0	1726.9

vival time t_S is the time between death and diagnosis. Note that the diffusion coefficient in white matter is simply five times that in grey matter for each tumour grade listed in Table 11.6. Note also that tumours located in the temporal lobe are associated with increased untreated life expectancy following diagnosis.

On the assumption of a uniform diffusion coefficient in homogeneous brain tissue we obtained an approximate survival in Section 11.2; namely,

$$\text{survival time} \approx \frac{1}{\sqrt{D\rho}} \left(\bar{r}_{\text{lethal}} - \bar{r}_{\text{detect}}\right). \tag{11.39}$$

We can make a rough comparison between the results in Table 11.6 if we take $\bar{r}_{\text{lethal}} - \bar{r}_{\text{detect}} = 1.5$ cm and, in the case of a high grade tumour, $\rho = 1.2 \times 10^{-2}$/day and a diffusion coefficient $1.3 \times 10^{-3} \leq D \leq 6.5 \times 10^{-3}$ cm^2/day, that is, a motility between the grey and white matter. We get an estimate of between 170 days and 380 days. For a low grade tumour with $\rho = 1.2 \times 10^{-3}$/day and $1.3 \times 10^{-4} \leq D \leq 6.5 \times 10^{-4}$ cm^2/day we get between 1698 days and 3798 days. The lower of these survival times is reasonably close to the values given in Table 11.6 for a high and low grade tumour in Position 3. In general this very rough estimate is not too unrealistic if we use the lower of the two (grey and white matter) diffusion coefficients. Burgess et al. (1997) solved the full spherically symmetric three-dimensional model and obtained, for the high grade tumour with $\rho = 1.2 \times 10^{-2}$/day and $D = 1.3 \times 10^{-3}$ cm^2/day, a survival duration of 179 days and for a low grade tumour with $\rho = 1.2 \times 10^{-3}$/day and $D = 1.3 \times 10^{-4}$ cm^2/day of 1796 days. When we compare the approximation with the homogeneous situation the comparison is very good. Position 3 has the best prognosis as to survival duration so, for tumours in other positions the approximate survival duration is very much an overestimate. In the case of a tumour located at Position 1 in the high grade case it overestimates survival duration by approximately 50% and for a low grade tumour by approximately 85%.

From Figure 11.13, we see that the geometry of the temporal lobe white matter tends to lead tumour cells into the deep cerebral nuclei (grey matter), thereby con-

straining the invasion of the tumour from Position 3 and providing the best prognosis; see Table 11.6. Similarly comparing Figures 11.13 and 11.15, we see that the tumour in Position 2 is constricted superiorly and medially and has direct access to the white matter corona radiata corpus callosum. The tumour in Position 1 has the worst prognosis because it is adjacent to corona radiata white matter and has little interaction with anatomic boundaries, being restricted only laterally.

The results in Table 11.6, as might be expected, indicate that high grade gliomas generally have the worst prognosis while low grade tumours have the best with intermediate grade tumours having intermediate survival times. However. the highly proliferative intermediate grade glioma has a better prognosis than the highly diffuse intermediate grade tumours and that the highly diffuse intermediate grade tumour in Position 1 has a prognosis even worse than that of the high grade gliomas. This suggests that the diffusion abilities of a tumour are a stronger indicator of prognosis than the growth rate. None of the prognoses are encouraging.

We now extrapolate theoretical survival curves based on tumour grade and location. For each tumour grade, we vary growth, ρ, and motility, D, by $\pm 50\%$ from their values in Table 11.6. This defines 9 hypothetical patients for each of the 4 growth and diffusion coefficient combinations. Survival times for tumours at various locations are given in Figure 11.17. Each of the 3 curves for a given tumour grade defines the survival times of the 9 hypothetical patients with untreated gliomas. Figure 11.17(a) represents high grade tumours (HH) defined by a high growth rate ρ and a high diffusion coefficient D. The opposite extreme (LL) is shown in Figure 11.17(d). The intermediate grade populations with high–low (HL) and low–high (LH) combinations of ρ and D are presented in Figures 11.17(b) and (c). Note that temporal lobe tumours (Position 3) consistently have the best prognoses. Although the curves look very similar, the timescales are very different in each plot. Clinical data are, to our knowledge, not available for comparison due to the fact that our simulated tumours are untreated. (We discuss the model amendments to consider various treatments below.) However, as noted above, even following surgical resection we can find now clinical results relating to different sites of gliomas.

The proportion of tumour detectable on enhanced CT decreases with increasing diffusion coefficient and decreasing growth rate, as might be expected. For a fixed growth rate, as diffusion increases, tumour cells migrate larger distances and, so, diffusion tends to smooth out the spatial distribution of glioma cells. For a fixed diffusion coefficient, as the growth rate decreases, tumour cells have less chance to build up to detectable levels. Interestingly, if the ratio of the growth rate to the diffusion coefficient is fixed while ρ and D change, the proportion of tumour detectable is fixed. This type of relationship can be very important in the study of individual patient cases where independent estimates for the diffusion and growth rate parameters are unrealistic.

We use a threshold of detection corresponding to a tumour cell density of 40,000 cells/cm^2. Above this threshold, the tumour is observable on enhanced CT while below it, it is not. Because of the diffuse nature of gliomas, we can only 'detect' a small portion of the actual tumour with currently available imaging techniques. This fact has been substantiated by Chicoine and Silbergeld (1995) and Silbergeld and Chicoine (1997) with their cultured tumour cells from histologically normal brain far from the bulk tumour location.

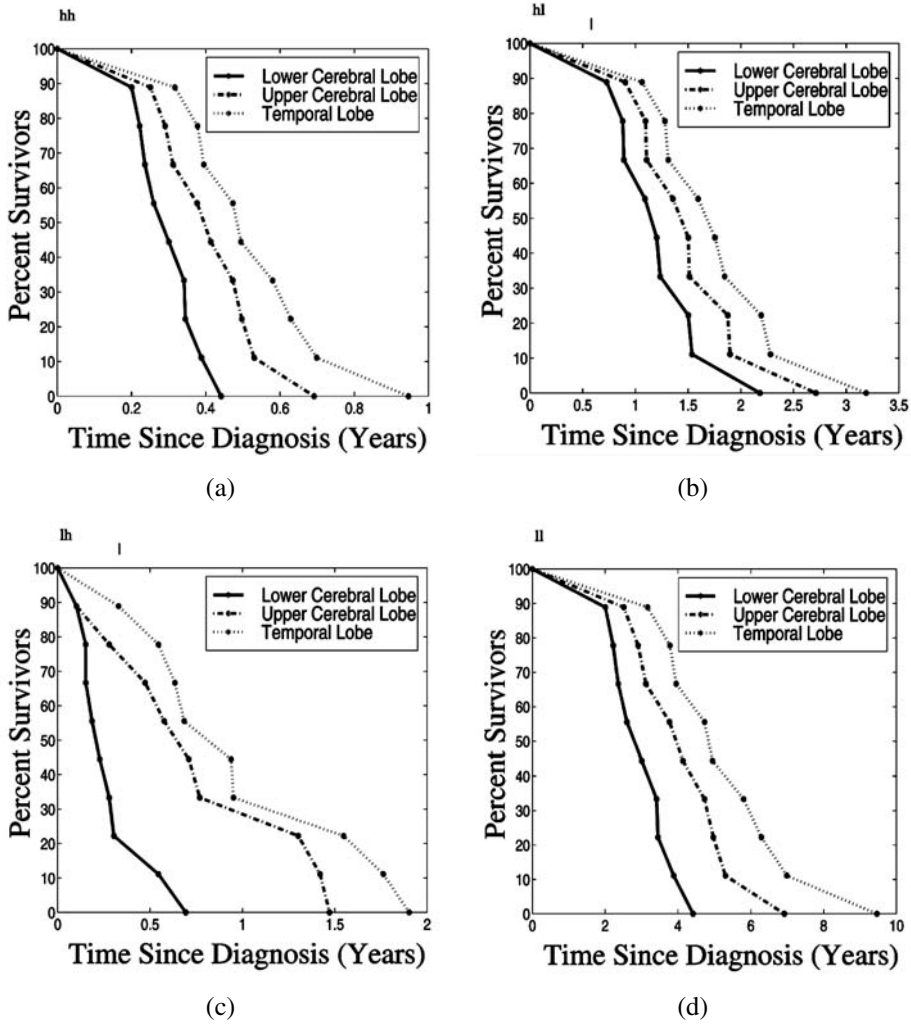

Figure 11.17. Theoretical survival curves for untreated gliomas of all grades: (**a**) represents high grade tumours with high growth (ρ) and high diffusion (D_g, D_w); (**b**) represents intermediate grade tumours with high growth (ρ) and low diffusion (D_g, D_w); (**c**) represents intermediate grade tumours with low growth (ρ) and high diffusion (D_g, D_w); (**d**) represents low grade tumours with low growth (ρ) and low diffusion (D_g, D_w).

An advantage of mathematical modelling is the ability to alter theoretically any parameter and analyze its effect thereby simulating hypothetical experiments. By mathematically decreasing the threshold of detection in our model, we can visualize the usefulness of increasing detection capabilities in medical imaging. Figure 11.18 illustrates the effect of decreasing the threshold of detection on the proportion of the tumour we actually detect. Augmented detection abilities invariably increase the amount of tumour identifiable but the rate of increase varies among tumour positions and grade. Notice that detection of high and low grade tumours coincides. This suggests that the ratio be-

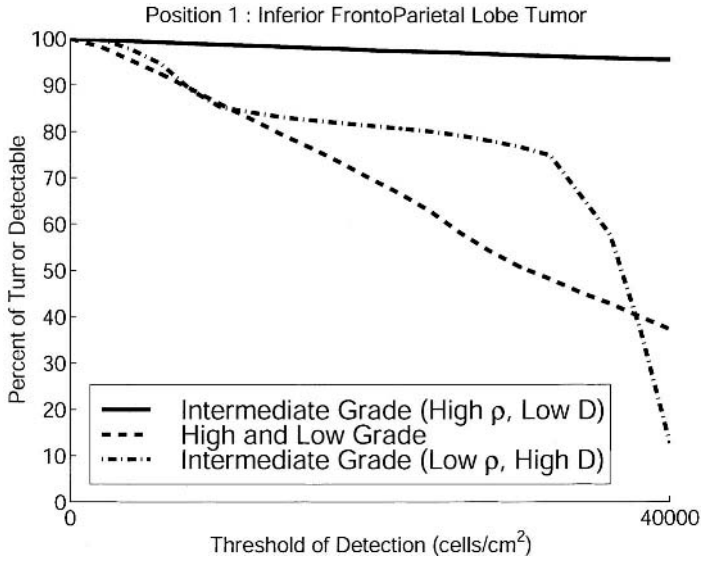

(a)

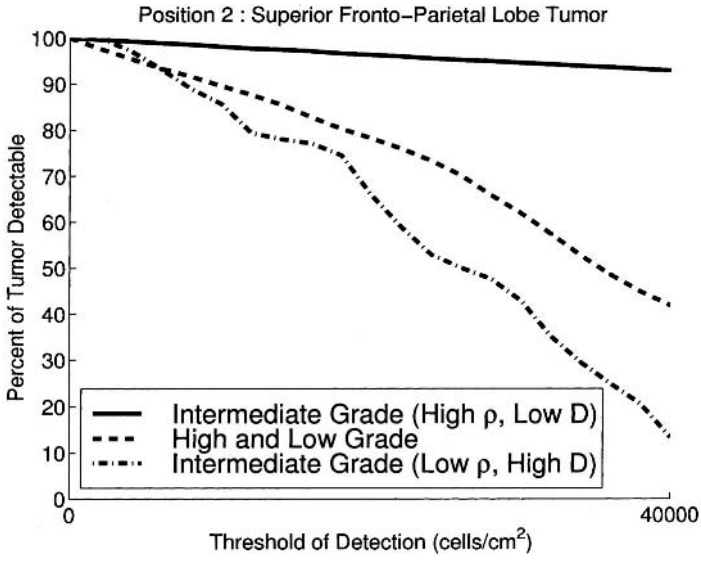

(b)

Figure 11.18. Percent of detectable tumour volume as a function of the detection threshold at various positions. The 40,000 cells/cm^2 represents the threshold of detection for a CT scan. (From Swanson et al. 2000)

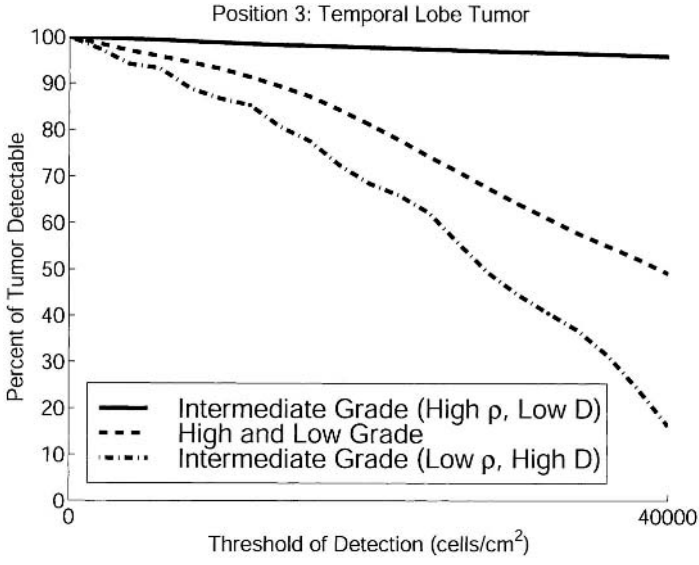

(c)

Figure 11.18. (continued)

tween the growth rate ρ and the diffusion coefficient D is critical to the determination of the proportion of tumour detectable. Again, it suggests that the invasive nature of the tumour is defined by the *ratio* D/ρ. So, another potential practical application of this model for patients is simplified since separate estimates for D and ρ are not necessary. The problem here, of course, is how to obtain an estimate for D/ρ.

Note in Figure 11.18 that the slowly growing and quickly diffusing intermediate grade tumours are associated with the least proportion of tumour that is detectable at diagnosis. This is clearly due to the extensive invasive abilities of those tumours. High and low grade tumours are associated with the same proportion of tumour detectable as a function of the threshold of detection. The difference between the high and low grade tumours is the timescale on which the growth and invasion occurs. It takes high grade tumours a very short time to invade. Low grade tumours may follow the invasion path of high grade tumours but much more slowly.

All of the results presented in this section can be obtained for any other sagittal, coronal or horizontal slice of the brain.

The key question we must now ask is how a three-dimensional simulation of the model might affect these results. The numerical simulation is clearly much more complex. Burgess et al. (1997) investigated the three-dimensional constant diffusion spherically symmetric situation and studied the interaction of growth rates and diffusion coefficients on the spatial spread both with and without resection. They were particularly interested in quantifying the effect of the size of the resected volume on the increased life expectancy. With the more accurate model here, three-dimensional simulations have also been carried out. Figure 11.19 is an example of such a simulation

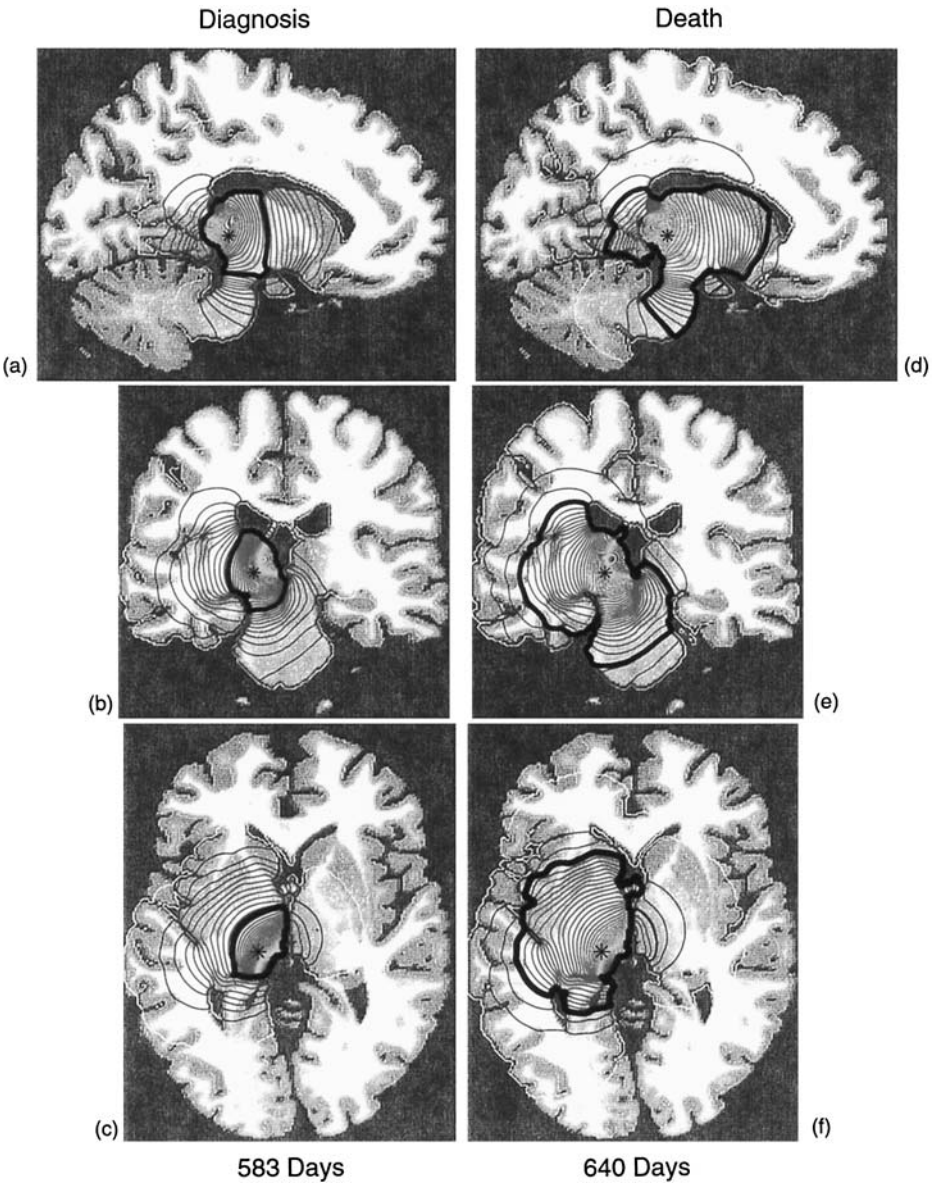

Figure 11.19. The spatial spread of the cancer cells at time of death for a virtual tumour introduced at Position 3 (Figure 11.13), denoted by the asterisk, for three cross-sections through the three dimensional tumour, namely sagittal, coronal and horizontal which intersect at the tumour site. (**a**)–(**c**) are at diagnosis while (**d**)–(**f**) are at death. The dark line defines the edge of the tumour detected by a CT scan in which the threshold is 40,000 cells/cm^2. (From Swanson et al. 2000)

for an untreated tumour initiated at Position 3 (see Figure 11.13) and shows the cell distribution at time of death.

Recap of the Model Assumptions and Limitations

Before discussing various treatment scenarios we should perhaps recall the various assumptions in the modelling. The model assumes that glioma tumour cells grow with a constant exponential rate, ρ. We have not included any necrotic core formation (which can be incorporated by using a logistic growth dynamics for the cells): it is evident in some gliomas, but only the highly proliferative, slowly diffusive tumours are significantly affected by necrosis. In fact, our experimental data were taken from a tumour without necrosis (anaplastic astrocytoma). Tracqui et al. (1995), Woodward et al. (1996) and Burgess et al. (1997) have shown that results from our model with logistic growth for the cells differ little from the model with exponential growth. Tracqui et al. (1995) showed that logistic growth decreased the amount of time before identification of the tumour and decreased the life expectancy as the necrotic cell density decreased.

Diffusion begins after about 23 generations when the tumour contains approximately 4×10^3 cells; at this point we consider the model equation (11.6) to start governing the tumour growth and invasion. Without this limitation no local tumour mass appears to form, corresponding to certain cases of gliomatosis cerebri.

We have taken the diffusion coefficient as approximately 5 times larger in white matter than in grey matter (by way of example). There is probably some anisotropy to the diffusion along individual white matter fibres but the network of fibres is very complicated on the whole brain scale. There are several pathways which help facilitate lateral diffusion such as the corpus callosum and, to a limited degree, fronto-parietally. A change in the overall diffusion coefficient could perhaps be sufficient to simulate the increased motility of gliomas in white matter. There is some justification for this possibility in view of the good comparison the results of Burgess et al. (1997) had with patient data.

The tumour is detectable above a critical density of 40,000 cells/cm^2 corresponding to the detectable threshold on enhanced CT. This value was determined by the analysis of patient data from histological sections obtained at autopsy and terminal CT scans (Tracqui et al. 1995). The tumour is diagnosed, on average, when the detectable area covers $\pi(1.5)^2$ cm^2 (the area equivalent to a 1.5-cm radius circular tumour). The tumour is fatal when it is detected at twice the diameter at diagnosis (that is, covering an area of 9π cm^2). These choices were based on average size of gliomas in a large number of scanned or autopsied patients, but the range is very wide.

Although brain boundaries and tissue heterogeneity are taken into account, we do not define any destruction to the normal tissue by the tumour cell invasion. It is presently a point of contention experimentally whether the tumour cells have the ability to break down the normal brain parenchyma distant from the tumour site and affect the time to death.

Our simulations can be done in both two and three dimensions. Three dimensions are, of course, better and are much easier to visualize with respect to two-dimensional CT or MRI scans. Practically, we expect to fit the model to data obtained from two-dimensional CT scans (schematically shown in Figure 11.5) for patients. The use of two-dimensional computations is certainly not inappropriate.

In spite of the many assumptions involved the model has allowed us to obtain many clinically potentially useful results. In particular, we have identified that temporal lobe tumours may have a better prognosis than fronto-parietal lobe tumours. Although the difference in survival times between temporal and fronto-parietal lobe tumours may be statistically insignificant in clinical studies, it may account for at least some of the clinical variability. It has also let us include a significant measure of heterogeneity in brain tissue to account for asymmetric tumour geometries. We have also been able to simulate clinically observed tumour geometries and suggest survival times of patients. This, of course, requires further clinical analysis to see whether or not they are consistent with clinical data. With the availability of a detailed description of the local composition of grey and white matter throughout the brain, the model has still a lot of unexplored potential some of which we discuss in the following sections.

11.6 Modelling Treatment Scenarios: General Comments

As we have already commented, the prognosis for a patient with a glioma is not encouraging and depends on many factors, among them the type of neoplasm and the grade of malignancy. The relatively simple mathematical model we propose takes into account the growth and diffusion rates of the glioma and tissue heterogeneity. As we have seen, the results in the previous sections are reasonably consistent with clinical data (Cruywagen et al. 1995, Tracqui et al. 1995, Cook et al. 1995, Woodward et al. 1996, Burgess et al. 1997, Swanson et al. 2000), so we believe that the model could be used to make predictions regarding the survival time of the patient following various types of treatment including surgical resection, radiation and chemotherapy.

A major problem with present treatment strategies is the local focus of therapy when the action of the tumour growth and invasion is elsewhere (see, for example, Gaspar et al. 1992 and Liang and Weil 1998). The failure of glioma treatment regimes represents a large portion of glioma clinical and experimental literature (for example, Yount et al. 1998 and other references there). Local therapies are desirable, of course, to reduce the bulk tumour which is mostly responsible for pressure-induced symptoms. However, they can not control the motile invading cells responsible for recurrence (Silbergeld and Chicoine 1997).

The most appropriate treatment for a given glioma tumour is often not at all clear, irrespective of whether or not the subsequent quality of remaining life is taken into account. Because of their invasive characteristics, malignant gliomas can rarely be cured by surgical or radiological resection alone. There is much new research on quite different treatments, such as tumour-attacking viruses. Varying degrees of resection have been shown to increase survival time only marginally for glioblastoma multiforme although the increase is generally more significant for the lower grade (anaplastic) astrocytomas. With the general failure of surgical resection alone, to increase the survival time of patients, multi-modality treatments have been developed combining resection, radiation and chemotherapies and other therapies. Giese and Westphal (1996) in their review article discuss the perspectives for antiinvasive therapy. Numerous clinical studies have attempted to demonstrate the effectiveness of various treatments and combinations (see, for example, Ramina et al. 1999 and numerous other references there). Counterintu-

itively, some combinations of therapies have been shown, for various reasons, to be less effective than each of the therapies separately. Fairly recently, it was found that ionizing radiation can inhibit chemotherapy-induced cell death (apoptosis) in certain glioblastoma cells (Yount et al. 1998). (There have also been suggestions that antioxidants may in fact be exploited by the cancer cells to help prevent their destruction.) This type of multimodality treatment failure can be attributed to the induced mutation of cells exposed to harsh chemicals or radiation. Cancer cells are, by definition, mutated 'normal' cells, so with the accumulation of mutations, the cancerous cells progressively become more malignant and treatment-resistant. We discuss polyclonal models later when we discuss a modification of the basic model to consider chemotherapy treatment.

Clearly, there is a threshold of treatment sustainable by a given patient and determining the optimal minimal strategies is of major importance. Not only that, even with similar tumour sizes, histologic malignancy and anatomic location, certain treatments work better on some patients than on others. There is no one universal treatment, but in deciding the best course of treatment for patients it is necessary to take into account all of the available information regarding the cancer before proceeding. We believe that realistic modelling can help to address this complicated issue by quantifying certain virtual glioma behaviours with and without treatment.

As we shall see, with relatively slight alterations, our model can take into account the effects of chemotherapy, radiation and resection on the spatiotemporal behaviour of the tumour. This capability lets us compare projected growths and invasion of the tumour under various treatment scenarios, thereby giving some insight into the optimal therapeutic course. Given a sense of the location, size, shape, diffusion coefficient and growth rate of a specific tumour, our model can help to suggest the best type of therapy to maximize survival time, that is, the difference between the time of diagnosis and death.

11.7 Modelling Tumour Resection in Homogeneous Tissue

Earlier uses of our model by Cook (Dr. J. Cook, personal communication 1994), Woodward et al. (1996) and Burgess et al. (1997) considered the effect of resection on patient survival time for the spatially homogeneous model (11.3) in two spatial dimensions. Their analyses suggest that surgery adds little more than two extra months of life. The recurrence (on a CT scan) of the tumour is due to the low density infiltrated tumour cells far afield from the gross tumour site.

Mathematically, surgical resection is simulated by the removal of all tumour cells within a defined location. Death was assumed to occur either when the visible tumour reached a defined radius or when the total cancer cell count reached a critical value. Given an initial tumour size, grade and location these models can then simulate the effects of various resection sizes and geometries on survival time. Woodward et al. (1996) took as initial conditions (11.12) and then, when the tumour had a visibly (CT) detectable area equivalent to a circle of radius 1.5 cm a region was resected. Woodward et al. (1996) estimated the diffusion coefficient differently to the methods discussed above; the method is described in detail in Cruywagen et al. (1995) and Tracqui et al. (1995). They took patient CT scans from three levels through the tumour (idealized in

Figure 11.5) to calculate the tumour area at each level. With the proliferation parameter, ρ, given they then numerically solved the model equation and determined the diffusion coefficient which gave the best fit when the cell density was at the observed threshold on the scans at each level. This gave three estimates for the diffusion coefficient, one at each level and they took the average: interestingly (and fairly crucial in fact) the variation in values for D did not vary markedly for each scan level. We discuss the procedure in more detail in Section 11.10.

With the estimated values for the model parameters, Woodward et al. (1996) then carried out hypothetical resections of different diameters on the tumour when it had reached the CT detectable size of 3 cm in diameter. With this resected state as the initial condition they numerically solved the model equation until the recurring tumour had the equivalent size to the lethal size, that is, of a circle of diameter 6 cm. The shape of the tumour of course was no longer a disk but rather an annulus with low cell density inside and far afield outside. The simulations were carried out with anatomical constraints including the ventricles (as was also done by Tracqui et al. 1995 and Cruywagen et al. 1995 in their modelling of chemotherapy treatment); these constraints had a major effect on the results as we found and illustrated in the previous sections. The accumulation of cells within a restricted area effectively slows down the spatial spread of the tumour. Cook (Dr. J. Cook, personal communication 1994) developed an analytical procedure to study this problem and obtained limits on the parameter values when the prediagnostic distribution of cells was defined by the same growth characteristics as occur later. We discuss his results in the next section.

Woodward et al. (1996) considered three excision diameters, denoted by S, namely, $S = 3$, 4, and 5 cm. In each case the cell density outside the resected area is, of course, less than the detectable level. Medically $S = 3$ cm simulates the 'gross total resection' of the tumour when diagnosed and treated. So, the larger resections are much more extensive. Death, assumed to occur when the visually detectable area is equivalent to a circle of radius 3 cm, represents a volume of about 113 cm^3.

Figure 11.20(a) shows cumulative survival curves by assuming a uniform population by nine idealized patients with all possible combinations of three values of ρ and three values of D. Each population is subjected to four extents of surgery: $S = 0$ represents 'biopsy only' (no resection), $S = 3$ represents 'gross total resection' while $S = 4$ and $S = 5$ represent increasing resections of the margin of the tumour; we cannot consider $S = 6$ since that is considered fatal. Figure 11.20(b) compares the computed survival curves with those of 115 actual patients reported by Kreth et al. (1993), two groups of patients with glioblastoma, one subjected to biopsy plus radiation (58 patients) and the other subjected to surgical resection plus radiation (57 patients). All of them died within 100 weeks. The median survival times for the biopsy group was 32 weeks and for the resection group, 39.5 weeks. The median increase in survival time of 7.7 weeks between $S = 0$ cm and $S = 4$ cm resection compares well with the median value of 7.5 weeks found by Kreth et al. (1993). In our simulations, however, we required a 1-cm more extensive resection which could be accounted for in our estimate of the threshold number of cells or, of course, how extensive the resections of Kreth et al. (1993) really were. It is surprising that even with such a relatively simple model, simulated with homogeneous tissue but including brain boundaries, the results are so well correlated with patient data.

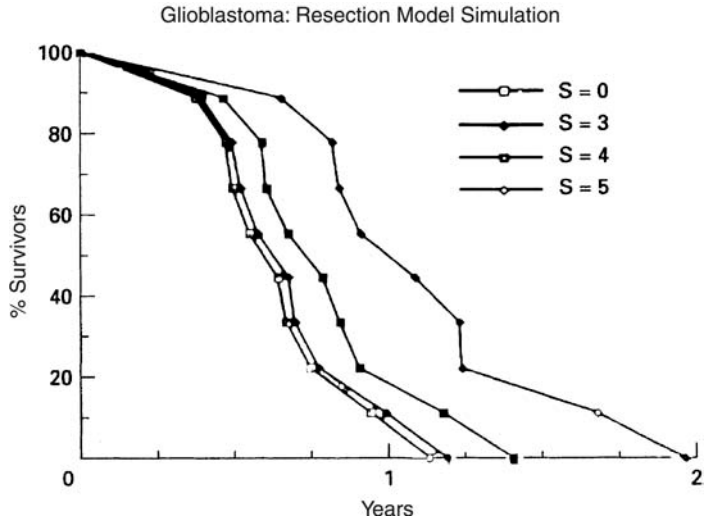

(a)

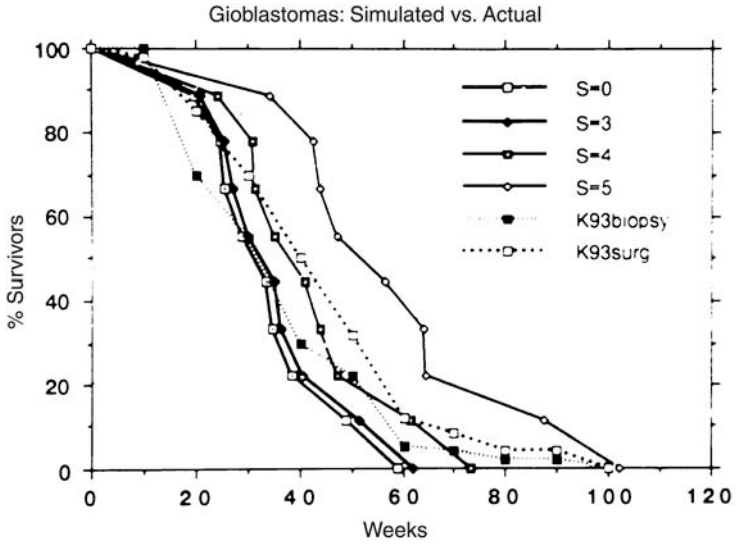

(b)

Figure 11.20. (**a**) Simulated cumulative survival times of 9 patients with high rates of growth and high diffusion. The 4 curves represent resected areas of $S = 0, 3, 4, 5$-cm diameter of the tumour and surrounding infiltrated tissue. Each curve is composed of 9 patients with all possible combinations of growth rate $\rho = 0.8 \times 10^{-2}, 1.2 \times 10^{-2}$ or 2.4×10^{-2}/day and $D = 4.32 \times 10^{-4}, 1.0 \times 10^{-4}$ or 1.3×10^{-3} cm^2/day. The median survival times are 33.4 weeks without resection ($S = 0$) and 35.0, 41.1 and 52.6 weeks with resection. (**b**) Superimposed actual survival curves from Kreth et al. (1993) following biopsy only (K93biopsy) or extensive surgical resection (K93surg), both groups of patients also receiving postoperative X-irradiation. (From Woodward et al. 1996)

Woodward et al. (1996) went on to explore the effect of varying ρ and D tenfold from the low and high values they used in Figure 11.20 to mimic the four tumour grades discussed above, starting with high ρ and high D (HH) down to the low grade tumour (LL). Populations of nine hypothetical patients for each of the four combinations were formed by allowing 50% variation in each of these values and survival times calculated. Figure 11.21 shows the results. Figure 11.21(a), the highest grade tumour, is the same as Figure 11.20(a), included for comparison, while Figure 11.21(d) gives the results for the lowest grade.

Although the curves in Figure 11.21 look quite similar the timescales are very different. The curves have progressively decreasing slopes from the high ρ – high D grade tumour to the low ρ – low D one. When all curves are put on the same timescale they can then be compared directly with the actual patient results summarised by Alvord

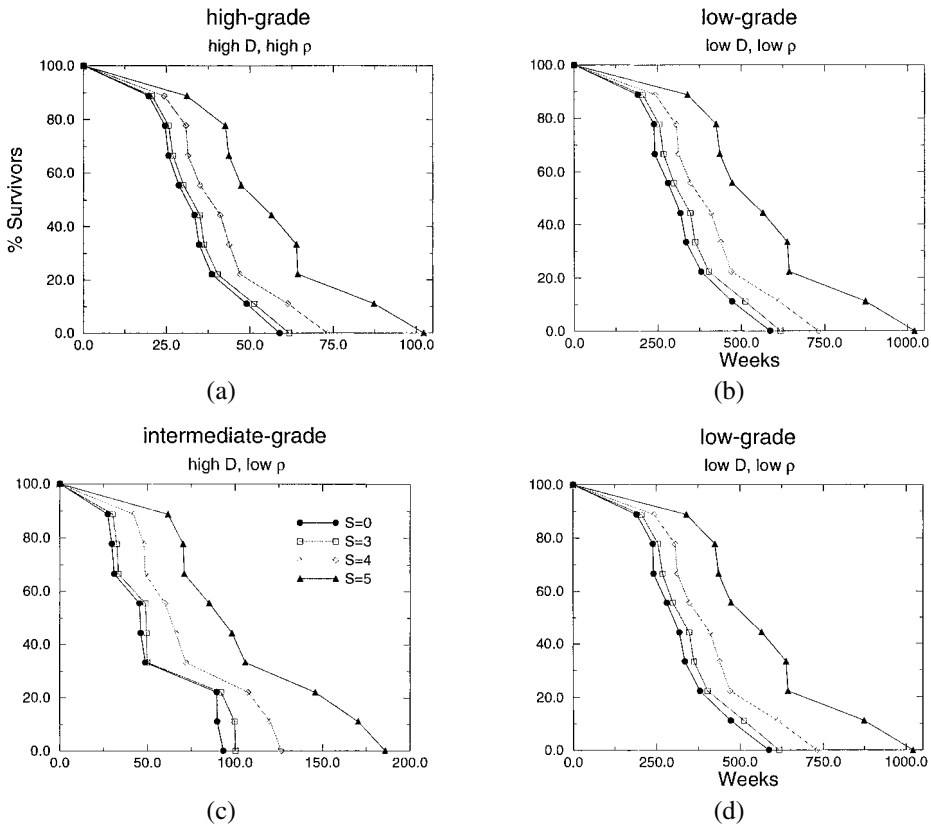

Figure 11.21. Survival times following various resection extents for a population of 9 hypothetical patients formed by allowing 50% variation in the growth and diffusion rates. Each family of four curves includes the various extents of resection $S = 0, 3, 4, 5$-cm diameter of the tumour and surrounding infiltrated tissue. (**a**) High grade, that is, a high–high combination (HH) of ρ and D, (**b**) intermediate grade, high–low (HL), (**c**) intermediate grade, low–high (LH) and (**d**) low grade tumour, low–low (LL), with a low ρ and low D. (From Woodward et al. 1996)

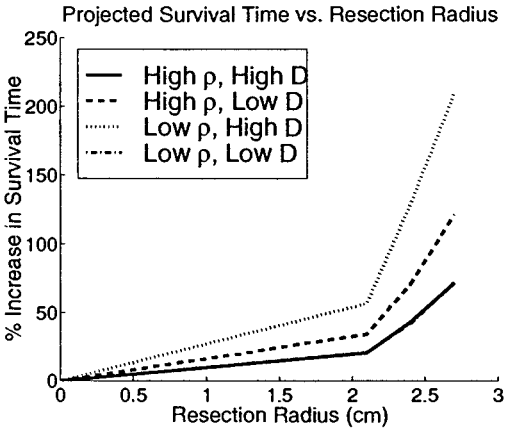

Figure 11.22. Spatially homogeneous model projected increase in survival time following various extents of resection. (From Woodward et al. 1995)

(1992). His results show a very wide range of glioma behaviour which is also found, not surprisingly, by the model results here. We should add that there is no general agreement as to how to grade gliomas medically. Perhaps another possible use of a theory is to provide a basis for such a classification.

Assuming a radius of 3 cm of detectable tumour size as fatal, Figure 11.22 shows the effects of various resection radii on subsequent survival time. The figure suggests that only slowly diffusing gliomas are significantly affected by resection as we would expect from the above. Again, we find that diffusion is fundamental to glioma treatment difficulties and recurrence.

One of the major conclusions that come out of the above detailed analysis and comparison with patient data is that there is no clear evidence that resection surgery increases survival, at least in patients with intermediate and high grade astrocytomas. This was also the conclusion of Nazzaro and Neuwalt (1990) who reviewed 33 major reports over the previous 50 years. Kreth et al. (1993) noted a statistically insignificant increase of 7.5 weeks. Kreth et al. (1993) said they found it equally difficult to define the benefit of resection even in low grade tumours.

Although we have varied the growth rate of the tumour cells we have assumed that for a given tumour it is constant. As commented by Woodward et al. (1996) it is generally believed that the tumour margin contains the less malignant-looking cells, but they are still cancerous and grow no matter how much of the tissue outside the (CT) visible tumour is excised.

11.8 Analytical Solution for Tumour Recurrence After Resection

Cook (Dr. J. Cook, personal communication 1994) considered the effect of resection in a homogeneous tissue analytically. As we noted above, mathematically, surgical resection is simulated by the removal of all tumour cells within a defined location centred on the tumour. It is his analysis that we present here. As explained, the cancer is assumed to be fatal either when the visible size reaches an equivalently defined circle of radius 3 cm

or when the total cancer cell count reaches a critical value. We expect the bulk effect of resection is reasonably quantified by the homogeneous case but subtleties associated with tumour location and local tissue heterogeneity could adjust these results; below we discuss this situation.

The dimensionless model is that derived in Section 11.2 and defined by (11.10) and (11.11) with boundary conditions (11.8). The nondimensionalisation is given by (11.9). Without spatial heterogeneity in the diffusion coefficient, that is, $D(\mathbf{x}) \equiv 1$, the model equation is

$$\frac{\partial c}{\partial t} = \nabla^2 c + c. \tag{11.40}$$

Before and after resection the tumour cell population satisfies this equation but with different initial conditions.

For simplicity, and in view of the surprisingly good results (when compared with patient data) from the two-dimensional studies above, we consider the post-resection problem in two spatial dimensions in polar coordinates. We consider the tumour was initiated by a point source of N cells at the origin and so the pre-resection problem satisfies (11.38) for $0 < t < t_r$, where t_r denotes the time of the resection, with initial conditions $c_{\text{preresect}}(r, \theta, 0) = N\delta(r)$. On the infinite domain the solution is given by (11.13), which, in dimensionless form at time t_r, is

$$c_{\text{preresect}}(r, \theta, t_r) = \frac{N}{4\pi t_r} \exp\left(t_r - \frac{r^2}{4t_r}\right). \tag{11.41}$$

At resection, a central core of radius R_r is removed, so the post-resection problem satisfies (11.38) for $t > t_r$ with initial conditions ($t = t_r$),

$$\begin{aligned} c_{\text{postresect}}(r, \theta, t_r) &= F(r, \theta) \\ &= N H(r - R_r) c_{\text{preresect}}(r, \theta, t_r) \\ &= H(r - R_r) \frac{N}{4\pi t_r} \exp\left(t_r - \frac{r^2}{4t_r}\right), \end{aligned} \tag{11.42}$$

where H is the Heaviside function.

By superposition, the solution of the post-resection problem with these initial conditions can be represented as the integral

$$c_{\text{postresect}}(r, \theta, t) = \int_0^{2\pi} \int_0^{\infty} K(r, \theta, t; \xi, \alpha, t_r) F(\xi, \alpha) \xi \, d\xi \, d\alpha \quad \text{for} \quad t > t_r,$$

where K is the fundamental solution of (11.38) for a point source at $(r, \theta) = (\xi, \alpha)$ introduced at $t = t_r$,

$$K(r,\theta,t;\xi,\alpha,t_r)=\frac{1}{4\pi(t-t_r)}\exp\left(t-t_r-\frac{r^2+\xi^2-2r\xi\cos(\theta-\alpha)}{4(t-t_r)}\right).$$

Now

$$c_{\text{postresect}}(r,\theta,t)=N\frac{\exp\left(t-\frac{r^2}{4(t-t_r)}\right)}{(4\pi)^2t_r(t-t_r)}\int_{R_r}^{\infty}\xi\exp\left(-\frac{\xi^2}{4t_r}-\frac{\xi^2}{4(t-t_r)}\right)\left[\int_0^{2\pi}\exp\left(\frac{2r\xi}{4(t-t_r)}\cos(\theta-\alpha)\right)d\alpha\right]d\xi.$$

Consider the second integral, in square brackets, which we denote by $\mathcal{I}$ and introduce the change of variables $\nu=\theta-\alpha$, and so

$$\mathcal{I}=\int_0^{2\pi}e^{A\cos(\theta-\alpha)}\,d\alpha=\int_{\theta-2\pi}^{\theta}e^{A\cos\nu}\,d\nu, \tag{11.43}$$

where $A=2r\xi/(4(t-t_r))$. Since we are interested in eventually integrating $\mathcal{I}$ from $\xi=R_r$ to ∞ and A is proportional to ξ, A large is the limit we are interested in. Additionally, from numerical simulations, we find that the nondimensional time $t=\rho\bar{t}$ is at most O(1) for the range of growth rates ρ we consider. These two observations support exploiting the limit for A large. For A large, we can use Laplace's method (see, for example, Murray 1984) to approximate $\mathcal{I}$; this method exploits the fact that the integral is dominated by the contribution over a region near the maximum of the exponent: the maximum of $\cos\nu=1$ so $\nu=0$ or 2π. Rescaling near $\nu=0$ we have, for large A,

$$\mathcal{I}=2\int_0^{\epsilon}e^{A(1-(\nu^2/2)\ldots)}\,d\nu\sim e^A\int_{-\infty}^{\infty}e^{-A(\nu^2/2)}\,d\nu\sim e^A\sqrt{\frac{2\pi}{A}}.$$

With this

$$c_{\text{postresect}}(r,\theta,t)\sim N\frac{\sqrt{2\pi}\,e^{\left(t-\frac{r^2}{4(t-t_r)}\right)}}{16\pi^2t_r(t-t_r)}\int_{R_r}^{\infty}\frac{e^{-\frac{\xi^2}{4t_r}-\frac{\xi^2}{4(t-t_r)}+\frac{r\xi}{2(t-t_r)}}}{\sqrt{\frac{r\xi}{2(t-t_r)}}}\xi\,d\xi$$

$$=N\frac{e^t}{8t_r\sqrt{r\pi^3(t-t_r)}}\int_{R_r}^{\infty}\sqrt{\xi}\exp\left(-\frac{\xi^2}{4t_r}-\frac{(r-\xi)^2}{4(t-t_r)}\right)d\xi$$

as $A\to\infty$. Let

$$\mathcal{J}=\int_{R_r}^{\infty}\sqrt{\xi}\exp\left(-\frac{\xi^2}{4t_r}-\frac{(r-\xi)^2}{4(t-t_r)}\right)d\xi=\int_{R_r}^{\infty}g(\xi)e^{-xh(\xi)}\,d\xi,$$

where $g(\xi) = \sqrt{\xi}$, $h(\xi) = (\xi^2/r) + (rt_r/t) - 2(\xi t_r/t)$ and $x = rt/(4t_r(t-t_r))$ which we can approximate for x large again using Laplace's method. This is equivalent to assuming $t \approx t_r$ and $r \sim O(1)$ or $t \gg t_r$ and $r \gg 4t_r$. The asymptotic contribution comes from around the minimum of $h(\xi)$ which is at $\xi = rt_r/t$. There are two possibilities.

(i) The minimum lies in the range of integration: $(rt_r/t) > R_r$. Introducing a new variable $w = \xi - (rt_r/r)$ and expanding for large x gives

$$\mathcal{J} \sim \sqrt{4\pi r(t-t_r)}\,\frac{t_r}{t} e^{-r^2/4t_r} + O\left(\left[\frac{4t_r(t-t_r)}{rt}\right]^{3/2} e^{-r^2/4t_r}\right) \quad \text{as } x \to \infty. \tag{11.44}$$

(ii) The minimum does not lie in the range of integration: $rt_r/t < R_r$. Introducing a new variable $w = \xi - R_r$ and expanding for large x gives

$$\mathcal{J} \sim \frac{2t_r(t-t_r)\sqrt{R_r}}{R_r t - rt_r} \exp\left(-\frac{R_r^2}{4t_r} - \frac{(r-R_r)^2}{4(t-t_r)}\right) + O\left(\exp\left(-\frac{R_r(R_r t - t_r r)}{4t_r(t-t_r)}\right)\left[\frac{4t_r(t-t_r)}{rt}\right]^2\right) \quad \text{as} \quad x \to \infty. \tag{11.45}$$

We now gather these results together to obtain the solution, following resection, as

$$c_{\text{postresect}}(r,\theta,t) \sim \begin{cases} \dfrac{N}{4(R_r t - rt_r)}\sqrt{\dfrac{(t-t_r)R_r}{r\pi^3}}\, e^{t-(R_r^2/4t_r)-(r-R_r)^2/(4(t-t_r))} & \text{for } r < \dfrac{t}{t_r}R_r \\ \dfrac{N}{4\pi t} e^{(t-(r^2/4t_r))} & \text{for } r > \dfrac{t}{t_r}R_r \end{cases} \tag{11.46}$$

which is strictly only valid for $(t/2t_r)(rR_r/(2(t-t_r)))$ and $(rR_r/(2(t-t_r)))$ large. It is quite clear from this solution that irrespective of the resected area the solution will eventually grow (exponentially) to a critical size.

We are mainly interested in how different the tumour cell population growth and invasion is, with and without resection. So, we look at the front of tumour cells invading the tissue beyond the bulk tumour margin. From the asymptotic solution (11.43) we can deduce how the invading front of tumour cells has been slowed down as a consequence of resection. For $r > (t/t_r)R_r$, we can write the asymptotic solution following resection as

$$c_{\text{postresect}}(r,\theta,t) \sim \frac{N}{4\pi t}\exp\left(t - \frac{r^2}{4t_r}\right) = c_{\text{noresect}}(r,\theta,t)\exp\left(-\frac{r^2}{4t_r} + \frac{r^2}{4t}\right), \tag{11.47}$$

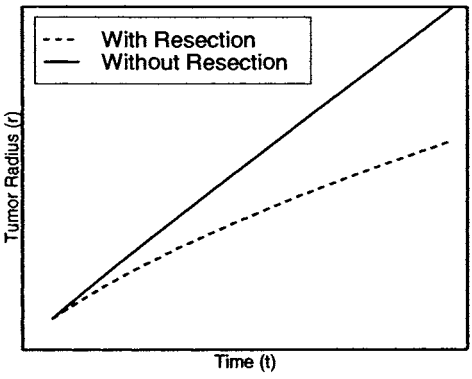

Figure 11.23. Tumour radius, with and without resection, from (11.49).

where (cf. (11.41)),

$$c_{\text{noresect}}(r,\theta,t) = \frac{N}{4\pi t}\exp\left(t - \frac{r^2}{4t}\right) \tag{11.48}$$

is the analytic solution if resection had not been performed. So, following resection, the tumour cell concentration ahead of the resected area is suppressed by a factor of $\exp(-(r^2/4t_r) + r^2/4t)$; this is only for the asymptotic parameters (defined above) sufficiently large. If we assume cell density is detectable (by CT) at the threshold c^*, the outer radius of the detectable tumour then satisfies

$$r^2_{\text{postresect}} \sim 4tt_r\left(1 - \frac{\ln(4\pi t c^*/N)}{t}\right) < 4t^2\left(1 - \frac{\ln(4\pi t c^*/N)}{t}\right) = r^2_{\text{noresect}} \tag{11.49}$$

for $t_r < t < (r/R_r)t_r$. Figure 11.23 gives the detectable tumour radius with and without resection using the asymptotic form in the last equation.

11.9 Modelling Surgical Resection with Brain Tissue Heterogeneity

Swanson (1999) reconsidered resection in the case of an anatomically accurate brain such as we described above. The principle is the same as in the last section but the mathematical problem is considerably more complex. The difference is in the spatial heterogeneity of the diffusion coefficient due to the white and grey matter distribution in the brain. As before, following resection, the tumour cell population continues to be governed by the model system developed in Section 11.2. The mathematical problem with resection is given by the dimensionless system

$$\frac{\partial c}{\partial t} = \nabla\cdot(D(\mathbf{x})\nabla c) + c \tag{11.50}$$

for $t > t_r$, where

$$D(\mathbf{x}) = \begin{cases} 1 & \text{for } \mathbf{x} \in \text{ White Matter} \\ \gamma = \dfrac{D_g}{D_w} & \text{for } \mathbf{x} \in \text{ Grey Matter} \end{cases} \tag{11.51}$$

with $c(\mathbf{x}, t_r) = F(\mathbf{x})$, the initial distribution of cells after resection and $\mathbf{n} \cdot D(\mathbf{x})\nabla = 0$ for $\mathbf{x}$ on ∂B (the boundary of the brain).

We are interested here in the effects of resection on tumour growth and invasion. With the procedures described above for the untreated tumour growth we can look at the effects of resection on tumours at different locations in the brain. The solutions are necessarily numerical. As a detailed example we focus specifically on Position 1 (inferior fronto-parietal) tumours and consider only a high grade tumour, that is, high growth rate and high diffusion; Swanson (1999) gives further results for all grades of tumour. The growth rate ρ does not appear in the dimensionless model but, of course, in the nondimensionalisation (refer to (11.9)).

Figure 11.24 is the simulated response of a high grade glioma at Position 1 (see Figure 11.13) following gross total resection, that is, removal of the detectable (by CT) portion of the tumour. Figure 11.25 shows the evolution of the same tumour following extensive resection, that is, removal of an area twice the size of the detectable portion of the tumour. Recall that a gross total resection corresponds to removal of an area of tumour equivalent to a circle with radius 1.5 cm; in other words the total resected area (as seen on a CT scan) is $\pi(1.5)^2$ cm^2. As mentioned above, the term 'gross total resection' is commonly used by neurosurgeons to describe a successful removal of the tumour such that just after surgery there is no detectable tumour observable on enhancement of a CT scan. The maximum extensive resection corresponds to removal of an area of tumour equivalent to a circle with radius 3 cm; that is, the total resected area (as seen on a CT scan) is $\pi 3^2$ cm^2. In the work of Woodward et al. (1996) the maximum resection they considered was equivalent to a circle with radius 2.5 cm. This scenario defines the recent trend to remove not only the detectable tumour but some radius of normal-appearing tissue surrounding the grossly visible tumour. It makes little difference to the final outcome.

Figure 11.24(a) represents the detectable portion (by a CT scan) of the tumour at diagnosis; that is, $t = t_r$. This is immediately followed by gross total resection, Figure 11.24(b), which shows the actual extent of the tumour using the threshold we used in Section 11.7. We see that the resection succeeded in removing only a fraction of tumour, 36.9% in fact, of the total tumour volume (see Table 11.7). After 60 days, the detectable portion of the tumour has increased from an area of 0 to $\pi(1.5)^2$ cm^2; in other words the tumour has recurred. The recurrent tumour is represented by a ring of detectable tumour surrounding the bed of resection, which is a common characteristic of human gliomas. The CT detectable portion of the recurrent tumour and the actual tumour are shown in Figures 11.24(c) and (d), respectively. Assuming no other treatment is considered, the tumour is fatal 130 days following resection.

If we carry out an extensive resection (see Figure 11.25(b)), 86.7% of the total tumour volume is removed (see Table 11.7). The tumour recurs after 225 days. The

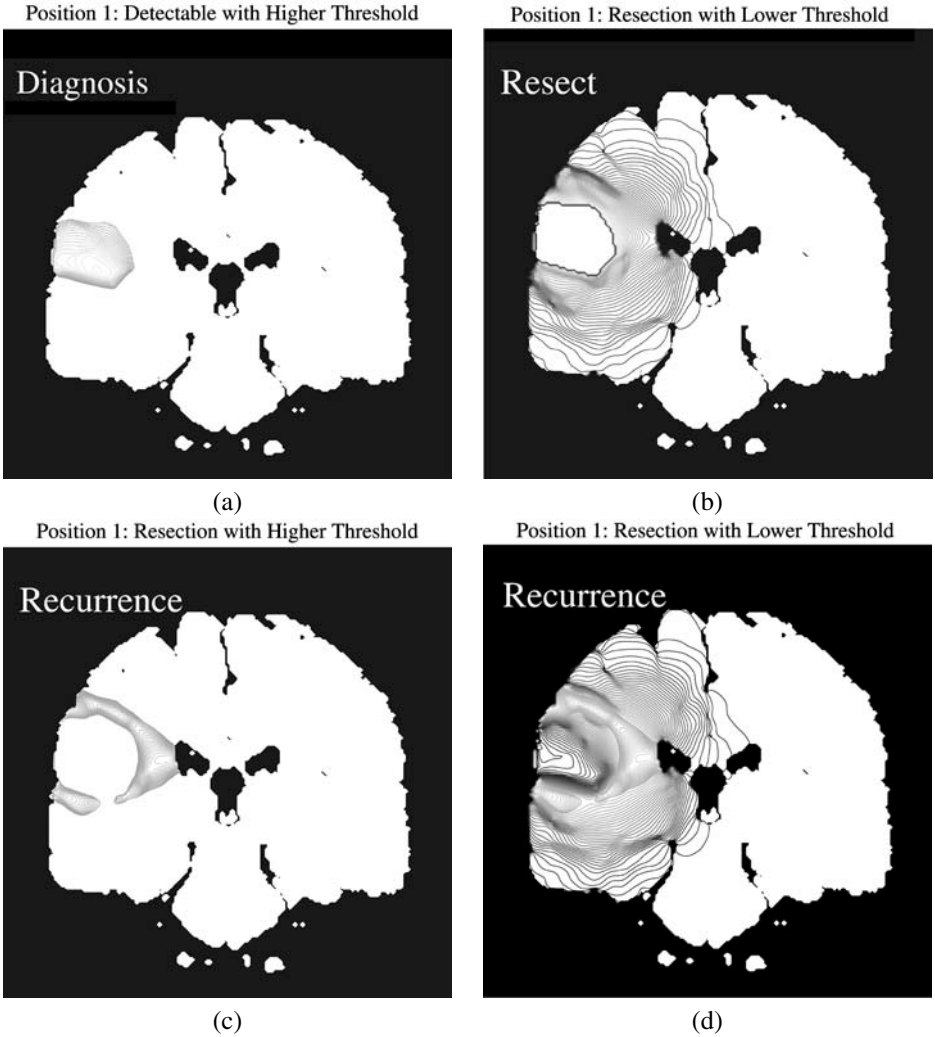

Figure 11.24. Simulation of tumour invasion of a high grade glioma in Position 1 in the inferior fronto-parietal lobe following gross total resection: (**a**) at diagnosis (preresection); (**b**) just after resection of the identifiable tumour, that is, gross total resection; (**c**) and (**d**) at recurrence (60 days later); (**a**) and (**c**) are as seen on the CT scans; (**b**) and (**d**) are as calculated out to 5% of the threshold (boundary) cell concentration defined by CT. (From Swanson 1999) (See the comment in parentheses in Figure 11.10.)

recurrent tumour does not form a ring around the tumour bed but forms isolated tumour islands near the edge of the resection bed (see Figure 11.25(c)). Clearly recurrence following extensive resection is significantly affected by the boundaries of the brain. The three islands of recurrent tumour are located at or near the boundary. Since the concentrations of tumour cells are fairly low after the resection, a single bulk tumour does not form. The tumour cells that remain after resection continue to diffuse and, on encountering boundaries, there is a build-up of tumour cells. An example of clinically

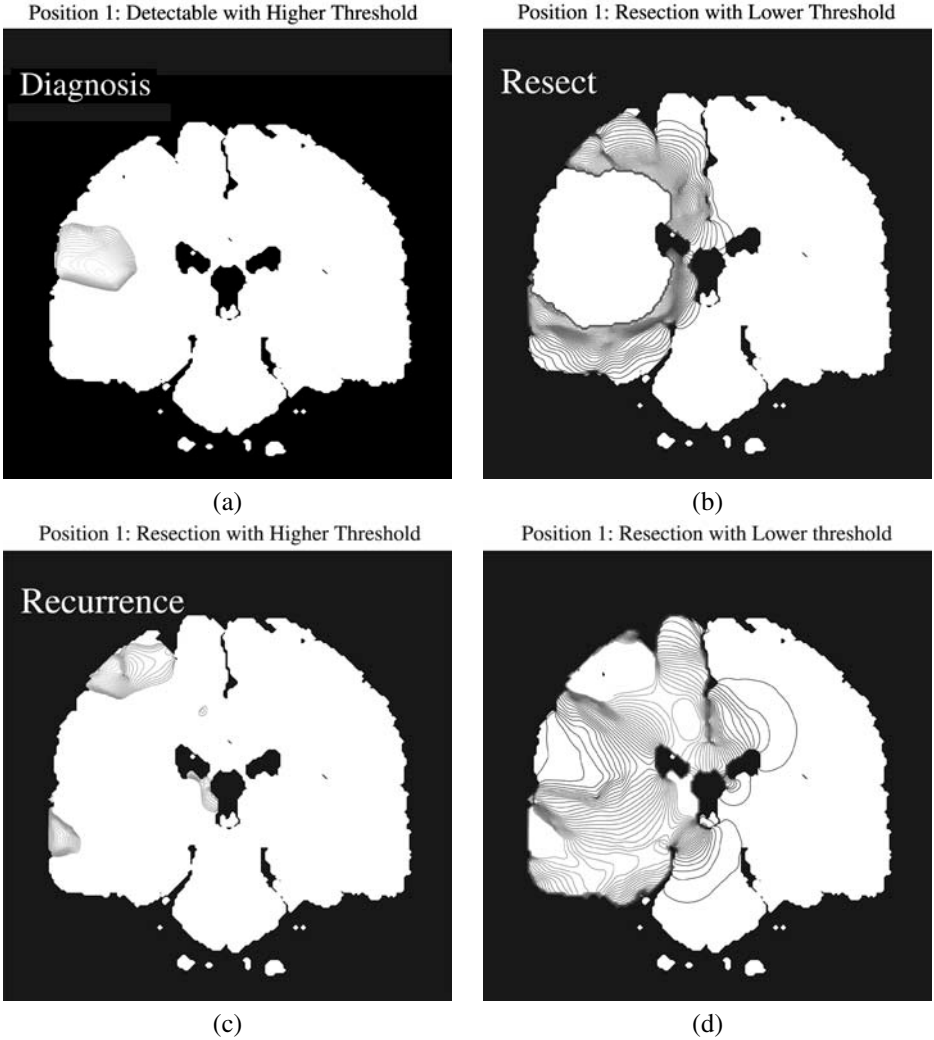

Figure 11.25. Simulation of tumour invasion of a high grade glioma in Position 1 in the inferior fronto-parietal lobe following extensive resection beyond the (CT) detectable margin of the tumour: (**a**) at diagnosis (preresection); (**b**) after resection of the extended region outside the detectable tumour; (**c**) and (**d**) at recurrence (253 days later); (**a**) and (**c**) are as seen on the CT scan; (**b**) and (**d**) are as calculated out to 5% of the threshold (boundary) cell concentration defined by CT. (From Swanson 1999) (See the comment in parentheses in Figure 11.10.)

observed multifocal recurrence is shown in Figure 11.26. The simulated tumour is fatal 253 days following resection, assuming no other treatment regime is attempted, that is, an increase in survival time of 123 days or about 100%. This type of recurrence after *extensive* resection is often considered a 'new' tumour separate from that which was resected. The model suggests that, in fact, this regrowth is part of the same tumour, namely, the diffusively invaded portion that has now become detectable.

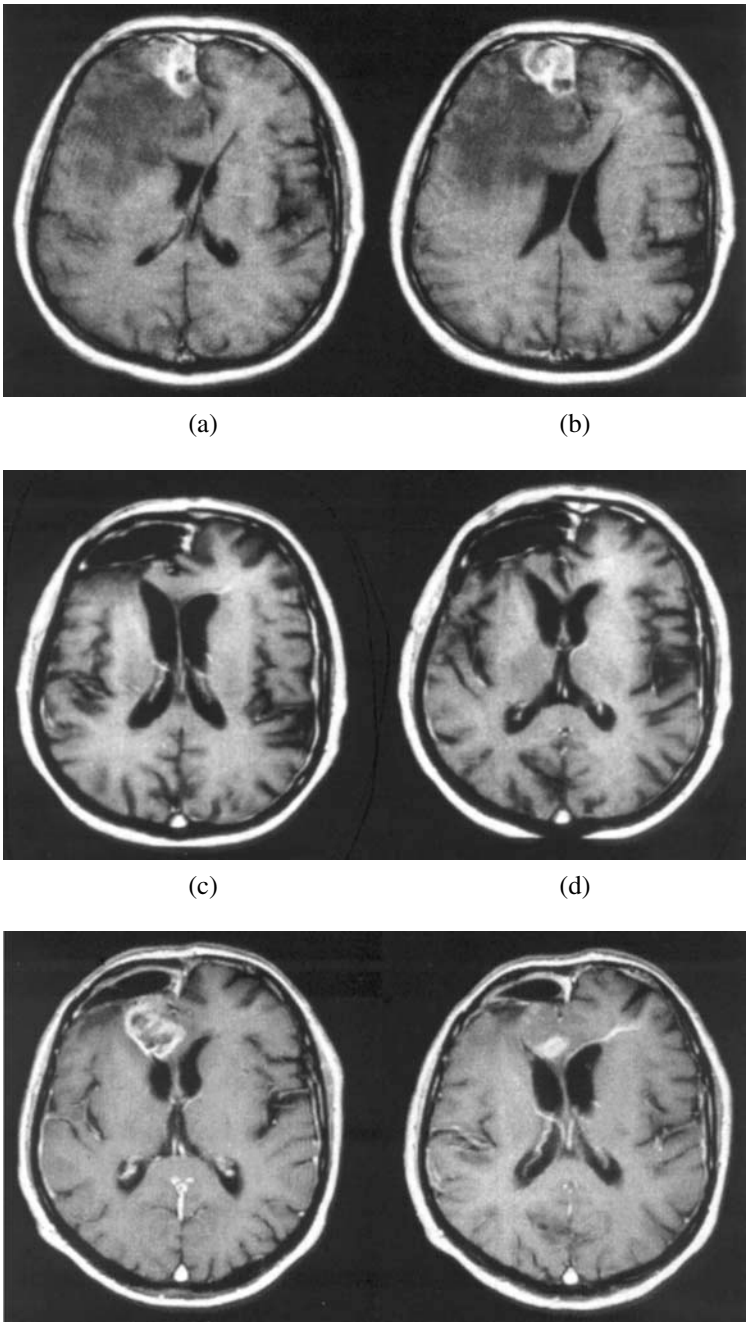

Figure 11.26. Typical clinical example of multifocal recurrence following resection of a glioblastoma. The images are of a 58-year-old man diagnosed with a glioblastoma. Images (**a**) and (**b**) show the histological invasion. Images (**c**) and (**d**) show the gross total resection which was followed by radiation and chemotherapy. Images (**e**) and (**f**) show local recurrence after 6 months. (Data and images were kindly provided by Dr. Alf Giese)

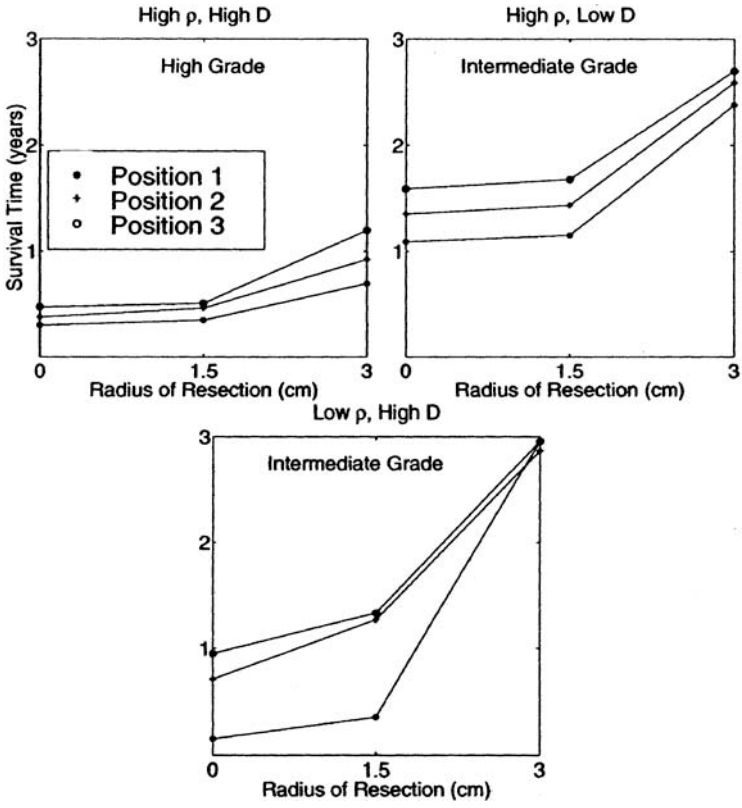

Figure 11.27. Survival time as a function of resection radius. Low grade glioma survival is 10 times that for high grade gliomas. (From Swanson 1999)

Survival Time Following Tumour Resection in Heterogeneous Medium

Although it is clear that diffusely invaded tumour cells contribute directly to the survival time of patients it is instructive to consider the model implications of the idealized fatal tumour size we have used throughout this work. We performed simulations similar to those described above for tumours in the other positions marked in Figure 11.13, namely Positions 2 and 3; these simulation results are given in Swanson (1999). Figure 11.27 shows the survival time associated with tumours at all three positions for high grade and two intermediate grade tumours. Low grade gliomas are not given since their behaviour is essentially the same as that of high grade gliomas but on a much slower timescale.

Tables 11.7 and 11.8 summarize the results on survival time and resection. We tabulate the portion of the total tumour volume removed following gross total or extensive resection. Under our model assumptions, a gross total resection can remove as little as 12% of the total tumour since it is already so diffuse at diagnosis. An extensive resection can remove greater than one-half of the tumour. The effectiveness of the resection depends, of course, on the ratio of the diffusion coefficient D and the growth rate ρ. Also, as we have commented on above, the location of the tumour with respect to the boundaries significantly affects the survival times predicted by our model.

Table 11.7. Percent of tumour volume resected with survival time for all positions with gross total resections for high grade and two intermediate grade tumours. (From Swanson 1999)

Position	ρ (/day)	D (cm^2/day)	Gross Total % Resected	Survival Time (days)
1	1.2×10^{-2}	1.3×10^{-3}	36.9	127.3
	1.2×10^{-2}	1.3×10^{-3}	95.5	420.8
	1.2×10^{-4}	1.3×10^{-4}	12.5	129.6
2	1.2×10^{-2}	1.3×10^{-3}	41.3	169.0
	1.2×10^{-2}	1.3×10^{-3}	92.9	525.5
	1.2×10^{-4}	1.3×10^{-4}	13.1	462.9
3	1.2×10^{-2}	1.3×10^{-3}	48.3	185.6
	1.2×10^{-2}	1.3×10^{-3}	95.8	613.9
	1.2×10^{-4}	1.3×10^{-4}	15.9	486.1

Table 11.8. Percent of tumour volume resected with survival time for all positions with extensive resections. (From Swanson 1999)

Position	ρ (/day)	D (cm^2/day)	Extensive % Resected	Survival Time (days)
1	1.2×10^{-2}	1.3×10^{-3}	86.7	253.7
	1.2×10^{-2}	1.3×10^{-3}	99.9	868.5
	1.2×10^{-4}	1.3×10^{-4}	55.7	1078.7
2	1.2×10^{-2}	1.3×10^{-3}	92.4	337.0
	1.2×10^{-2}	1.3×10^{-3}	99.9	945.0
	1.2×10^{-4}	1.3×10^{-4}	44.2	1046.3
3	1.2×10^{-2}	1.3×10^{-3}	96.2	438.0
	1.2×10^{-2}	1.3×10^{-3}	99.8	985.6
	1.2×10^{-4}	1.3×10^{-4}	52.8	1078.7

The relationship between the amount of tumour resected and survival time clearly depends on many factors. In particular, it is very important to have a sense of physical environment of the tumour location such as proximity to boundaries and the white and grey matter distributions. With such information we can use this approach to deduce more accurately the effectiveness of resection treatment. There are others and we discuss a major one of these, chemotherapy below.

11.10 Modelling the Effect of Chemotherapy on Tumour Growth

In this section we describe the model developed by Cruywagen et al. (1995) and Tracqui et al. (1995) to quantify the effect of chemotherapy on tumour growth. It is based in

part on quantitative image analysis of histological sections of a human brain glioma and especially on cross-sectional area/volume measurements of serial CT images while the patient was undergoing chemotherapy. We estimated the model parameters using optimization techniques to give the best fit of the simulated tumour area to the CT scan data. We carried out numerical simulations on a two-dimensional domain, which took into account the geometry of the brain (only the ventricles and the skull) and its natural barriers to diffusion. The results were used to determine the effect of chemotherapy on the spatiotemporal growth of the tumour. (Shochat et al. (1999) have used computer-based simulations of various basic ordinary differential equation models to evaluate the efficacy of chemotherapy protocols on breast cancer.)

One of the reasons for discussing this work is that it is a somewhat different approach and it shows how the model parameters are estimated from clinical data obtained from successive computerized tomograms (CT) of a patient with an anaplastic astrocytoma who received radiotherapy and chemotherapy. This approach is a feasible one when other methods or independent data are not available. As before the time course of the treatments was incorporated in the model, and, by using optimization techniques to fit the model response to the experimental data, an evaluation of the effectiveness of the chemotherapy was obtained by identifying parameters characterizing the rate of death of tumour cells.

Just as with the above discussions, once the feasibility of reconstructing some of the kinetic events in invasion from histological sections has been established, the hope is to be able to use such modelling to investigate other gliomas with different characteristic growth patterns and geometries and the effects of various forms of therapy using the same types of data from other patients.

Experimental Data

Since many patients with brain tumours die too soon after detection of their tumour without a sufficient number of follow-up scans, we were fortunate to be able to study one patient with an anaplastic astrocytoma who had been diagnosed and treated with X-irradiation three years previously. The tumour recurred and was re-treated chemotherapeutically with moderate success, while CT scans were taken repeatedly during the 12 months before the patient's death. From these scans one or more of the pieces of tumour were observed. The tumour area of the largest piece (piece a) was measured at three different levels (referred to as levels 1, 2 and 3; recall Figure 11.3) of the brain using a digitizing tablet and computerized area measurement technique. Since the levels at which the areas had been recorded were not always exactly the same for all the scans, some data points were obtained by linear interpolation between the neighboring upper and lower levels.

During the same terminal year, the patient received two different chemotherapies (Figure 11.28). The first one was a course of six drugs (6-thioguanine, procarbazine, dibromodulcitol, CCNN, 5-florouracil, and hydroxyurea given over 15 days and repeated every six to eight weeks to allow for recovery of bone marrow) applied five times. The second consisted of two courses of cisplatinum given at month intervals. In addition, the patient received neutron beam irradiation during the last three weeks.

The tumour cell density was determined by image analysis of a biopsy obtained at the time of the first scan. The number of nuclei in the tumour tissue detected per mm^2

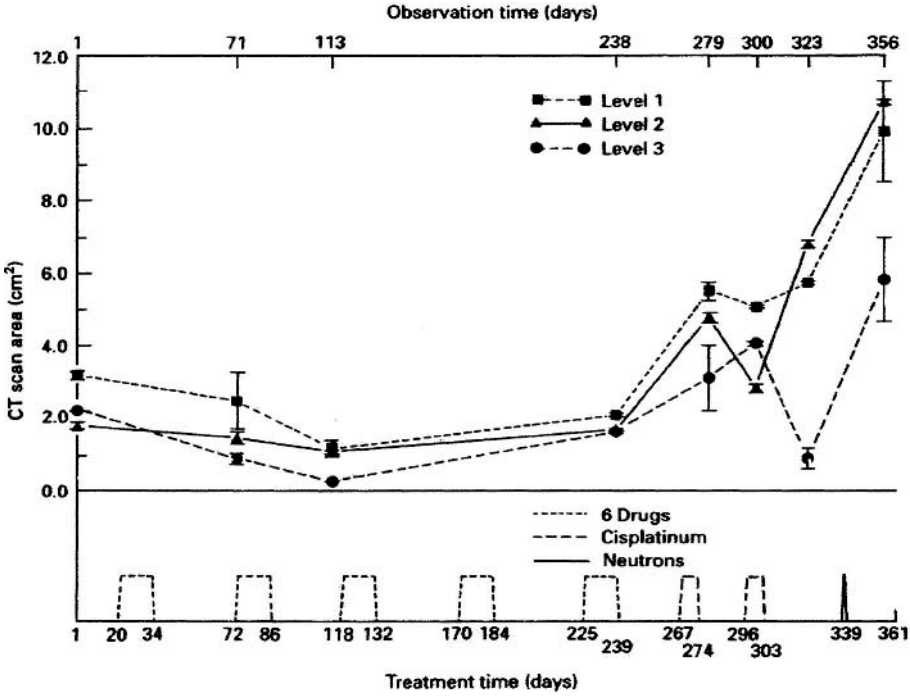

Figure 11.28. Tumour area measured at different levels (recall Figure 11.5), referred to as levels 1, 2 and 3 of the brain, from 8 CT scans taken during the 12 months before the patient's death. During the same terminal year, the patient received 5 cycles of 6 drugs (UW protocol), two cycles of cisplatinum, and neutron beam irradiation. (From Tracqui et al. 1995)

was averaged over five images. This cell density was used as a starting condition for the model. Another evaluation of tumour cell density was performed on autopsy material. From the autopsy tissue, the number of nuclei detected per mm^2 in normal tissue was also averaged over five images. This cell density was used as the threshold in the model over which the area was determined to be tumorous.

Mathematical Model

Here we consider the tissue to be homogeneous, that is, we take the diffusion coefficient and growth rate parameter to be constant. The basic mathematical model, without including the effect of chemotherapy, is given by (11.3) with zero flux boundary conditions on the brain boundaries.

We now have to quantify the effect of the chemotherapy. We do this by assuming that the cell death due to the chemotherapy can be modelled by a linear removal rate, $K(t)c(\mathbf{x}, t)$, where the function $K(t)$ describes the temporal profile of the treatment. We further assume that, for the timescale considered here, the action of the chemotherapy can be modelled, as a first approximation, by a step function with a constant amplitude, such that

$$K(t) = \begin{cases} k_1 & \text{if } t_{1,i} \le t \le t_{1,i+1} \quad i = 1, 3, \ldots, 9 \\ k_2 & \text{if } t_{2,j} \le t \le t_{2,j+1} \quad j = 1, 3 \\ 0 & \text{otherwise} \end{cases}, \tag{11.52}$$

where $t_{1,i}$ and $t_{1,i+1}$ are the starting and finishing times, respectively, of each of the five treatments of the first six-drug course of chemotherapy, while $t_{2,j}$ and $t_{2,j+1}$ correspond to the starting and finishing times of the second cisplatinum chemotherapy course as illustrated in Figure 11.29. With this and equation (11.3) the basic (single cell type) equation is

$$\frac{\partial c}{\partial t} = D\nabla^2 c + \rho c - K(t)c. \tag{11.53}$$

We now need initial and boundary conditions. Theoretically, the tumour started out as one cancerous cell, but the time of appearance of this original cell and the type of

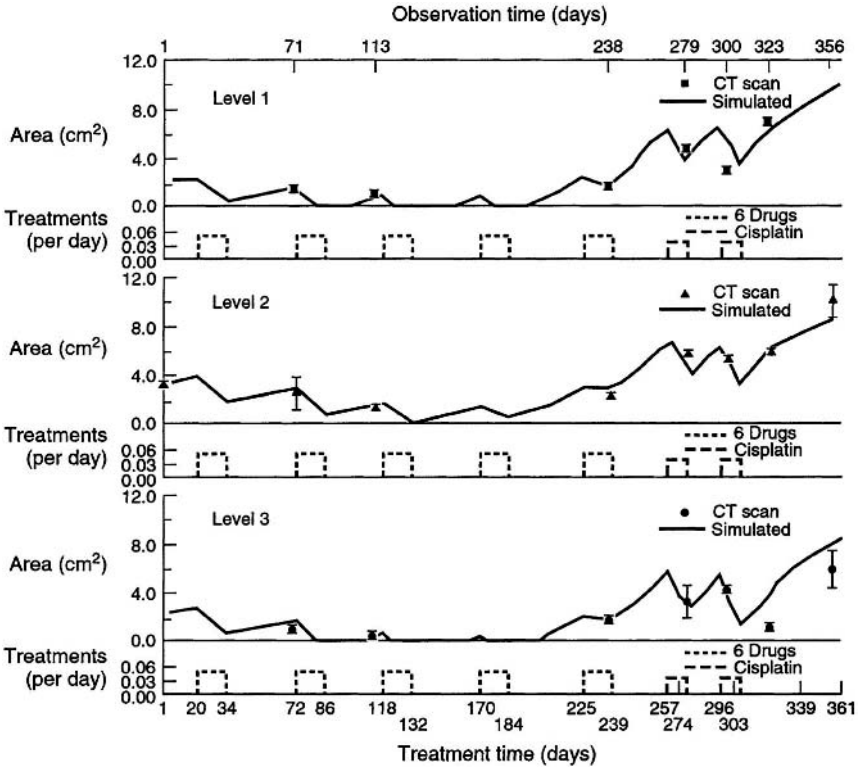

Figure 11.29. The simulated time evolution of the tumour area at each of the three brain levels considered. The model system (11.56)–(11.59) was solved numerically on a two-dimensional grid which takes into account the different brain and ventricle boundaries at each level. The optimisation routine determined the parameters which give the best least squares fit of the simulated tumour area to the CT scan data. The effect of the chemotherapies on each level is also shown. (From Tracqui et al. 1995)

growth and the spread of the early cancer cells are unknown. Since approximate initial conditions must be provided, we assumed, as above, that at the time of the first scan the diffusion process has already broken any previous possibly uniform distribution of the cells. So, we assumed that the cells were normally distributed with a maximum cell density, a, at the centre, $\mathbf{x}_0$, of the tumour for the considered level; that is,

$$c(\mathbf{x}, 0) = a \exp\left(\frac{-|\,\mathbf{x} - \mathbf{x}_0\,|^2}{b}\right), \tag{11.54}$$

where b is a measure of the spread of tumour cells.

As boundary conditions, we require zero flux of cells to the outside of the brain or into the ventricles, so, at the boundaries of the domain we again have

$$\mathbf{n} \cdot \nabla c(\mathbf{x}, t) = 0, \tag{11.55}$$

where $\mathbf{n}$ is the unit vector normal to the boundary.

The initial attempt to represent the spatiotemporal variation of the tumour under the hypothesis of a single cell population with the above model was unsuccessful because it could not account for the qualitative changes in behaviour seen in the clinical data. In particular, it was not possible to capture the sharp increase observed in the tumour area at the end of the first chemotherapy as seen in Figure 11.28, which indicates the failure of this treatment. This suggested that a polyclonal model, which incorporated cell mutations, was necessary and a reasonable first modification.

It was necessary, therefore, to modify the model to include two cell populations. The first cell type, denoted by $c_1(\mathbf{x}, t)$ and which is sensitive to both the first course of chemotherapy (UW protocol of six drugs) and the second course (cisplatinum), comprises most (actually calculated to be over 90%) of the tumour at the time of the first scan. The second cell type, denoted by $c_2(\mathbf{x}, t)$ and which is assumed resistant to the first course of chemotherapy, but possibly sensitive to the second course, comprises the remainder of the cancerous cell population. To model the effect of chemotherapy we considered that cell death is proportional to the number of cells present during the chemotherapy that are sensitive to the particular treatment. The second type of tumour cells could have originated from an earlier genetic mutation, either spontaneous or induced by the radiation therapy three years earlier, or by a similar mutation induced at the beginning of the chemotherapy itself. Under this hypothesis, the proliferation of the second cell population is determined by the initial density of this cell type. A different model could consider a different hypothesis to include the probability of mutation per cell generation as suggested by Goldie and Coldman (1979). We further assumed that both populations of cells have the same properties with regard to diffusion but they may have different growth rates.

Two-Cell Population Model

In the model here we do not view the second cell population as a mutation but rather a cell line in its own right. In the following section on polyclonality we describe such a model. Here, we consider two cell populations, $c_1(\mathbf{x}, t)$ and $c_2(\mathbf{x}, t)$, with the same

diffusion coefficient D, but possibly different growth rates, r_1 and r_2. Then, with the same model (11.53) as the basis, the model we take for the two cell populations is now

$$\begin{aligned}\frac{\partial c_1}{\partial t} &= D\nabla^2 c_1 + r_1 c_1 - K_1(t)c_1 - K_2(t)c_1\\ \frac{\partial c_2}{\partial t} &= D\nabla^2 c_2 + r_2 c_2 - K_2(t)c_2.\end{aligned} \tag{11.56}$$

Here we assume the first cell type, c_1, is sensitive to both treatments, and the second cell type, c_2, is resistant to the first chemotherapy but sensitive to the second course of drugs; that is,

$$\begin{aligned}K_1(t) &= \begin{cases} k_1 & \text{if } t_{1,i} \le t \le t_{1,i+1} \quad i = 1,3,5,7,9\\ 0 & \text{otherwise}\end{cases}\\ K_2(t) &= \begin{cases} k_2 & \text{if } t_{2,1}+4 \le t \le t_{2,2}+6\\ k_2 & \text{if } t_{2,3} \le t \le t_{2,4}+2\\ 0 & \text{otherwise}\end{cases}.\end{aligned} \tag{11.57}$$

The times, $t_{1,1}$, $i = 1, 10$ and $t_{2,j}$, $j = 1, 4$, are directly related to those given in Figure 11.29. Here (and in the numerical simulations) we consider the first chemotherapy to act from the time treatment begins to the time treatment ends, but the second chemotherapy does not start acting until 0 to 4 days after the date of treatment and is still effective 2 days after the last administration. The exact timing is unknown but these assumptions give a better fit to the clinical data.

The associated boundary conditions are (cf. (11.55))

$$\mathbf{n}\cdot\nabla c_1 = 0, \qquad \mathbf{n}\cdot\nabla c_2 = 0 \tag{11.58}$$

and the initial spatial conditions (cf. (11.54))

$$c_1(\mathbf{x},0) = a_1 \exp\left(\frac{-|\,\mathbf{x}-\mathbf{x}_0\,|^2}{b}\right), \quad c_2(\mathbf{x},0) = a_2 \exp\left(\frac{-|\,\mathbf{x}-\mathbf{x}_0\,|^2}{b}\right). \tag{11.59}$$

The parameter $a = a_1 + a_2$ is the maximum initial density of cells (located at the centre of the tumour, $\mathbf{x}_0$), and the parameter, b, measures the spread of the tumour cells.

Initial values of a and b are estimated from the cell densities determined by the biopsy at the time of the first scan and the first scan area, so that at the time of the first scan the simulated value of the area of the tumour is close to the one determined experimentally. The parameter a_1 (the maximum initial density of cells in the first population) still has to be estimated. Assuming an initial homogeneous three-dimensional diffusion of the tumour away from the boundaries, different initial conditions were chosen for the initial cell concentration at the different levels corresponding to the different initial areas as measured at the first scan. The initial cell density a at the centre of the tumour at level 2 is thus larger than those at levels 1 and 3. Accordingly, the coefficient b, characterizing the initial dispersion of the cells is slightly larger for the level 2 compared to

Table 11.9. The model parameters for each level determined by the optimisation routine to give the best least squares fit to the simulated area to the CT scan areas. Here D is the cell diffusion coefficient, r_1 and r_2 are the growth rates and Td_1 and Td_2 are the cell doubling times. The parameters k_1 and k_2 are the cell death rates caused by the two chemotherapies. We assume that at the time of the first scan ('initial' conditions) the cells were normally distributed with the parameter, a, measuring the density of cells at the centre of the tumour and parameter, b, characterising the initial dispersion of the cells. The initial percentage of type 2 cells is determined by the optimisation routine. The weighted least-square error sum is used as a measure of the fit of the simulated tumour area to the CT scan data. (From Tracqui et al. 1995)

	Level 1	Level 2	Level 3
Model Parameters			
D (cm^2/day)	1.11×10^{-2}	1.08×10^{-2}	1.05×10^{-2}
D (cm^2/sec)	1.29×10^{-7}	1.24×10^{-7}	1.21×10^{-7}
r_1 (1/day)	1.05×10^{-2}	1.03×10^{-2}	1.07×10^{-2}
Td_1 (days)	66.0	67.4	64.7
r_2 (1/day)	1.24×10^{-2}	1.10×10^{-2}	1.14×10^{-2}
Td_2 (days)	55.7	63.2	60.6
k_1 (1/day)	3.91×10^{-2}	5.5×10^{-2}	5.10×10^{-2}
k_2 (1/day)	2.85×10^{-2}	2.99×10^{-2}	3.23×10^{-2}
Initial Conditions			
a	706	1120	814
b (cm^2)	5.68	5.68	5.68
initial % of type 2	6.66%	7.95%	9.09%
least square error sum	1480	158	155

the other two levels. Table 11.9 shows how these parameter estimates compare at each level.

Numerical Methods and Results

The two cell populations, $c_1(\mathbf{x}, t)$ and $c_2(\mathbf{x}, t)$ were obtained by the numerical integration of the model system (11.56)–(11.59). An immediate problem is the values to assign to the parameters. As in the evaluation of the tumour area from the CT scan, the numerical determination of the simulated area involves a threshold, c_{th}, in cell density. Mathematically we can choose that to be whatever we want. However, since we are using the model here in conjunction with the data we have to use a different approach. According to the experimental data obtained from the comparisons of histological sections obtained at autopsy with terminal CT scans, the retained value of the normalized threshold is taken as 40% of the biopsy density. This is a reasonable estimate, but obviously it would be much better to have an independent estimation of the threshold from brain slice scans. We can, however, illustrate quantitatively the effect of a variation of the threshold value on the model parameters. For example, a rather large decrease of 25% in the detection threshold has less than a 10% effect on the other parameters, characterized by slight increases in the values of D and k_1 and slight decreases in the values of the growth rates, r_1 and r_2; we come back to this below. The numerical simulation details are given in Tracqui et al. (1995) and Cruywagen et al. (1995).

Initial values of the model parameters, which gave results in good agreement with the observed data, were determined heuristically; we have some idea of these values from the literature such as described in earlier sections but here they were originally estimated from experimental data on cell doubling times from Alvord and Shaw (1991) and *in vitro* motility from Chicoine and Silbergeld (1995). The model parameters, given in Table 11.9, are those obtained by the optimization procedure. Subsequently, a global procedure was used to improve the fit of the model solution to the data through an optimization[2] of the six unknown model parameters.

With this model the unknown parameters are the diffusion coefficient, D, the two growth rates r_1 and r_2 of the first and second cell populations respectively, and the values k_1 and k_2 characterising the death rates of the two cell populations during the two different chemotherapies. The percentage of type 1 cells and type 2 cells at the starting time (that is, at the time of the first scan) is also an unknown parameter.

The total density of cancerous cells, $c(\mathbf{x}, t) = c_1(\mathbf{x}, t) + c_2(\mathbf{x}, t)$ was obtained by the numerical solution. The anatomic boundaries of the skull and of the ventricles associated with each level were taken into account.

Figure 11.29 shows the simulated time evolution of the tumour area at each of the levels 1, 2 and 3. In the simulations, the tumour area increases up to the beginning of the first chemotherapy. As expected, the decrease in the tumour area is larger for a higher value of the effect of the first chemotherapy, k_1, whereas increasing the value of the diffusion coefficient, D, or the growth rate, r_1, has the opposite effect. To generate an increase of the tumour area before the end of the first chemotherapy, the effect of k_1 must be counterbalanced by the growth rate of the second cell population, r_2. The effect of the second chemotherapy is measured by k_2. The value of these parameters, as well as the initial composition of the tumour, are thus critical for determining the spatial-temporal variation of the tumour. The inclusion of the physical brain boundaries and the position of the ventricles in the model has a considerable effect on the results: not only do the boundaries contribute towards a higher tumour cell density due to the accumulation of cells within a restricted area, but also there is clearly a maximum value for the tumour area, which is the brain area without the ventricles.

The evolution of the tumour area simulated by the model is in good agreement with the experimental data. A good fit is obtained for all three levels, which is encouraging for the model validity considering the wide variations in the data points observed in the latter part of the experimental curves, that is, during the second chemotherapy (see Figure 11.28). It is also encouraging to see from Table 11.9 that similar values are obtained for the model parameters for each of the three levels considered, as expected if no specific differences in cell behaviour and properties between the different levels are assumed. Larger inter-level variations are observed for the parameters k_1 and k_2

[2]The minimized criterion was a least square function F, where each term is weighted by the variance of the data point (Ottaway 1973), with

$$F = \sum_{i=1}^{m} \frac{\sum_{j=1}^{n} (S_{ij} - S_i^*)^2}{\sum_{j=1}^{n} (S_{ij} - \bar{S}_i)^2},$$

where m is the number of data points, n is the number of measurements at each data point, $\bar{S}_i$ is the mean value of the area and S_i^* is the simulated area at each data point. The optimization algorithm was coupled with the numerical integration procedure which provided the simulated values at each of the observation times.

measuring the efficiency of the chemotherapies. However, the sawtoothlike shape of the curve in Figure 11.30, resulting from the successive treatments, is sensitive to any small change in the starting and finishing time of each step function modelling each stage of the chemotherapy. So, such variations are to be expected in the absence of more detailed information on the kinetics of the treatment, which would allow for a more precise modelling of the chemotherapy action with time.

Tracqui et al. (1995) reran the optimisation with a 25% decrease in the detection threshold and essentially the same optimisation criterion value to see what effect this had on the parameter estimates. They found that it causes a much smaller change, less than 10%, in the other parameters estimated, with slightly increased values of D and k_1 and slightly decreased values of the growth rates, r_1 and r_2. They also carried out simulations to give the spatiotemporal variation in the tumour in terms of the total cancerous cells and also the two subpopulations. They found, as expected from the model basis that although type 1 cells decreased, type 2 cells increased and it is clear that the patient's death was due to the emergence of a subpopulation of type 2 cells.

Figure 11.30 shows the two-dimensional images of the simulated tumour, and, for comparison, the pictures of the tumour obtained from scans at days 113 and 300. The assumption of a homogeneous medium leads to a simulated tumour shape more regular than the observed one. The variation in the scan levels, with the concomitant modification of the location of the ventricles, prevents a precise tracking of the evolution in tumour shape, a problem not encountered with the approach of Swanson (1999) discussed above.

As mentioned above, the model parameters were estimated from the clinical data. The basic parameters, the cell proliferation and diffusion parameters, are robust in that small changes to their values give quantitatively similar results. On the other hand, the parameters measuring the strength and duration of the chemotherapy treatments are more sensitive to small changes, as described. Even more important than the agreement between the parameters for each level is the agreement between simulated and observed values determined in other experiments and also from various other biological data as given in Tables 11.5 and 11.6. This lends further credence to the method used to estimate the parameters.

The initial cell density (Day 1) corresponds to an average value of 1026 cells/mm^2 measured by the biopsy carried out after the first scan. The cell density given by the model at the end of the simulation time (Day 356) gave an average of 710 cells/mm^2, which is very close to the one measured at autopsy, specifically an average of 750 cells/mm^2.

The growth rate of the second mutant cell population estimated by the model is not significantly different from that of the first cell population. The associated doubling times are 66 days for the first cell population and 60 days for the second cell type (Table 11.9), which is in agreement with the values reported for this type of neoplasm (Alvord and Shaw 1991).

The value of the diffusion coefficient in Table 11.9 (here given in cm^2/day) was determined by using a scale factor of $(5/2.2)^2$ between the scan and the real brain size. The mean value identified from the model is 1.25×10^{-7} cm^2/sec. This value can be compared with estimation of the rate of migration of cancerous cells *in vitro* (Chicoine and Silbergeld 1995). Using the experimental speed value of $v = 15$ microns/hour and

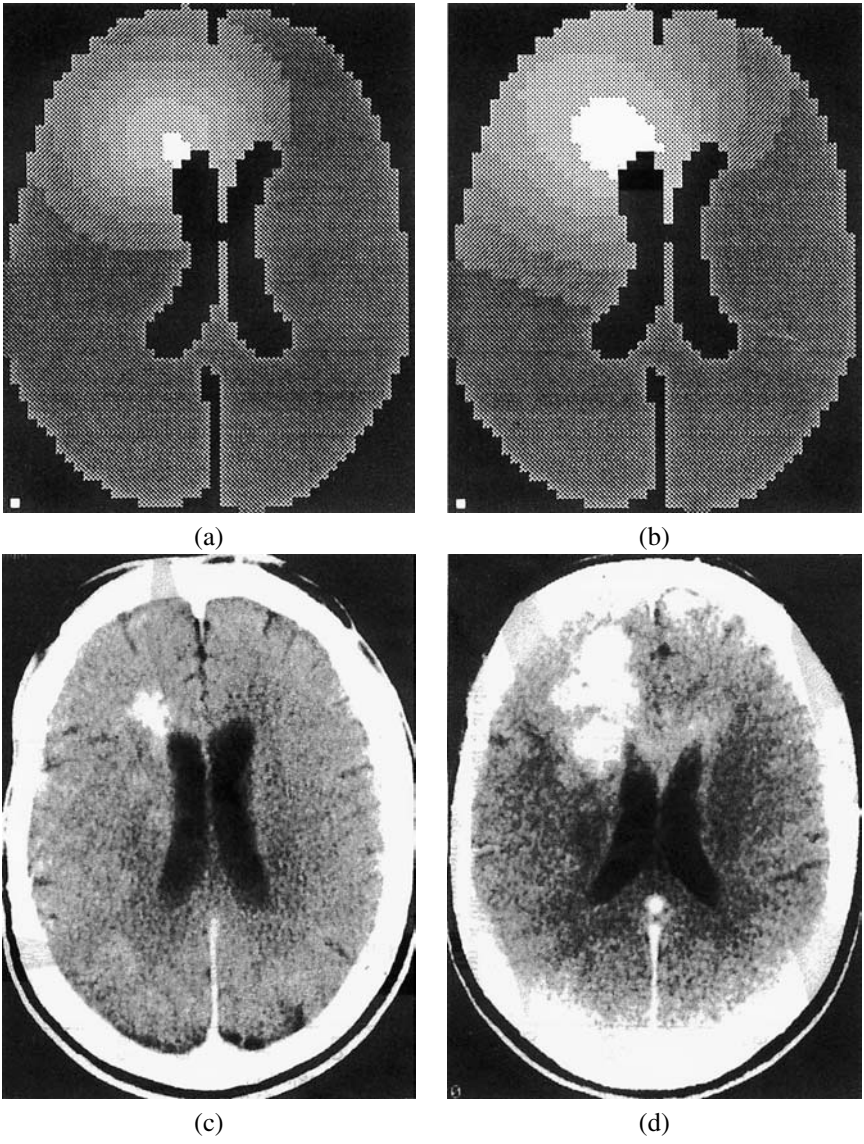

Figure 11.30. The image of the spatial spreading of the tumour inside the brain at (**a**) day 113 and (**b**) day 300 and, for comparison, the CT scans themselves at the same times are given in (**c**) and (**d**). (From Tracqui et al. 1995)

the mean value of the growth rates identified from the model, $\rho = 1.2 \times 10^{-2}$/day, we get an estimate of $D = v^2/4\rho = 3.13 \times 10^{-7}$ cm^2/s; see also Table 11.5.

Obviously other cases must be analysed to determine the ranges of the various parameters defined in the present case. To analyse other cases, at least a few MRI or CT scans over a time period (preferably at least a year) must be available, as well as histologic samples of the tumour and its margins from biopsy or autopsy. Since astrocytomas have estimated doubling times varying from one week to one year or more, in general correlating with their histological degree of malignancy, we anticipate that corresponding differences in r_1 and r_2 will be definable by the model in other cases. Of course, astrocytomas also respond to radio- and/or chemo-therapies in unpredictable degrees, so we anticipate corresponding differences in the parameters, k_1 and k_2.

Perhaps one of the most critical questions is how much the diffusion coefficient D varies from one glioma to another. Another question is whether the cell concentration or the cell type contributes independently to D.

Current therapies of gliomas are limited by the tolerance of normal brain for X-irradiation and of hematopoetic tissues for chemotherapies, but it is a reasonable expectation that, as additional therapies are developed, definitions of the parameters in the model will be helpful in planning the dose and timing of these therapies.

The prediction of tumour response to therapy is a goal which mathematical models can help to reach. This benefit should appear especially true for chemotherapy, which is a treatment suffering from a great lack of knowledge concerning drug pharmacokinetics and the existence of drug-resistant subpopulations within large populations of cells (both factors varying from patient to patient). A knowledge of the generic values of the model parameters for a given type of brain tumour will provide a first estimation of the tumour growth response to the routine treatment. Online adaptation of the parameters in space with the specific data obtained from each new CT or MRI scan of the treated patient will provide necessary corrections needed to approach optimal patterns of drug delivery.

We should voice, again, a word of caution on the use of models. A large series of cautious explorations and validations of the model predictions have to be made before an optimal clinical strategy can be reached. But this approach allows an improvement of cancer treatment which does not imply or depend on the discovery of completely new drugs, but rather suggests an optimal use and *in situ* evaluation of the already existing ones.

There are, of course, some obvious limitations of the model. Tumour heterogeneity can be taken into account by considering various populations with specific kinetics and possibly competitive interactions which can affect tumour growth dynamics (Michelson et al. 1987). The effect of different therapy scheduling can easily be investigated by shifting the time boundary values of the step functions modelling chemotherapy, and additional knowledge on the pharmacokinetics of the drugs can furthermore be introduced to modulate the shape of these latter functions. The effect of different extents of surgical excision was explored with this type of model by Woodward et al. (1996) and more recently by Swanson (1999) and Swanson et al. (2000), which crucially included facilitated diffusion in the direction of white fibre tracts. Although we model motility by diffusion it is not likely that tumour cells diffuse passively through normal brain tissue, which is too viscous to allow much passive diffusion. Instead, as shown experimentally

(Chicoine and Silbergeld 1995), tumour cells probably migrate by active amoeboid processes. The mathematical framework in which the present model has been developed is general enough to formalize these specificities, as exemplified by different models in population dynamics such as described in this book. Tracqui (1995) discusses this aspect by comparing the approach discussed in this section to the minimal hypotheses relating cell motility and cell traction forces. Other limitations and suggestions for improving the model are given by Tracqui et al. (1995).

With the approach here to parameter estimation, additional work is needed to determine to what extent modelling the tumour as a three-dimensional object significantly modifies the estimation of the model parameters, especially the diffusion coefficient. A major contribution to this is given by the work of Swanson (1999) and Swanson et al. (2000). She has also applied her approach (Swanson 1999) to the problem of chemotherapy treatment. However, the benefit of a more accurate description of the phenomena will necessitate a three-dimensional analysis of the brain and ventricular boundaries together with the heterogeneous distribution of grey and white matter.

11.11 Modelling Tumour Polyclonality and Cell Mutation

With the exception of the last section we have assumed that the tumour cell population is homogeneous involving only one cell type. In spite of the good quantitative comparison with data, such as regards life expectancy after resection, in the last section we saw that variable sensitivity to chemotherapeutic drugs exhibited by gliomas necessitated a model with tumour cell heterogeneity. Gliomas are known to be heterogeneous (polyclonal) with heterogeneity generally increasing with grade. The more malignant cells are believed to have a stronger propensity to mutate thus increasing heterogeneity. Therefore, we expect to see different types of cells within the tumour (for example, Pilkington 1992). The basic model can be extended to consider the case of a polyclonal tumour as we saw in the last section by simply creating two (or more) cell populations within the tumour that may have different diffusivity and growth rates. In the model equation (11.3) (the homogeneous tissue situation) the cell density $\bar{c}$ becomes the vector of cell densities $\bar{\mathbf{c}}$ and the diffusion coefficient D and the growth rate ρ now become diagonal matrices of diffusion coefficients and growth rates, respectively. The total tumour population, at a given point in space and time $(\bar{\mathbf{x}}, \bar{t})$, is the sum of the components of the $\bar{\mathbf{c}}$ vector. In the chemotherapy model in the last section we took the two cell populations to be independent. Often, however, the subpopulations are not independent but are connected by mutational events transferring cancer cells from cell population i to cell population j. A fairly general but basic model to account for population polyclonality can be written in the dimensional form

$$\frac{\partial \bar{\mathbf{c}}}{\partial \bar{t}} = \bar{\nabla} \cdot (D \bar{\nabla} \bar{\mathbf{c}}) + \rho \bar{\mathbf{c}} + T \bar{\mathbf{c}}, \tag{11.60}$$

where T is a matrix representing transfer between subpopulations. To complete the mathematical problem we use initial and boundary conditions

$$\bar{\mathbf{n}} \cdot D\bar{\nabla}\bar{\mathbf{c}} = 0 \qquad \text{for } \bar{\mathbf{x}} \text{ on } \partial B \text{ (the boundary of the brain)}$$
$$\bar{\mathbf{c}}(\bar{\mathbf{x}}, 0) = \bar{\mathbf{f}}(\bar{\mathbf{x}}) \qquad \text{for } \bar{\mathbf{x}} \text{ in } B \text{ (the brain domain)}.$$

We expect that the introduction of multiple cell populations in the tumour introduces more heterogeneity in the growth patterns of the simulated tumour. Clinical and experimental results have shown fingering and branching of the visible tumour.

In this section we consider, by way of example, the existence of two clonal subpopulations within a tumour with mutational transfer. To be specific we assume one population has a high growth and low diffusion coefficient while the second population has a moderate growth rate and high diffusion coefficient; there are various other scenarios we could take. Let

$$\bar{\mathbf{c}} = \begin{pmatrix} \bar{u} \\ \bar{v} \end{pmatrix}, \quad D = \begin{pmatrix} D_1 & 0 \\ 0 & D_2 \end{pmatrix}, \quad \rho = \begin{pmatrix} \rho_1 & 0 \\ 0 & \rho_2 \end{pmatrix}, \quad T = \begin{pmatrix} -k & 0 \\ k & 0 \end{pmatrix},$$

where the D's, ρ's and k's are constant parameters, and (11.60) becomes

$$\begin{aligned} \frac{\partial \bar{u}}{\partial \bar{t}} &= \bar{\nabla} \cdot (D_1 \bar{\nabla} \bar{u}) + \rho_1 \bar{u} - k\bar{u}, \\ \frac{\partial \bar{v}}{\partial \bar{t}} &= \bar{\nabla} \cdot (D_2 \bar{\nabla} \bar{v}) + \rho_2 \bar{v} + k\bar{u} \end{aligned} \tag{11.61}$$

with given initial conditions $\bar{u}(\bar{\mathbf{x}}, 0) = \bar{f}(\bar{\mathbf{x}})$ and $\bar{v}(\bar{\mathbf{x}}, 0) = \bar{g}(\bar{\mathbf{x}})$. With $\bar{u}$ the more rapidly proliferating population and $\bar{v}$ the more rapidly diffusing population, $D_2 > D_1$ and $\rho_1 > \rho_2$. We further assume $\bar{u}$ cells are the only tumour cells initially present ($\bar{f}(\bar{\mathbf{x}}) > 0$ and $\bar{g}(\bar{\mathbf{x}}) = 0$). With some small probability, $k \ll \rho_1$, $\bar{u}$ cells mutate to form $\bar{v}$ cells. Although we do not include it here, each of the cell populations could retain the ability to diffuse faster in white matter regions.

Initially, let us suppose there is a source of $\bar{u}$ tumour cells that have mutated from healthy cells and can proliferate faster then the neighboring normal cells thereby starting to form a tumour. We can think of k as a measure of the probability of $\bar{u}$ tumour cells mutating to become the rapidly diffusing tumour cell population $\bar{v}$.

Introduce the nondimensional variables

$$\mathbf{x} = \sqrt{\frac{\rho_1}{D_1}}\,\bar{\mathbf{x}}, \quad t = \rho_1 \bar{t}, \quad \beta = \frac{\rho_2}{\rho_1} < 1, \quad \alpha = \frac{k}{\rho_1}, \quad \nu = \frac{D_2}{D_1}, \tag{11.62}$$

$$u(\mathbf{x}, t) = \frac{D_1}{\rho_1 u_0} \bar{u}\left(\sqrt{\frac{\rho_1}{D_1}}\,\bar{\mathbf{x}}, \rho_1 \bar{t}\right), \quad v(\mathbf{x}, t) = \frac{D_1}{\rho_1 u_0} \bar{v}\left(\sqrt{\frac{\rho_1}{D_1}}\,\bar{\mathbf{x}}, \rho_1 \bar{t}\right), \tag{11.63}$$

where $u_0 = \int \bar{f}(\bar{\mathbf{x}}) d\bar{\mathbf{x}}$, the total original cancer cell population. Growth is measured on the timescale of the $\bar{u}$ population proliferation and diffusion is on the spatial scale of the $\bar{u}$ cell diffusion.

Equations (11.61) now become

$$\frac{\partial u}{\partial t} = \nabla^2 u + u - \alpha u, \tag{11.64}$$

$$\frac{\partial v}{\partial t} = \nu \nabla^2 v + \beta v + \alpha u. \tag{11.65}$$

The parameter $\alpha = k/\rho_1 \ll 1$ is the proportion of the first subpopulation's growth lost to mutation.

In one space dimension on an infinite domain we can write down the analytical solutions from which some interesting and highly relevant conclusions can be deduced as we shall see. In one space dimension

$$\frac{\partial u}{\partial t} = \frac{\partial^2 u}{\partial x^2} + u - \alpha u, \tag{11.66}$$

$$\frac{\partial v}{\partial t} = \nu \frac{\partial^2 v}{\partial x^2} + \beta v + \alpha u. \tag{11.67}$$

Let us take the initial source of u tumour cells to be $u(x, 0) = \delta(x)$ and take $v(x, 0) = 0$. The v population diffuses faster than u so $\nu > 1$. The growth rate of the u population is larger than v so $\beta < 1$. The growth rate of u is much higher than the probability of mutation so $\alpha \ll 1$.

The solution of (11.66) can be solved separately from the v equation and has the solution

$$u(x, t) = \frac{1}{\sqrt{4\pi t}} \exp\left((1 - \alpha)t - \frac{x^2}{4t}\right), \tag{11.68}$$

which on substituting this result into the v equation (11.67) gives

$$\frac{\partial v}{\partial t} = \nu \frac{\partial^2 v}{\partial x^2} + \beta v + \alpha \frac{1}{\sqrt{4\pi t}} \exp\left((1 - \alpha)t - \frac{x^2}{4t}\right). \tag{11.69}$$

We use a Fourier transform in the spatial variable x to solve this equation. With the transform and its inverse defined by

$$\mathcal{F}[f(x, t)](t; \omega) = \int_{-\infty}^{\infty} f(x, t) e^{-i\omega x}\, dx,$$

$$\mathcal{F}^{-1}[F(t; \omega)](x, t) = \frac{1}{2\pi} \int_{-\infty}^{\infty} F(t; \omega) e^{i\omega x}\, d\omega$$

the transformed equation for v is then

$$\frac{\partial V}{\partial t} = \nu(i\omega)^2 V + \beta V + \alpha e^{(1-\alpha-\omega^2)t} \quad \text{with} \quad V(t = 0; \omega) = 0,$$

where $V(t; \omega) = \mathcal{F}[v(x, t)]$. The solution for V is then given by

$$V(t; \omega) = \frac{\alpha\left[e^{(1-\alpha-\omega^2)t} - e^{(\beta-\nu\omega^2)t}\right]}{1 - \alpha - \beta + \omega^2(\nu - 1)}. \tag{11.70}$$

Taking the inverse transform gives, after some algebra, $v(x,t)$ as

$$\begin{aligned} v(x,t) &= \mathcal{F}^{-1}[V(t;\omega)] \\ &= \alpha\mathcal{F}^{-1}\left[e^{(1-\alpha-\omega^2)t} - e^{(\beta-\nu\omega^2)t}\right] * \mathcal{F}^{-1}\left[\frac{1}{1-\alpha-\beta+\omega^2(\nu-1)}\right] \\ &= \alpha e^{(1-\alpha)t}\int_{\xi=-\infty}^{\infty} \frac{\exp\left(-\frac{(x-\xi)^2}{4t}\right)}{\sqrt{4\pi t}} \frac{\exp\left(-A|\,\xi\,|\right)}{A(\nu-1)}\,d\xi \\ &\quad - \alpha e^{\beta t}\int_{\xi=-\infty}^{\infty} \frac{\exp\left(-\frac{(x-\xi)^2}{4\nu t}\right)}{\sqrt{4\pi\nu t}} \frac{\exp\left(-A|\,\xi\,|\right)}{A(\nu-1)}\,d\xi. \end{aligned} \tag{11.71}$$

If we now assume $1-\alpha-\beta > 0$, integration of the convolution integrals gives

$$\begin{aligned} v(x,t) = \frac{\alpha \exp\left(\frac{\nu(1-\alpha-\beta)}{\nu-1}t\right)}{2A(\nu-1)} &\left[e^{-Ax}\left(\operatorname{erf}\left[\frac{x-2At}{2\sqrt{t}}\right] - \operatorname{erf}\left[\frac{x-2A\nu t}{2\sqrt{\nu t}}\right]\right)\right. \\ &\left. - e^{Ax}\left(\operatorname{erf}\left[\frac{x+2At}{2\sqrt{t}}\right] - \operatorname{erf}\left[\frac{x+2A\nu t}{2\sqrt{\nu t}}\right]\right)\right], \end{aligned} \tag{11.72}$$

where $A = \sqrt{(1-\alpha-\beta)/(\nu-1)}$. An important implication of this solution is that for certain values of α, we see that the initially nonexistent subpopulation v can eventually dominate the growth of the tumour. Swanson (1999) computed the two populations using this solution and Figure 11.31 shows the transition of dominance from the rapidly growing u population to the rapidly diffusing v population. Although the initial tumour consisted of only u cells, for large time the v subpopulation can dominate depending on the value of the mutation probability parameter α. Yet again, we find that the diffusion is more important to glioma growth and invasion then proliferation.

There are two relevant ways to view transition of dominance: (i) the total tumour cell population volume is dominated at later times by the second, more aggressive, tumour subpopulation v; or, (ii) v dominates at a single point or neighborhood of points, say, near the centre of the tumour, but does not necessarily fill the volume.

When performing a biopsy of a tumour, the sample of tissue is extracted from a fairly random location within the tumour. Analysis of this piece of tissue is expected to give an accurate portrayal of the tumour composition. Since it is often the case that different grades of tumour cells are histologically (physically) distinct, a pathologist could quantify the proportion of the tumour that is of a certain grade from the tissue biopsy. In particular, we expect that a biopsy would reveal information about the clonal distribution of the total tumour volume and the results would not be significantly different from that if the entire tumour were analyzed (as is possible postmortem). From Swanson's (1999) analysis below and our discussion of transmission of dominance at a given location and in volume, it is not necessarily clear that a biopsy will, in fact, define an accurate representation of the total tumour cell composition (tumour volume).

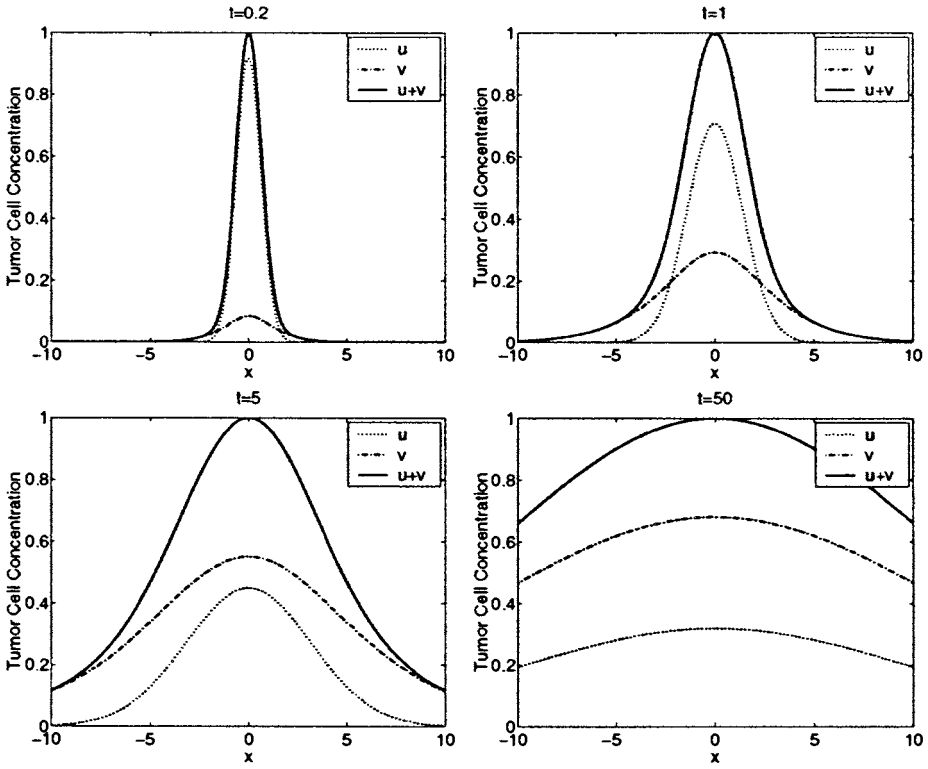

Figure 11.31. Transition of dominance from u to v. Between $t = 0.2$ and $t = 50$, there is a transition in dominance from the highly proliferative u subpopulation to rapidly diffusing v subpopulation. Parameters: $\alpha = 0.5$, $\nu = 10$, and $\beta = 0.1$. (From Swanson 1999)

Transition of Dominance at a Given Location

To determine if the subpopulation v eventually dominates the tumour composition at a given location, say, the centre of the tumour $x = 0$ where a biopsy would be performed, we consider the ratio of the two subpopulations $v(x,t)/u(x,t)$. Certainly, for small t, this ratio is less than 1 since u is initially the only population present. The v subpopulation becomes dominant if this ratio $v/u > 1$.

For large t, the ratio of the two subpopulations is approximated by

$$\frac{v(x,t)}{u(x,t)} \sim \frac{2\alpha}{1-\alpha-\beta} - \frac{\alpha(\nu-1)}{(1-\alpha-\beta)^2}\left(\frac{1}{t}\right) - \frac{\alpha x^2[x^2(1-\alpha-\beta)-4(\nu-1)]}{16(1-\alpha-\beta)}\left(\frac{1}{t^2}\right) + O\left(\frac{1}{t^3}\right). \quad (11.73)$$

So, for large time, the ratio tends to a constant value $2\alpha/(1-\alpha-\beta)$. If $2\alpha/(1-\alpha-\beta) > 1$ then the second subpopulation v dominates for large time. The condition

for the diffuse population v dominance at a point ($x = 0$) is then given by

$$\frac{2\alpha}{1-\alpha-\beta} > 1 \implies \beta > 1 - 3\alpha. \tag{11.74}$$

Note that this parameter condition does not depend on ν, the ratio of the diffusion coefficients of u and v. We can also use the asymptotic expression (11.73) to estimate the time at which the transition of dominance occurs. Setting (11.73) equal to 1 and solving for t, we find that the time at which transition of dominance at $x = 0$ occurs $t_{\text{dominance}}$, say, is given approximately by

$$t_{\text{dominance}} \sim -\frac{\alpha(\nu-1)}{(2\alpha+\beta-1)^2-\alpha}, \tag{11.75}$$

which does depend on ν and is positive if the condition (11.74) for transition of dominance at a point is satisfied. For large ν, the diffusion coefficient of the v cells is much higher than the u cells and the time to transition of dominance is large. However, if the parameters α and β satisfy the parametric condition (11.74), the time to this transition can be quite short if the diffusion coefficients are nearly equivalent ($\nu \approx 1$).

Transition of Dominance in Volume

Let us now consider the situation in which we can analyze the entire tumour and determine the proportion of the tumour volume occupied by u and v cells separately. This is biologically analogous to a detailed postmortem analysis of the entire brain. In this case, transition of dominance occurs if the volume occupied by v cells exceeds that occupied by u cells.

The model equations (11.66) and (11.67) define the spatiotemporal dynamics of the u and v subpopulations. By integrating these equations over all space, we can determine the temporal behavior of the tumour cell subpopulation volumes. Define $V_u(t)$ and $V_v(t)$ to be the volume of the tumour occupied by u and v cells, respectively, then

$$V_u(t) = \int_{-\infty}^{\infty} u(x,t)\,dx \quad \text{and} \quad V_v(t) = \int_{-\infty}^{\infty} v(x,t)\,dx. \tag{11.76}$$

Integrating equations (11.66) and (11.67) over all space (the infinite domain) we get

$$\frac{dV_u}{dt} = (1-\alpha)V_u \qquad \text{with} \quad V_u(0) = 1,$$

$$\frac{dV_v}{dt} = \beta V_v + \alpha V_u \qquad \text{with} \quad V_v(0) = 0.$$

Solving the first equation gives

$$V_u(t) = e^{(1-\alpha)t} \tag{11.77}$$

and V_v then satisfies

$$\frac{dV_v}{dt} = \beta V_v + \alpha e^{(1-\alpha)t} \quad \text{with} \quad V_v(0) = 0 \tag{11.78}$$

which has solution

$$V_v(t) = \frac{\alpha\left(e^{(1-\alpha)t} - e^{\beta t}\right)}{1-\alpha-\beta}. \tag{11.79}$$

Transition of dominance in the volume occurs if the ratio $V_v/V_u = 1$ at some finite time. So,

$$\begin{aligned} \frac{V_v}{V_u} = 1 &\implies e^{(1-\alpha-\beta)t} = \frac{\alpha}{2\alpha+\beta-1} \\ &\implies t_{\text{dominance}} = \frac{1}{1-\alpha-\beta}\ln\left(\frac{\alpha}{2\alpha+\beta-1}\right), \end{aligned} \tag{11.80}$$

where the time of transition of dominance exists (that is, positive) if

$$1-\alpha-\beta > 0 \quad \text{and} \quad 2\alpha+\beta-1 > 0.$$

Equivalently, the condition on the parameters for transition of dominance in volume is

$$1-2\alpha < \beta < 1-\alpha. \tag{11.81}$$

Figure 11.32 shows the parameter domains (in the α–β plane) for transition of dominance at a point, in volume and both. The shaded region of Figure 11.32(a) represents the parameter domain for which transition of dominance at a point (say, the origin) occurs while Figure 11.32(b) represents the parameter values for which transition of dominance by volume is possible. Clearly, there are values of α and β for which transition of dominance at a point occurs and that of volume does not. This indicates a failure for accurate biopsies of tumours. Analysis of a portion of tissue extracted from the centre of a tumour will not necessarily reveal the actual total tumour composition.

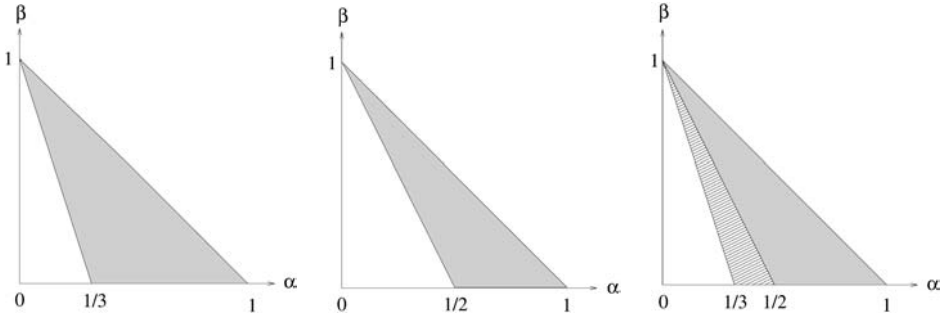

(a) (b) (c)

Figure 11.32. Parameter domains for which transition of dominance occurs: (**a**) at a point (taken to be $x = 0$ here); (**b**) by volume; (**c**) both. (From Swanson 1999)

Multi-Cell Model with Tumour Polyclonality

We now briefly consider a simple model with homogeneous diffusion in which there is mutation from one cell line to another but in which there are n lines: the formulation mimics what we did above but there is the possibility of very much more complex spatiotemporal dynamics. The general problem is then, in appropriate dimensionless form,

$$\frac{\partial \mathbf{c}}{\partial t} = \nabla \cdot (D\nabla \mathbf{c}) + P\mathbf{c} + T\mathbf{c} \tag{11.82}$$

with $\mathbf{c}$ satisfying

$$\mathbf{n} \cdot D\nabla \mathbf{c} = 0 \quad \text{for } \mathbf{x} \text{ on } \partial B, \quad \mathbf{c}(\mathbf{x}, 0) = \mathbf{f}(\mathbf{x}), \tag{11.83}$$

where D, P and T are respectively the diffusion coefficient matrix, growth rate matrix and transfer matrix between the populations.

Define the eigenvalue problem by

$$\nabla \cdot (D\nabla \mathbf{W}) + K^2 \mathbf{W}(\mathbf{x}) = 0, \quad \mathbf{n} \cdot D\nabla \mathbf{W} = 0, \tag{11.84}$$

where K denotes the eigenvalues. We now look for solutions (cf. Chapter 2) in the form

$$\mathbf{c}(\mathbf{x}, t; K_i) \propto e^{(P+T-K^2 I)t}, \tag{11.85}$$

where the K_i are the discrete eigenvalues and I is the identity matrix. Keep in mind that the exponent of the exponential is a matrix. The spatiotemporal behaviour on a linear basis is that determined by the eigenvalues $\sigma(\rho_i, K_i, D_i)$, where the ρ_i and D_i are components in the growth matrix and diffusion matrix respectively. The eigenvalues are given by

$$| P + T - (K_i^2 + \sigma) I | = 0. \tag{11.86}$$

The analysis of the spatiotemporal behaviour of the solutions here is a generalisation of the two-species model systems we have discussed extensively in many chapters of the book. The implications for tumour growth and invasion governed by this type of model are still unexplored.

Some Concluding Comments

Cancer is no single disease. We have only considered some of the basic models for the growth and control of brain tumours. We have seen that, even with such simple linear models as discussed in this chapter, there is a surprising richness of potentially applicable results. There is clearly much still to be done with this modelling approach.

There is a large literature on models for other tumours and it is impossible to mention them all. One place to start is with several of the articles on cancer and related topics in the book edited by Chaplain et al. (1999). Other tumours can involve a wide range of biological phenomena such as angiogenesis and capillary networks (Chaplain and An-

derson 1999), pattern formation in cancer macrophage dynamics (Owen and Sherratt 1997), role of inhibitors and cell-adhesion (Byrne and Chaplain 1995, 1996) and cell traction (Holmes and Sleeman 2000). What seems very clear is that the use of realistic models can help to elucidate many of the complex processes (or at the very least pose informative questions) that take place in the growth of malignant tumours; the closer the connection to the medical situation the more useful are the results.

A very good example of how such a close connection between experiment and theory can be so productive is given by the new approach to cancer treatment, notably melanoma, which has been developed by Jackson and her colleagues (Jackson 1998, Jackson et al. 1999a,b,c). Her work is directed to improving the efficacy of chemotherapeutic agents for treating cancer. It involves a two-step process which is designed to minimize the toxicity to the body while at the same time maximizing the toxicity in the cancer. The treatment involves enzyme-conjugated antibodies (ECA) in combination with prodrugs. Basically an antibody that binds to a tumour-associated antigen is conjugated to an enzyme not present in the host and then injected into the bloodstream. The ECA distributes itself in the tissue throughout the body and after some time is localized within the tumour because of high binding affinity. The prodrug is then injected into the body and the enzyme then converts the prodrug back into the toxic form. In this way the drug penetrates the tumour with minimal penetration into normal tissues and the bloodstream. The modelling involves taking this scenario and the basic biochemistry and constructing a realistic model which can be tested experimentally *in vitro*. The model mechanism involves space and time and gives rise to a different type of system of nonlinear coupled partial differential equations. Because of the experimental interdisciplinary collaboration, Jackson (1998) was able to assign realistic parameter values to her model, which makes the comparison with experiment so relevant and her approach important. The close quantitative agreement she was able to get with the experiments (several of which were motivated by the theory) is particularly encouraging for this approach to chemotherapy regimens for various cancers, but not, unfortunately for brain tumours.

Appendix A. General Results for the Laplacian Operator in Bounded Domains

In Chapter 2, Section 2.9, we used the result that a function $u(x)$ with $u_x = 0$ on $x = 0, 1$ satisfies

$$\int_0^1 u_{xx}^2 \, dx \geq \pi^2 \int_0^1 u_x^2 \, dx \tag{A4.1}$$

and the more general result

$$\int_B | \nabla^2 \mathbf{u} |^2 \, d\mathbf{r} \geq \mu \int_{\partial B} \| \nabla \mathbf{u} \|^2 \, d\mathbf{r}, \tag{A4.2}$$

where B is a finite domain enclosed by the simply connected surface ∂B on which zero-flux (Neumann) conditions hold; namely, $\mathbf{n} \cdot \nabla \mathbf{u} = 0$ where $\mathbf{n}$ is the unit outward normal to ∂B. In (A4.2), μ is the least positive eigenvalue of $\nabla^2 + \mu$ for B with Neumann conditions on ∂B and where $\| \cdot \|$ denotes a Euclidean norm. By the Euclidean norm here we mean, for example,

$$\| \nabla \mathbf{u} \| = \max_{r \in B} \left[\sum_{i,j} \left(\frac{\partial u_i}{\partial x_j} \right)^2 \right]^{1/2} \tag{A4.3}$$

$$\mathbf{r} = (x_j), \quad j = 1, 2, 3; \quad \mathbf{u} = (u_i), \quad i = 1, 2, \ldots, n.$$

We prove these standard results in this section: (A4.1) is a special case of (A4.2) in which $\mathbf{u}$ is a single scalar and $\mathbf{r}$ a single space variable.

By way of illustration we first derive the one-dimensional result (A4.1) in detail and then prove the general result (A4.2).

Consider the equation for the scalar function $w(x)$, a function of the single space variable x, given by

$$w_{xx} + \mu w = 0, \tag{A4.4}$$

where μ represents the general eigenvalue for solutions of this equation satisfying Neumann conditions on the boundaries; namely,

$$w_x(x) = 0 \quad \text{on} \quad x = 0, 1. \tag{A4.5}$$

The orthonormal eigenfunctions $\{\phi_k(x)\}$ and eigenvalues $\{\mu_k\}$, where $k = 0, 1, 2, \ldots$, for (A4.4) and (A4.5) are

$$\phi_k(x) = \cos \mu_k^{1/2} x, \quad \mu_k = k^2\pi^2, \quad k = 0, 1, \ldots. \tag{A4.6}$$

Any function $w(x)$, such as we are interested in, satisfying the zero-flux conditions (A4.5) can be written in terms of a series (Fourier) expansion of eigenfunctions $\phi_k(x)$ and so also can derivatives of $w(x)$, which we assume exist. Let

$$w_{xx}(x) = \sum_{k=0}^{\infty} a_k \phi_k(x) = \sum_{k=0}^{\infty} a_k \cos(k\pi x), \tag{A4.7}$$

where, in the usual way,

$$a_k = 2\int_0^1 w_{xx}(x)\cos(k\pi x)\,dx, \quad k > 0$$

$$a_0 = \int_0^1 w_{xx}(x)\,dx = [w_x(x)]_0^1 = 0.$$

Then, integrating (A4.7) twice and using conditions (A4.5) gives

$$w(x) = \sum_{k=1}^{\infty} -\frac{a_k}{\mu_k}\phi_k(x) + b_0\phi_0,$$

where b_0 and ϕ_0 are constants. Thus, since $a_0 = 0$,

$$\begin{aligned}
\int_0^1 w_x^2(x)\,dx &= [ww_x]_0^1 - \int_0^1 ww_{xx}\,dx \\
&= -\int_0^1 ww_{xx}\,dx \\
&= \int_0^1 \left[\sum_{k=1}^{\infty} \frac{a_k}{\mu_k}\cos(k\pi x)\right]\left[\sum_{k=1}^{\infty} a_k \cos(k\pi x)\right] dx \\
&\quad + b_0\phi_0 \int_0^1 \left[\sum_{k=1}^{\infty} a_k \cos(k\pi x)\right] dx \\
&= \frac{1}{2}\sum_{k=1}^{\infty} \frac{a_k^2}{\mu_k} \\
&\le \frac{1}{2\mu_1}\sum_{k=1}^{\infty} a_k^2 \\
&= \frac{1}{\mu_1}\int_0^1 w_{xx}^2\,dx = \frac{1}{\pi^2}\int_0^1 w_{xx}^2\,dx,
\end{aligned}$$

which is (A4.1); μ_1 is the smallest positive eigenvalue μ_k for all k.

The proof of the general result (A4.2) simply mirrors the one-dimensional scalar version.

Again let the sequence $\{\boldsymbol{\phi}_k(\mathbf{r})\},\ k = 0, 1, 2, \ldots$ be the orthonormal eigenvector functions of

$$\nabla^2 \mathbf{w} + \mu \mathbf{w} = 0,$$

where $\mathbf{w}(\mathbf{r})$ is a vector function of the space variable $\mathbf{r}$ and μ is the general eigenvalue. Let the corresponding eigenvalues for the $\{\boldsymbol{\phi}_k\}$ be the sequence $\{\mu_k\},\ k = 0, 1, \ldots,$ where they are so ordered that $\mu_0 = 0, 0 < \mu_1 < \mu_2 \cdots$. Note in this case also that $\boldsymbol{\phi}_0 =$ constant.

Let $\mathbf{w}(\mathbf{r})$ be a function defined for $\mathbf{r}$ in the domain B and satisfying the zero-flux conditions $\mathbf{n} \cdot \nabla \mathbf{w} = 0$ for $\mathbf{r}$ on ∂B. Then we can write

$$\begin{aligned} \nabla^2 \mathbf{w} &= \sum_{k=0}^{\infty} a_k \boldsymbol{\phi}_k(\mathbf{r}), \\ a_k &= \int_B \langle \nabla^2 \mathbf{w}, \boldsymbol{\phi}_k \rangle \, d\mathbf{r}, \\ a_0 &= \langle \boldsymbol{\phi}_0, \int_B \nabla^2 \mathbf{w} \, d\mathbf{r} \rangle = \langle \boldsymbol{\phi}_0, \int_{\partial B} \nabla \mathbf{w} \, d\mathbf{r} \rangle = 0. \end{aligned} \tag{A4.8}$$

Here $\langle \cdot \rangle$ denotes the inner (scalar) product. Integrating $\nabla^2 \mathbf{w}$ twice we get

$$\mathbf{w}(\mathbf{r}) = \sum_{k=1}^{\infty} -\frac{a_k}{\mu_k} \boldsymbol{\phi}_k(\mathbf{r}) + b_0 \boldsymbol{\phi}_0,$$

where b_0 and $\boldsymbol{\phi}_0$ are constants. With this expression together with that for $\nabla^2 \mathbf{w}$ we have, on integrating by parts,

$$\begin{aligned} \int_B \| \nabla \mathbf{w} \|^2 \, d\mathbf{r} &= \int_{\partial B} \langle \mathbf{w}, \mathbf{n} \cdot \nabla \mathbf{w} \rangle d\mathbf{r} - \int_B \langle \mathbf{w}, \nabla^2 \mathbf{w} \rangle d\mathbf{r} \\ &= \sum_{k=1}^{\infty} \frac{a_k^2}{\mu_k} \\ &\leq \frac{1}{\mu_1} \sum_{k=1}^{\infty} a_k^2 \\ &= \frac{1}{\mu_1} \int_B | \nabla^2 \mathbf{w} |^2 d\mathbf{r}, \end{aligned}$$

which gives the result (A4.2) since μ_1 is the least positive eigenvalue.

Bibliography

[1] N.S. Adzick and M.T. Longaker, editors. *Fetal Wound Healing*. Elsevier, New York, 1991.

[2] K.I. Agladze and V.I. Krinskii. Multi-armed vortices in an active chemical medium. *Nature*, 286:424–426, 1982.

[3] K.I. Agladze, E.O. Budrene, G. Ivanitsky, and V.I. Krinskii. Wave mechanisms of pattern formation in microbial populations. *Proc. R. Soc. Lond. B*, 253:131–135, 1993.

[4] P. Alberch. Ontogenesis and morphological diversification. *Amer. Zool.*, 20:653–667, 1980.

[5] P. Alberch. Developmental constraints in evolutionary processes. In J.T. Bonner, editor, *Evolution and Development, Dahlem Conference Report*, volume 20, pages 313–332. Springer-Verlag, Berlin-Heidelberg-New York, 1982.

[6] P. Alberch. The logic of monsters: evidence for internal constraint in development and evolution. *Geo. Bios, Mémoire Spéciale*, 12:21–57, 1989.

[7] P. Alberch and E. Gale. Size dependency during the development of the amphibian foot. Colchicine induced digital loss and reduction. *J. Embryol. Exp. Morphol.*, 76:177–197, 1983.

[8] B. Alberts, D. Bray, J. Lewis, M. Raff, K. Roberts, and J.D. Watson. *Molecular Biology of The Cell (3rd edition)*. Garland, New York and London, 1994.

[9] M.A. Allessie, F.I.M. Bonke, and F.G.J. Schopman. Circus movement in rabbit atrial muscle as a mechanism of tachycardia. *Circ. Res.*, 33:54–62, 1973.

[10] M.A. Allessie, F.I.M. Bonke, and F.G.J. Schopman. Circus movement in rabbit atrial muscle as a mechanism of tachycardia. II. The role of nonuniform recovery of excitability in the occurrence of unidirectional block, as studied with multiple microelectrodes. *Circ. Res.*, 39:168–177, 1976.

[11] M.A. Allessie, F.I.M. Bonke, and F.G.J. Schopman. Circus movement in rabbit atrial muscle as a mechanism of tachycardia. III. The 'leading circle' concept: a new model of circus movement in cardiac tissue without the involvement of an anatomical obstacle. *Circ. Res.*, 41:9–18, 1977.

[12] W. Alt and D.A. Lauffenburger. Transient behaviour of a chemotaxis system modelling certain types of tissue inflammation. *J. Math. Biol.*, 24:691–722, 1987.

[13] E.C. Alvord, Jr. Simple model of recurrent gliomas. *J. Neurosurg.*, 75:337–338, 1991.

[14] E.C. Alvord, Jr. Is necrosis helpful in grading of gliomas? *J. Neuropathol. and Exp. Neurology*, 51:127–132, 1992.

[15] E.C. Alvord, Jr. and C.M. Shaw. Neoplasms affecting the nervous system in the elderly. In S. Duckett, editor, *The Pathology of the Aging Human Nervous System*, pages 210–281. Lea and Febiger, Philadelphia, 1991.

[16] V. R. Amberger, T. Hensel, N. Ogata, and M. E. Schwab. Spreading and migration of human glioma and rat C6 cells on central nervous system myelin *in vitro* is correlated with tumor malignancy and involves a metalloproteolytic activity. *Cancer Res.*, 58:149–158, 1998.

[17] T. Amemiya, S. Káár, P. Kettunen, and K. Showalter. Spiral wave formation in three-dimensional excitable media. *Phys. Rev. Lett.*, 77:3244–3247, 1996.

[18] R.M. Anderson, H.C. Jackson, R.M. May, and A.M. Smith. Population dynamics of fox rabies in Europe. *Nature*, 289:765–771, 1981.

[19] J. Andersson, A.-K. Borg-Karlson, and C. Wiklund. Sexual cooperation and conflict in butterflies: A male-transferred anti-aphrodisiac reduces harassment of recently mated females. *Proc. R. Soc. Lond. B*, 267:1271–1275, 2000.

[20] J. Ando and A. Kamiya. Flow-dependent regulation of gene expression in vascular endothelial cells. *Japanese Heart J.*, 37:19–32, 1996.

[21] J. Ando, T. Komatsuda, C. Ishikawa, and A. Kamiya. Fluid shear stress enhanced DNA synthesis in cultured endothelial cells during repair of mechanical denudation. *Biorheology*, 27:675–684, 1990.

[22] J. Ando, H. Nomura, and A. Kamiya. The effect of fluid shear stress on the migration and proliferation of cultured endothelial cells. *Microvascular Res.*, 33:62–70, 1987.

[23] L. Andral, M. Artois, M.F.A. Aubert, and J. Blancou. Radio-tracking of rabid foxes. *Comp. Immun. Microbiol. Infect. Dis.*, 5:285–291, 1982.

[24] J.L. Aragón, C. Varea, R.A. Barrio, and P.K. Maini. Spatial patterning in modified Turing systems: application to pigmentation patterns on marine fish. *Forma*, 13:213–221, 1998.

[25] C. Archer, P. Rooney, and L. Wolpert. The early growth and morphogenesis of limb cartilage. In J. Fallon and A. Kaplan, editors, *Limb Development and Regeneration*, pages 267–276, part A. A.R. Liss, New York, 1983.

[26] P. Arcuri and J.D. Murray. Pattern sensitivity to boundary and initial conditions in reaction-diffusion models. *J. Math. Biol.*, 24:141–165, 1986.

[27] B.T. Arriaza, P. Cárdenas-Arroyo, E. Kleiss, and J.W. Verano. South American mummies: culture and disease. In A. Cockburn, E. Cockburn, and T.A. Reyman, editors, *Mummies, Diseases and Ancient Cultures*, pages 190–236. Cambridge University Press, Cambridge, UK, 1998.

[28] M. Artois and N.F.A. Aubert. Structure des populations (age et sexe) de renard en zones indemnés ou atteintés de rage. *Comp. Immun. Microbiol. Infect. Dis.*, 5:237–245, 1982.

[29] G. Asaad and B. Shapiro. Hallucinations: theoretical and clinical overview. *Amer. J. Psychiatry*, 143:1088–1097, 1986.

[30] M. Aubert. Current status of animal rabies in France. *Medicine Tropicale*, 57:45–51, 1997.

[31] P.J. Bacon, editor. *Population Dynamics of Rabies in Wildlife*. Academic, New York, 1985.

[32] J.T. Bagnara and M.E. Hadley. *Chromatophores and Colour Change: The Comparative Physiology of Animal Regenration*. Prentice-Hall, New Jersey, 1973.

[33] J.B.L. Bard. A unity underlying the different zebra striping patterns. *J. Zool. (Lond.)*, 183:527–539, 1977.

[34] J.B.L. Bard. A model for generating aspects of zebra and other mammalian coat patterns. *J. Theor. Biol.*, 93:363–385, 1981.

[35] J.B.L. Bard. *Morphogenesis: The Cellular and Molecular Processes of Developmental Anatomy*. Cambridge University Press, Cambridge, UK, 1990.

[36] M. Barinaga. Looking to development's future. *Science*, 266:561–564, 1994.

[37] F.R. Barkalow, R.B. Hamilton, and R.F. Soots. The vital statistics of an unexploited gray squirrel population. *J. Wildl. Mgmnt.*, 34:489–500, 1970.

[38] F.S. Barkalow. A record Grey squirrell litter. *J. Mammal.*, 48:141, 1967.

[39] R.D. Barnes. *Invertebrate Zoology*. Saunders, Philadelphia, 1980.

[40] V.H. Barocas and R.T. Tranquillo. Biphasic theory and in vitro assays of cell-fibril mechanical interactions in tissue-equivalent gels. In V.C. Mow, F. Guilak, R. Tran-Son-Tay, and R.M. Hochmuth, editors, *Cell Mechanics and Cellular Engineering*, volume 119. Springer-Verlag, New York, 1994.

[41] V.H. Barocas and R.T. Tranquillo. An isotropic biphasic theory of tissue-equivalent mechanics: the interplay among cell traction, fibrillar network deformation, fibril alignment and cell contact guidance. *J. Biomech. Eng.*, 119:137–145, 1997a.

[42] V.H. Barocas and R.T. Tranquillo. A finite element solution for the anisotropic biphasic theory of tissue-equivalent mechanics: the effect of contact guidance on isometric cell traction measurement. *J. Biomech. Eng.*, 119:261–268, 1997b.

[43] V.H. Barocas, A.G. Moon, and R.T. Tranquillo. The fibroblast-populated collagen microsphere assay of cell traction force—Part 2: Measurement of the cell traction parameter. *J. Biomech. Eng.*, 117:161–170, 1995.

[44] J. Barrat and M.F. Aubert. Current status of fox rabies in Europe. *Onderstepoort J. Veterinary Res.*, 60:357–363, 1993.

[45] R.A. Barrio, C. Varea, and J.L. Aragón. A two-dimensional numerical study of spatial pattern formation in interacting systems. *Bull. Math. Biol.*, 61:483–505, 1999.

[46] W.M. Bement, P. Forscher, and M.S. Mooseker. A novel cytoskeletal structure involved in purse string wound closure and cell polarity maintenance. *J. Cell Biol.*, 121:565–578, 1993.

[47] E. Ben-Jacob. From snowflake formation to growth of bacterial colonies II: Cooperative formation of complex colonial patterns. *Contemporary Physics*, 38:205–241, 1997.

[48] E. Ben-Jacob, I. Cohen, I. Golding, and Y. Kozlovsky. Modeling branching and chiral colonial patterning of lubricating bacteria. In P.K. Maini and H.G. Othmer, editors, *Mathematical Models for Biological Pattern Formation*, pages 211–253. Springer-Verlag, New York, 2000.

[49] E. Ben-Jacob, O. Shochet, I. Cohen, A. Tenenbaum, A. Czirók, and T. Vicsek. Cooperative strategies in formation of complex bacterial patterns. *Fractals*, 3:849–868, 1995.

[50] G. Ben-Yu, A.R. Mitchell, and B.D. Sleeman. Spatial effects in a two-dimensional model of the budworm-balsam fir ecosystem. *Comp. and Maths. with Appls. (B)*, 12:1117–1132, 1986.

[51] D.E. Bentil. *Aspects of Dynamic Pattern Formation in Embryology and Epidemiology*. PhD thesis, University of Oxford, 1990.

[52] D.E. Bentil and J.D. Murray. Pattern selection in biological pattern formation mechanisms. *Appl. Maths. Letters*, 4:1–5, 1991.

[53] D.E. Bentil and J.D. Murray. On the mechanical theory of biological pattern formation. *Physica D*, 63:161–190, 1993.

[54] C. Berding. On the heterogeneity of reaction-diffusion generated patterns. *Bull. Math. Biol.*, 49:233–252, 1987.

[55] J. Bereiter-Hahn. Epidermal cell migration and wound repair. In J. Bereiter-Hahn, A.G. Matoltsy, and K.S. Richards, editors, *Biology of the Integument*, volume 2 (*Vertebrates*), pages 443–471. Springer-Verlag, Berlin-Heidelberg-New York, 1986.

[56] H.C. Berg. *Random Walks in Biology*. Princeton University Press, Princeton, NJ, 1983.

[57] H.C. Berg and L. Turner. Chemotaxis of bacteria in glass capillary arrays. *Biophys. J.*, 58:919–930, 1990.

[58] C.N. Bertolami, V. Shetty, J.E. Milavec, D.G. Ellis, and H.M. Cherrick. Preparation and evaluation of a nonpropietary bilayer skin subsitute. *Plastic and Reconstructive Surg.*, 87:1089–1098, 1991.

[59] J. Blancou. Ecology and epidemiology of fox rabies. *Rev. Infect. Dis.*, 10(Suppl. 4):S606–S609, 1988.

[60] F.G. Blankenberg, R.L. Teplitz, W. Ellis, M.S. Salamat, B.H. Min, L. Hall, D.B. Boothroyd, I.M. Johnstone, and D.R. Enzmann. The influence of volumetric tumor doubling time, DNA ploidy, and histologic grade on survival of patients with intracranial astrocytomas. *Amer. J. Neuroradiology*, 16:1001–1012, 1995.

[61] K. Boegel, H. Moegle, F. Steck, W. Krocza, and L. Andral. Assessment of fox control in areas of wildlife rabies. *Bull. WHO*, 59:269–279, 1981.

[62] T. Boehm, J. Folkman, T. Browder, and M.S. O'Reilly. Antiangiogenic therapy of experimental cancer does not induce acquired drug resistance. *Nature*, 390:404–407, 1997.

[63] S. Bonotto. *Acetabularia* as a link in the marine food chain. In S. Bonotto, F. Cinelli, and R. Billiau, editors, *Proc. 6th Intern. Symp. on Acetabulria. Pisa, 1984*, pages 67–80, Mol, Belgium, 1985. Belgian Nuclear Center, C.E.N.-S.C.K.

[64] W. Born. Monsters in Art. *CIBA Symp.*, 9:684–696, 1947.

[65] R.H. Brady. The causal dimension of Goethe's morphology. *J. Social Biol. Struct.*, 7:325–344, 1984.

[66] P.M. Brakefield and V. French. Eyespot development on butterfly wings: the epidermal response to damage. *Dev. Biol.*, 168:98–111, 1995.

[67] D. Bray, editor. *Cell Movements*. Garland Publishing, New York, 1992.

[68] J.H. Breasted. *Edwin Smith Surgical Papyrus*. University of Chicago Press, Chicago, 1930.

[69] M.P. Brenner, L.S. Levitov, and E.O. Budrene. Physical mechanisms for chemotactic pattern formation by bacteria. *Biophys. J.*, 74:1677–1693, 1998.

[70] J.F. Bridge and S.E. Angrist. An extended table of roots of $J_n'(x)Y_n(bx) - J_n(bx)Y_n'(x) = 0$. *Math. Comp.*, 16:198–204, 1962.

[71] N.F. Britton. *Reaction-Diffusion Equations and Their Applications to Biology*. Academic, New York, 1986.

[72] N.F. Britton and J.D. Murray. Threshold wave and cell-cell avalanche behaviour in a class of substrate inhibition oscillators. *J. Theor. Biol.*, 77:317–332, 1979.

[73] G. Brugal and J. Pelmont. Existence of two chalone-like substances in intestinal extract from the adult newt, inhibiting embryonic intestinal cell proliferation. *Cell Tiss. Kinet.*, 8:171–187, 1975.

[74] E.O. Budrene and H.C. Berg. Complex patterns formed by motile cells of *Escherichia coli*. *Nature*, 349:630–633, 1991.

[75] E.O. Budrene and H.C. Berg. Dynamics of formation of symmetrical patterns of chemotactic bacteria. *Nature*, 376:49–53, 1995.

[76] B. Bunow, J.-P. Kernevez, G. Joly, and D. Thomas. Pattern formation by reaction-diffusion instabilities: application to morphogenesis in *Drosophila*. *J. Theor. Biol.*, 84:629–649, 1980.

[77] P.C. Burger, E.R. Heinz, T. Shibata, and P. Kleihues. Topographic anatomy and CT corrrelations in the untreated glioblastoma multiforme. *J. Neurosurg.*, 68:698–704, 1988.

[78] P. K. Burgess, P. M. Kulesa, J. D. Murray, and E. C. Alvord, Jr. The interaction of growth rates and diffusion coefficients in a three-dimensional mathematical model of gliomas. *J. Neuropath. and Exp. Neurology*, 56(6):704–713, June 1997.

[79] R. Burton. *The Anatomy of Melancholy*. J.M. Dent, London, 1652.

[80] H.M. Byrne and M.A.J. Chaplain. Mathematical models for tumour angiogenesis: numerical simulations and nonlinear wave solutions. *Bull. Math. Biol.*, 57:461–486, 1995.

[81] H.M. Byrne and M.A.J. Chaplain. On the role of cell-cell adhesion in models for solid tumour growth. *Math. Comp. Modelling*, 24:1–17, 1996.

[82] R. S. Cantrell and C. Cosner. The effects of spatial heterogeneity in population dynamics. *J. Math. Biol.*, 29:315–338, 1991.

[83] G.A. Carpenter. Bursting phenomena in excitable membranes. *SIAM J. Appl. Math.*, 36:334–372, 1979.

[84] S.B. Carroll, J. Gates, D.N. Keyes, S.W. Paddock, G.R.F. Panganiban, J.E. Selegue, and J.A. Williams. Pattern formation and eyespot determination in butterfly wings. *Science*, 265:109–114, 1994.

[85] H.S. Carslaw and J.C. Jaeger. *Conduction of Heat in Solids*. Clarendon Press, Oxford, second edition, 1959.

[86] V. Castets, E. Dulos, J. Boissonade, and P. De Kepper. Experimental evidence of a sustained standing Turing-type nonequilibrium chemical pattern. *Phys. Rev. Lett.*, 64:2953–2956, 1990.

[87] M.A.J. Chaplain and A.R.A. Anderson. Modelling the growth and form of capillary networks. In M.A.J. Chaplain, G.D. Singh, and J.C McLachlan, editors, *On Growth and Form. Spatio-Temporal Pattern Formation in Biology*, pages 225–249. John Wiley, New York, 1999.

[88] M.A.J. Chaplain, G.D. Singh, and J.C. McLachlan, editors. *On Growth and Form. Spatio-Temporal Pattern Formation in Biology*. John Wiley, New York, 1999.

[89] G. Chauvet. Hierarchical functional organisation of formal biological systems: a dynamical approach. I, II and III. *Phil Trans. Roy. Soc. Lond. B*, 339:425–481, 1993.

[90] W.F. Chen. Mechanism of retraction of the trailing edge during fibroblast movement. *J. Cell Biol.*, 90:198–200, 1981.

[91] W.F. Chen and E. Mizuno. *Nonlinear Analysis in Soil Mechanics*. Elsevier, New York, 1990.

[92] M. R. Chicoine and D. L. Silbergeld. Assessment of brain tumor cell motility *in vivo* and *in vitro*. *J. Neurosurg.*, 82:615–622, 1995.

[93] D.G. Christopherson. Note on the vibration of membranes. *Quart. J. Math. Oxford Ser.*, 11:63–65, 1940.

[94] C.M. Chuong and G.M. Edelman. Expression of cell-adhesion molecules in embryonic induction. I, Morphogenesis of nestling feathers. *J. Cell Biol.*, 101:1009–1026, 1985.

[95] M. Cinotti. *The Complete Works of Bosch*. Rizzoli, New York, 1969.

[96] R.A.F. Clark. Cutaneous tissue repair: basic biological considerations. *J. Amer. Acad. Dermatol.*, 13:701–725, 1985.

[97] R.A.F. Clark. Overview and general considerations of wound repair. In R.A.F. Clark and P.M. Henson, editors, *The Molecular and Cellular Biology of Wound Repair*, pages 3–33. Plenum, New York, 1988.

[98] R.A.F. Clark. Wound repair. *Curr. Op. Cell Biol.*, 1:1000–1008, 1989.

[99] R.A.F. Clark. Cutaneous wound repair. In L.A. Goldsmith, editor, *Physiology, Biochemistry, and Molecular Biology of the Skin*, pages 576–601. Oxford University Press, New York, 1991.

[100] R.A.F. Clark and P.M. Henson, editors. *The Molecular and Cellular Biology of Wound Repair*. Plenum, New York, 1988.

[101] T. Clutton-Brock. Mammalian mating systems. *Proc. R. Soc. Lond. B*, 236:339–372, 1989.

[102] G. Cocho, R. Pérez-Pascual, J.L. Rius, and F. Soto. Discrete systems, cell-cell interactions and color pattern of animals. I. Conflicting dynamics and pattern formation. II. Clonal theory and cellular automata. *J. Theor. Biol.*, 125:419–447, 1987.

[103] E.A. Coddington and N. Levinson. *Theory of Ordinary Differential Equations*. McGraw-Hill, New York, 1972.

[104] D.S. Cohen and J.D. Murray. A generalized diffusion model for growth and dispersal in a population. *J. Math. Biol.*, 12:237–249, 1981.

[105] D.S. Cohen, J.C. Neu, and R.R. Rosales. Rotating spiral wave solutions of reaction-diffusion equations. *SIAM J. Appl. Math.*, 35:536–547, 1978.

[106] D. L. Collins, A. P. Zijdenbos, V. Kollokian, J. G. Sled, N. J. Kabani, C. J. Holmes, and A. C. Evans. Design and construction of a realistic digital brain phantom. *IEEE Trans. Medical Imaging*, 17(3):463–468, June 1998.

[107] J. Cook. *Mathematical Models for Dermal Wound Healing: Wound Contraction and Scar Formation*. PhD thesis, Department of Applied Mathematics, University of Washington, Seattle, WA, 1995.

[108] J. Cook, D. E. Woodward, P. Tracqui, and J. D. Murray. Resection of gliomas and life expectancy. *J. Neuro-Oncol.*, 24:131, 1995.

[109] J.D. Cowan. Some remarks on channel bandwidths for visual contrast detection. *Bull. Neurosci. Res.*, 15:492–515, 1977.

[110] J.D. Cowan. Spontaneous symmetry breaking in large-scale nervous activity. *Intl. J. Quantum Chem.*, 22:1059–1082, 1982.

[111] J.D. Cowan. Brain mechanisms underlying visual hallucinations. In D. Paines, editor, *Emerging Syntheses in Science*. Addison-Wesley, New York, 1987.

[112] S.C. Cowin. Wolff's law of trabecular architecture at remodelling equilibrium. *J. Biomech. Engr.*, 108:83–88, 1986.

[113] S.C. Cowin, A.M. Sadegh, and G.M. Luo. An evolutionary Wolff law for trabecular architecture. *J. Biomech. Engr.*, 114:129–136, 1992.

[114] E.J. Crampin, E.A. Gaffney, and P.K. Maini. Reaction diffusion on growing domains: scenarios for robust pattern formation. *Bull. Math. Biol.*, 61:1093–1120, 1999.

[115] J. Crank. *The Mathematics of Diffusion*. Clarendon Press, Oxford, 1975.

[116] C.E. Crosson, S.D. Klyce, and R.W. Beuerman. Epithelial wound closure in the rabbbit cornea wounds. *Invest. Ophthalmol. Vis. Sci.*, 27:464–73, 1986.

[117] G.C. Cruywagen. *Tissue Interaction and Spatial Pattern formation*. PhD thesis, University of Oxford, 1992.

[118] G.C. Cruywagen and J.D. Murray. On a tissue interaction model for skin pattern formation. *J. Nonlinear Sci.*, 2:217–240, 1992.

[119] G.C. Cruywagen, P. Kareiva, M.A. Lewis, and J.D. Murray. Competition in a spatially heterogeneous environment: modelling the risk of spread of a genetically engineered population. *Theor. Popul. Biol.*, 49:1–38, 1996.

[120] G.C. Cruywagen, P.K. Maini, and J.D. Murray. Sequential pattern formation in a model for skin morphogenesis. *IMA J. Maths. Appl. in Medic. and Biol.*, 9:227–248, 1992.

[121] G.C. Cruywagen, P.K. Maini, and J.D Murray. Sequential and synchronous skin pattern formation. In H.G. Othmer, P.K. Maini, and J.D. Murray, editors, *Experimental and Theoretical Advances in Biological Pattern Formation*, volume 259 of *NATO ASI Series A: Life Sciences*, pages 61–64. Plenum, New York, 1993.

[122] G.C. Cruywagen, P.K. Maini, and J.D. Murray. Travelling waves in a tissue interaction model for skin pattern formation. *J. Math. Biol.*, 33:193–210, 1994.

[123] G.C. Cruywagen, P.K. Maini, and J.D. Murray. An envelope method for analyzing sequential pattern formation. *SIAM J. Appl. Math.*, 61:213–231, 2000.

[124] G.C. Cruywagen, D.E. Woodward, P. Tracqui, G.T. Bartoo, J.D. Murray, and E.C. Alvord, Jr. The modeling of diffusive tumours. *J. Biol. Systems*, 3(4):937–945, 1995.

[125] H. Cummins and C. Midlo. *Fingerprints, Palms and Soles. An Introduction to Dermatoglyphics*. Blakiston, Philadelphia, 1943.

[126] A.I. Dagg. External features of giraffe. *Extrait de Mammalia*, 32:657–669, 1968.

[127] T.F. Dagi. The management of head trauma. In S.H. Greenblatt, editor, *A History of Neurosurgery*, pages 289–344. American Association of Neurological Surgeons, Park Ridge, IL, 1997.

[128] F.W. Dahlquist, P. Lovely, and D.E. Koshland. Qualitative analysis of bacterial migration in chemotaxis. *Nature, New Biol.*, 236:120–123, 1972.

[129] P.D. Dale, J.A. Sherratt, and P.K. Maini. Corneal epithelial wound healing. *J. Biol. Sys.*, 3:957–965, 1995.

[130] P.D. Dale, J.A. Sherratt, and P.K. Maini. A mathematical model for collagen fibre formation during foetal and adult dermal wound healing. *Proc. R. Soc. Lond. B*, 263:653–660, 1996.

[131] J.C. Dallon and H.G. Othmer. A discrete cell model with adaptive signalling for aggregation of *Dictyostelium discoideum*. *Phil. Trans. R. Soc. Lond. B*, 352:391–417, 1997.

[132] J.C. Dallon and H.G. Othmer. A continuum analysis of the chemotactic signal seen by *Dictyostelium discoideum*. *J. Theor. Biol*, 194:461–484, 1998.

[133] J.C. Dallon, J.A. Sherratt, and P.K. Maini. Mathematical modelling of extracellular matrix dynamics using discrete cells: fiber orientation and tissue regeneration. *J. Theor. Biol*, 199:449–471, 1999.

[134] R.J. D'Amato, M.S. Loughmman, E. Flynn, and J. Folkman. Thalidomide is an inhibitor of angiogenesis. *Proc. Nat. Acad. Sci. (U.S.)*, 91:4082–4085, 1994.

[135] S. Danjo, J. Friend, and R.A. Throft. Conjunctival epithelium in healing of corneal epithelial wounds. *Invest. Opthalmol. Vis. Sci.*, 28:1445–1449, 1987.

[136] C. Darwin. *The Origin of Species*. John Murray, London, sixth edition, 1873.

[137] D. Davidson. The mechanism of feather pattern development in the chick. I. The time of determination of feather position. II. Control of the sequence of pattern formation. *J. Embryol. Exp. Morph.*, 74:245–273, 1983.

[138] P. De Kepper, Q. Ouyang, J. Boissonade, and J.C. Roux. Sustained coherent spatial structures in a quasi-1D reaction-diffusion system. *React. Kinet. Cat. Lett.*, 42:275–288, 1990.

[139] P. De Kepper, J.-J. Perraud, B. Rudovics, and E. Dulos. Experimental study of stationary Turing patterns and their interaction with traveling waves in a chemical system. *Intern. J. Bifurcation & Chaos*, 4:1215–1231, 1994.

[140] G. Dee and J.S. Langer. Propagating pattern selection. *Phys. Rev. Letters*, 50:383–386, 1983.

[141] D.C. Deeming and M.W.J. Ferguson. Environmental regulation of sex determination in reptiles. *Phil. Trans. R. Soc. Lond. B*, 322:19–39, 1988.

[142] D.C. Deeming and M.W.J. Ferguson. The mechanism of temperature dependent sex determination in crocodilians: a hypothesis. *Am. Zool.*, 29:973–985, 1989a.

[143] D.C. Deeming and M.W.J. Ferguson. In the heat of the nest. *New Scientist*, 25:33–38, 1989b.

[144] D.C. Deeming and M.W.J. Ferguson. Morphometric analysis of embryonic development in *Alligator mississippiensis, Crocodylus johnstoni* and *Crocodylus porosus*. *J. Zool. Lond.*, 221:419–439, 1990.

[145] Daniel Defoe. In E.W. Brayley, editor, *A Journal of the Plague Year; or Memorials of the Great Pestilence in London in 1665*. Thomas Tegg, London, 1722.

[146] P. Delvoye, P. Wiliquet, J.L. Leveque, B. Nusgens, and C. Lapiere. Measurement of mechanical forces generated by skin fibroblasts embedded in a three-dimensional collagen gel. *J. Invest. Dermatol.*, 97:898–902, 1991.

[147] E.J. Denton and D.M. Rowe. Bands against stripes on the backs of mackerel *Scomber scombrus L. Proc. R. Soc. Lond. B*, 265:1051–1058, 1998.

[148] D. Dhouailly. Formation of cutaneous appendages in dermoepidermal recombination between reptiles, birds and mammals. *Wilhelm Roux Arch. EntwMech. Org.*, 177:323–340, 1975.

[149] D. Dhouailly, M. Hardy, and P. Sengel. Formation of feathers on chick foot scales: a stage-dependent morphogenetic response to retinoic acid. *J. Embryol. Exp. Morphol.*, 58:63–78, 1980.

[150] R. Dillon and H.G. Othmer. A mathematical model for outgrowth and spatial patterning of the vertebrate limb bud. *J. Theor. Biol.*, 197:295–330, 1999.

[151] M.R. Duffy, N.F. Britton, and J.D. Murray. Spiral wave solutions of practical reaction-diffusion systems. *SIAM J. Appl. Math.*, 39:8–13, 1980.

[152] P. Duffy, J. Wolf, et al. Possible person-to-person transmission of Creitzfeldt–Jakob disease. *N. Engl. J. Med.*, 290:692–693, 1974.

[153] S.R. Dunbar. Travelling wave solutions of diffusive Lotka–Volterra equations. *J. Math. Biol.*, 17:11–32, 1983.

[154] S.R. Dunbar. Travelling wave solutions of diffusive Lotka–Volterra equations: a heteroclinic connection in R^4. *Trans. Amer. Math. Soc.*, 268:557–594, 1984.

[155] M.G. Dunn, F.H. Silver, and D.A. Swann. Mechanical analysis of hypertropic scar tissue: structural basis for apparent increased rigidity. *J. Investig. Derm.*, 84:9–13, 1985.

[156] G.M. Edelman. Cell adhesion molecules in the regulation of animal form and tissue pattern. *Annu. Rev. Cell Biol.*, 2:81–116, 1986.

[157] B.B. Edelstein. The dynamics of cellular differentiation and associated pattern formation. *J. Theor. Biol.*, 37:221–243, 1972.

[158] L. Edelstein-Keshet and G.B. Ermentrout. Models for contact-mediated pattern formation: cells that form parallel arrays. *J. Math. Biol.*, 29:33–58, 1990.

[159] L. Edelstein-Keshet and G.B. Ermentrout. Models for the length distributions of actin filaments: I. Simple polymerization and fragmentation. *Bull. Math. Biol.*, 60:449–475, 1998.

[160] A.G. Edmund. Dentition. In C. Gans, A.d'A. Bellairs, and T.S. Parson, editors, *Biology of the Reptilia I*, volume *Morphology A*, pages 115–200. Academic, London, 1960a.

[161] A.G. Edmund. Evolution of dental patterns in the lower vertebrates. In *Evolution: Its Science and Doctrine*. *R. Soc. Can. Studia Varia. Ser. 4*, pages 45–52, 1960b.

[162] H.P. Ehrlich. Wound closure: evidence of cooperation between fibroblasts and collagen matrix. *Eye*, 2:149–157, 1989.

[163] M. Eisinger, S. Sadan, I.A. Silver, and R.B. Flick. Growth regulation of skin cells by epidermal cell-derived factors: implications for wound healing. *Proc. Nat. Acad. Sci. U.S.A.*, 85:1937–1941, 1988a.

[164] M. Eisinger, S. Sadan, R. Soehnchen, and I.A. Silver. Wound healing by epidermal-derived factors: Experimental and preliminary chemical studies. In A. Barbul, E. Pines, M. Caldwell, and T.K. Hunt, editors, *Growth Factors and Other Aspects of Wound Healing*, pages 291–302. Alan R. Liss, New York, 1988b.

[165] S.V. Elling and F.C. Powell. Physiological changes in the skin during pregnancy. *Clin. Dermatol.*, 15:35–43, 1997.

[166] T. Elsdale and F. Wasoff. Fibroblast cultures and dermatoglyphics: the topology of two planar patterns. *Wilhelm Roux Arch.*, 180:121–147, 1976.

[167] I.R. Epstein and K. Showalter. Nonlinear chemical dynamics: oscillations, patterns, and chaos. *J. Phys. Chem.*, 100:13132–13147, 1996.

[168] C.A. Erickson. Analysis of the formation of parallel arrays in BHK cells in vitro. *Exp. Cell Res.*, 115:303–315, 1978.

[169] B. Ermentrout, J. Campbell, and G. Oster. A model for shell patterns based on neural activity. *The Veliger*, 28:369–388, 1986.

[170] G.B. Ermentrout. Stable small amplitude solutions in reaction-diffusion systems. *Q. Appl. Math.*, 39:61–86, 1981.

[171] G.B. Ermentrout. Stripes or spots? Nonlinear effects in bifurcation of reaction diffusion equations on the square. *Proc. R. Soc. Lond. A*, 434:413–417, 1991.

[172] G.B. Ermentrout and J. Cowan. A mathematical theory of visual hallucination patterns. *Biol. Cybern.*, 34:137–150, 1979.

[173] G.B. Ermentrout and L. Edelstein-Keshet. Models for the length distributions of actin filaments: II. Polymerization and fragmentation by gelsolin acting together. *Bull. Math. Biol.*, 60:477–503, 1998.

[174] C.R. Etchberger, M.A. Ewert, J.B. Phillips, and C.E. Nelson. Environmental and maternal influences on embryonic pigmentation in a turtle (*Trachemys scripta elegans*). *J. Zool. Lond.*, 230:529–539, 1993.

[175] R.F. Ewer. *The Carnivores*. Cornell University Press, Ithaca, NY, 1973.

[176] M.W.J. Ferguson. The structure and composition of the eggshell and embryonic membranes of *Alligator mississippiensis*. *Trans. Zool. Soc. Lond.*, 36:99–152, 1981a.

[177] M.W.J. Ferguson. The structure and development of the palate in *Alligator mississippiensis*. *Arch. Oral Biol.*, 26:427–443, 1981b.

[178] M.W.J. Ferguson. Developmental mechanisms in normal and abnormal palate formation with particular reference to aetiology, pathogenesis and prevention of cleft palate. *Brit. J. Orthodont.*, 8(3):115–137, 1981c.

[179] M.W.J. Ferguson. Review: The value of the American alligator (*Alligator mississippiensis*) as a model for research in craniofacial development. *J. Craniofacial Genetics*, 1:123–144, 1981d.

[180] M.W.J. Ferguson. Reproductive biology and embryology of the crocodilians. In C. Gans, F. Billet, and P. Maderson, editors, *Biology of the Reptilia*, volume 14A, pages 329–491. John Wiley, New York, 1985.

[181] M.W.J. Ferguson. Palate development. *Development Suppl.*, 103:41–61, 1988.

[182] M.W.J. Ferguson. Craniofacial malformations: towards a molecular understanding. *Nature Genetics*, 6:329–330, 1994.

[183] M.W.J. Ferguson and G.F. Howarth. Marsupial models of scarless fetal wound healing. In N.S. Adzick and M.T. Longaker, editors, *Fetal Wound Healing*, pages 95–124. Elsevier, New York, 1991.

[184] J.A. Feroe. Existence and stability of multiple impulse solutions of a nerve equation. *SIAM J. Appl. Math.*, 42:235–246, 1982.

[185] I. Ferrenq, L. Tranqui, B. Vailhé, P.Y. Gumery, and P. Tracqui. Modelling biological gel contraction by cells: Mechanocellular formulation and cell traction force quantification. *Acta Biotheoretica*, 45:267–293, 1997.

[186] R.J. Field and M. Burger, editors. *Oscillations and Travelling Waves in Chemical Systems*. John Wiley, New York, 1985.

[187] R.A. Fisher. The wave of advance of advantageous genes. *Ann. Eugenics*, 7:353–369, 1937.

[188] J. Folkman. Anti-angiogenesis: new concept for therapy of solid tumors. *Ann. Surg.*, 175:409–416, 1972.

[189] J. Folkman. The vascularization of tumors. *Sci. Amer.*, 234:58–73, 1976.

[190] J. Folkman. Clinical applications of research on angiogenesis. *New Eng. J. Med.*, 333:1757–1763, 1995.

[191] J. Folkman and C. Haudenschild. Angiogenesis *in vitro*. *Nature*, 288:551–556, 1980.

[192] J. Folkman and M. Klagsbrun. Angiogeneic factors. *Science*, 235:442–447, 1987.

[193] J. Folkman and A. Moscona. Role of cell shape in growth control. *Nature*, 273:345–349, 1978.

[194] R.M. Ford and D.A. Lauffenburger. Analysis of chemotactic bacterial distributions in population migration assays using a mathematical model applicable to steep or shallow attractant gradients. *Bull. Math. Biol.*, 53:721–749, 1991.

[195] J.S. Forrester, M. Fishbein, T.R. Helfan, and J. Fagin. A paradigm for restenosis based on cell biology: clues for the development of new preventive therapies. *J. Amer. Coll. Cardiology*, 17:758–769, 1993.

[196] A.C. Fowler. The effect of incubation time distribution on the extinction characteristics of a rabies epizootic. *Bull. Math. Biol.*, 62:633–655, 2000.

[197] J.M. Frantz, B.M. Dupuy, H.E. Kaufman, and R.W. Beuerman. The effect of collagen shields on epithelial wound healing in rabbits. *Am. J. Ophthalmol.*, 108:524–8, 1989.

[198] F. Fremuth. Chalones and specific growth factors in normal and tumor growth. *Acta Univ. Carol. Mongr.*, 110, 1984.

[199] V. French. Pattern formation on butterfly wings. In M.A.J. Chaplain, G.D. Singh, and J.C. McLachlan, editors, *On Growth and Form. Spatio-Temporal Pattern Formation in Biology*, pages 31–46. John Wiley, New York, 1999.

[200] V. French and P.M. Brakefield. Eyespot development on butterfly wings: The focal signal. *Dev. Biol.*, 168:112–123, 1995.

[201] R.R. Frerichs and J. Prawda. A computer simulation model for the control of rabies in an urban area of Colombia. *Management Science*, 22:411–421, 1975.

[202] Y.C. Fung. *Biomechanics. Mechanical Properties of Living Tissue*. Springer-Verlag, Berlin, 1993.

[203] Y.C. Fung and S.Q. Liu. Change of residual strains in arteries due to hypertrophy caused by aortic constriction. *Circ. Research*, 65:1340–1349, 1989.

[204] Y.C. Fung and S.Q. Liu. Changes of zero-stress state of rat pulmonary arteries in hypotoxic hypertension. *J. Appl. Physiol.*, 70:2455–2470, 1991.

[205] D.W. Furnas, M. Ashraf Sheikh, P. van den Hombergh, and I.M. Nunda. Traditional craniotomies of the Kisi tribe of Kenya. *Annals Plastic Surg.*, 15:538–556, 1985.

[206] G. Gabbiani and G. Majno. Dupuytren's contracture: fibroblast contraction? An ultrastructural study. *Amer. J. Pathol.*, 66:131–146, 1972.

[207] W.J. Gallin, C.-M. Chuong, L.H. Finkel, and G.M. Edelman. Antibodies to liver cell adhesion molecules perturb inductive interactions and alter feather pattern and structure. *Proc. Natl. Acad. Sci. USA*, 83:8235–8239, 1986.

[208] P. Garnerin and A.-J. Hazout, S. Valleron. Estimation of two epidemiological parameters of fox rabies: the length of incubation period and the dispersion distance of cubs. *Ecol. Mod.*, 33:123–135, 1986.

[209] L. E. Gaspar, B. J. Fisher, D. R. Macdonald, D. V. LeBer, E. C. Halperin, S. C. Schold, and J. G. Cairncross. Supratentorial malignant glioma: patterns of recurrence and implication for external beam local treatment. *Intern. J. Radiation Oncol. Biol. Phys.*, 24:55–57, 1992.

[210] V. Gáspár, J. Maselko, and K. Showalter. Transverse coupling of chemical waves. *Chaos*, 1:435–444, 1991.

[211] I. Geoffroy Saint-Hilaire. *Traité de Tératologie*, volume 1–3. Bailliére, Paris, 1836.

[212] A. Gerber. Die embryonale und postembryonale Pterylose der Alectromorphae. *Rev. Suisse Zool.*, 46:161–324, 1939.

[213] R.G. Gibbs. Travelling waves in the Belousov–Zhabotinskii reaction. *SIAM J. Appl. Math.*, 38:422–444, 1980.

[214] A. Gierer and H. Meinhardt. A theory of biological pattern formation. *Kybernetik*, 12:30–39, 1972.

[215] A. Giese and M. Westphal. Glioma invasion in the central nervous system. *Neurosurgery*, 39(2):235–252, 1996.

[216] A. Giese, L. Kluwe, B. Laube, H. Meissner, M. Berens, and M. Westphal. Migration of human glioma cells on myelin. *Neurosurgery*, 38(4):755–764, 1996a.

[217] A. Giese, B. Laube, S. Zapf, U. Mangold, and M. Westphal. Glioma cell adhesion and migration on human brain sections. *Anticancer Res.*, 18:2435–2448, 1998.

[218] A. Giese, M. A. Loo, N. Tran, D. Haskett, S. W. Coons, and M. E. Berens. Dichotomy of astrocytoma migration and proliferation. *Intern. J. Cancer*, 67:275–282, 1996b.

[219] A. Giese, R. Schroder, A. Steiner, and M. Westphal. Migration of human glioma cells in response to tumour cyst fluids. *Acta Neurochirurgica*, 138:1331–1340, 1996c.

[220] J.H. Goldie and A.J. Coldman. A mathematical model for realting the drug sensitivity of tumors to their spontaneous mutation rate. *Cancer Treatment Rep.*, 66:439, 1979.

[221] R. Goldschmidt. *Die quantitativen Grundlagen von Vererbung und Arbildung*. Springer-Verlag, Berlin, 1920.

[222] S. Goldstein and J.D. Murray. On the mathematics of exchange processes in fixed columns. III. The solution for general entry conditions, and a method of obtaining asymptotic expressions. IV. Limiting values, and correction terms, for the kinetic-theory solution with general entry conditions. V. The equilibrium-theory and perturbation solutions, and their connection with kinetic-theory solutions, for general entry conditions. *Proc. R. Soc. Lond. A*, 257:334–375, 1959.

[223] J. Gómez-Alonso. Rabies. a possible explanation for the vampire legend. *Amer. Acad. Neurology*, 51:856–859, 1998.

[224] B.C. Goodwin, J.D. Murray, and D. Baldwin. Calcium: the elusive morphogen in *Acetabularia*. In S. Bonotto, F. Cinelli, and R. Billiau, editors, *Proc. 6th Intern. Symp. on Acetabularia. Belgian Nuclear Center, C.E.N.-S.C.K. Mol, Belgium, 1984*, pages 101–108, Pisa, 1985.

[225] Gould, S.J. Anscheulich (Atrocious). *Natural History*, March:42–49, 2000.

[226] H. Green. Cultured cells for the treatment of disease. *Sci. Amer.*, 265(5):96–102, 1991.

[227] H. Green and J. Thomas. Pattern formation by cultured human epidermal cells: development of curved ridges resembling dermatoglyphs. *Science*, 200:1385–1388, 1978.

[228] J.M. Greenberg. Spiral waves for $\lambda - \omega$ systems. *Adv. Appl. Math.*, 2:450–455, 1981.

[229] S.H. Greenblatt, editor. *A History of Neurosurgery*. American Association of Neurological Surgeons, Park Ridge, IL, 1997.

[230] H.W. Greene. *Snakes: The Evolution of Mystery in Nature*. University of California Press, Berkeley, CA, 2000.

[231] C.T. Gregg. *Plague: An Ancient Disease in the Twentieth Century*. University of New Mexico Press, Albuquerque, 1985.

[232] I. Grierson, J. Joseph, M. Miller, and J.E. Day. Wound repair: the fibroblasts and the inhibition of scar formation. *Eye*, 2:135–148, 1988.

[233] P. Grindrod. *The Theory and Applications of Reaction-Diffusion Equations—Patterns and Waves*. Oxford University Press, New York, 1996.

[234] P. Grindrod, M.A. Lewis, and J.D. Murray. A geometrical approach to wave-type solutions of excitable reaction-diffusion systems. *Proc. R. Soc. Lond. A*, 433:151–164, 1991.

[235] P. Grindrod, J.D. Murray, and S. Sinha. Steady state spatial patterns in a cell-chemotaxis model. *J. Maths. Appl. Medic. and Biol.*, 6:69–79, 1989.

[236] C. Guidry. Extracellular matrix contraction by fibroblasts: peptide promoters and second messengers. *Cancer Metast. Rev.*, 11:45–54, 1992.

[237] C. Guidry and F. Grinnell. Contraction of hydrated collagen gels by fibroblasts: evidence for two mechanisms by which collagen fibrils are stabilized. *Collagen Rel. Res.*, 6:515–529, 1986.

[238] G.H. Gunaratne, Q. Ouyang, and H.L. Swinney. Pattern formation in the presence of symmetries. *Phys. Rev. E*, 50:2802–2820, 1994.

[239] W. Gurtler and E. Zimen. The use of baits to estimate fox numbers. *Comp. Immun. Microbiol. Infec. Dis.*, 5:277–283, 1982.

[240] E. Haeckel. *Die Radiolaren*. Georg von Reimer, Berlin, 1862. (Vol. I) 1862, (Vol. II) 1887.

[241] E. Haeckel. *Art Forms in Nature*. Dover, New York, 1974.

[242] P.S. Hagan. Spiral waves in reaction diffusion equations. *SIAM J. Appl. Math.*, 42:762–786, 1982.

[243] P.A. Hall and D.A. Levinson. Assessment of cell proliferation in histological material. *J. Clin. Pathology*, 43:184–192, 1990.

[244] V. Hamburger. Monsters in Nature. *CIBA Symposium*, 9:666–683, 1947.

[245] A.K. Harris. Traction, and its relations to contraction in tissue cell locomotion. In R. Bellairs, A. Curtis, and G. Dunn, editors, *Cell Behaviour*, pages 109–134. Cambridge University Press, Cambridge, UK, 1982.

[246] A.K. Harris, D. Stopak, and P. Warner. Generation of spatially periodic patterns by a mechanical instability: A mechanical alternative to the Turing model. *J. Embryol. Exp. Morph.*, 80:1–20, 1984.

[247] A.K. Harris, D. Stopak, and D. Wild. Fibroblast traction as a mechanism for collagen morphogenesis. *Nature*, 290:249–251, 1981.

[248] A.K. Harris, P. Ward, and D. Stopak. Silicon rubber substrata: a new wrinkle in the study of cell locomotion. *Science*, 208:177–179, 1980.

[249] L.G. Harrison, J. Snell, R. Verdi, D.E. Vogt, G.D. Zeiss, and B.D. Green. Hair morphogenesis in *Acetabularia mediterranea*: temperature-dependent spacing and models of morphogen waves. *Protoplasma*, 106:211–221, 1981.

[250] D. Hart, E. Shochat, and Z. Agur. The growth law of primary breast cancer as inferred from mammography screening trials data. *British J. Cancer*, 78:382–387, 1998.

[251] H. Hasimoto. Exact solution of a certain semi-linear system of partial differential equations related to a migrating predation problem. *Proc. Japan Acad.*, 50:623–627, 1974.

[252] A. Hastings, S. Harrison, and K. McCann. Unexpected spatial patterns in an insect outbreak match a predator diffusion model. *Proc. R. Soc. Lond. B*, 264:1837–1840, 1997.

[253] E. Hay. *Cell Biology of the Extracellular Matrix*. Plenum, New York, 1981.

[254] K. Hedges. Shamanistic aspects of California rock art. In L. Bean, editor, *California Indian Shamanism*, pages 67–88. Ballena, Menlo Park, CA, 1992.

[255] K. Hedges. Origines chamaniques de l'art rupestre dans l'Ouest Américain. *L'Anthropologie (Paris)*, 97:675–691, 1993.

[256] K. Henke. Vergleichende und experimentelle Untersuchungen an Lymatria zur Musterbildung auf dem Schmetterlingsfluegel. *Nachr. Akad. Wiss. Goettingen, Math.-Physik. (KI)*, pages 1–48, 1943.

[257] H. Hennings, K. Elgio, and O.H. Iversen. Delayed inhibition of epidermal DNA synthesis after injection of an aqueous skin extract (chalone). *Virchows Arch. Abt. B Zellpath.*, 4:45–53, 1969.

[258] I. Herán. *Animal Colouration: The Nature and Purpose of Colours in Invertebrates*. Hamlyn, London, 1976.

[259] G.J. Hergott, M. Sandig, and V.I. Kalnins. Cytoskeletal organisation of migrating retinal pigment epithelial cells during wound healing in organ culture. *Cell Motil*, 13:83–93, 1989.

[260] H. Hickerson. The Virginia deer and intertribal buffer zones in the upper Mississippi valley. In A. Leeds and A. Vayta, editors, *Man, Culture and Animals. The Role of Animals on Human Ecological Adjustments*, pages 43–65. Amer. Assoc. Adv. Sci., Washington, DC, 1965.

[261] J. Hinchliffe and D. Johnson. *The Development of the Vertebrate Limb*. Clarendon, Oxford, 1980.

[262] U.T. Hinderer. Prevention of unsatisfactory scarring. *Clinics in Plast. Surg.*, 4(2):199–205, 1977.

[263] N. Holder. Developmental constraints and the evolution of the vertebrate digit patterns. *J. Theor. Biol.*, 104:451–471, 1983.

[264] J. Holm. *Squirrels*. Whittet, London, 1987.

[265] M.J. Holmes and B.D. Sleeman. A mathematical model of tumour angiogenesis incorporating cellular traction and viscoelastic effects. *J. Theor. Biol.*, 202:95–112, 2000.

[266] R.L. Hoskinson and L.D. Mech. White-tailed deer migration and its role in wolf predation. *J. Wildl. Manag.*, 40:429–441, 1976.

[267] Y. Hosono. Singular perturbation analysis of travelling waves for diffusive Lotka–Volterra competitive models. In *Numerical and Applied Mathematics Part II (Paris, 1988) (IMACS Ann. Comput. Appl. Math., 1,2)*, pages 687–692, Baltzer, Basel, 1989.

[268] S.A. Houff and R.C. Burton. Human-to-human transmission of rabies virus by corneal transplantation. *N. Engl. J. Med.*, 300:603–604, 1979.

[269] L.N. Howard and N. Kopell. Slowly varying waves and shock structures in reaction-diffusion equations. *Studies in Appl. Math.*, 56:95–145, 1977.

[270] A.H. Howe. *A Theoretical Inquiry into the Physical Cause of Epidemic Diseases*. J. Churchill, London, 1865.

[271] J.B. Hoying and S.K. Williams. Measurement of endothelial cell migration using an improved linear migration assay. *Microcirculation*, 3(2):167–174, 1996.

[272] D.H. Hubel and T.N. Wiesel. Functional architecture of macaque monkey visual cortex. *Proc. R. Soc. Lond. B*, 198:1–59, 1977.

[273] D.H. Hubel, T.N. Wiesel, and S. LeVay. Plasticity of ocular dominance columns in monkey striate cortex. *Phil. Trans. R. Soc. Lond. B*, 278:131–163, 1977.

[274] J. Hubert. Embryology of the Squamata. In C. Gans and F. Billet, editors, *Biology of the Reptilia*, volume 14, pages 1–34. John Wiley, New York, 1985.

[275] J. Hubert and J.P. Dufaure. Table de developpment de la vipère aspic: *Vipera aspis*. *Bull. Soc. Zool. France*, 93:135–148, 1968.

[276] O. Hudlická and M.D. Brown. Physical forces and angiogenesis. In G.M. Rubanyi, editor, *Mechanoreception by the Vascular Wall*, pages 197–241. Futura, Mount Kisco, NY, 1993.

[277] A. Hunding. Turing structures of the second kind. In M.A.J. Chaplain, G.D. Singh, and J.C. McLachlan, editors, *On Growth and Form. Spatio-temporal Pattern Formation in Biology*, pages 75–88. John Wiley, New York, 1999.

[278] A. Hunding and R. Engelhardt. Early biological morphogenesis and nonlinear dynamics. *J. Theor. Biol.*, 173:401–413, 1995.

[279] A. Hunding and P.G. Sørensen. Size adaption of Turing prepatterns. *J. Math. Biol.*, 26:27–39, 1988.

[280] N. Ikeda, H. Yamamoto, and T. Sato. Pathology of the pacemaker network. *Math. Modelling*, 7:889–904, 1986.

[281] D.E. Ingber, D. Prusty, Z. Sun, H. Betensky, and N. Wang. Cell shape, cytoskeletal mechanics, and cell cycle control in angiogenesis. *J. Biomechanics*, 28:1471–1484, 1995.

[282] H.C. Jackson and L.G. Schneider. Rabies in the Federal Republic of Germany, 1950–81: the influence of landscape. *Bull. WHO*, 62:99–106, 1984.

[283] T.L. Jackson. *Mathematical Models in Two-Step Cancer Chemotherapy*. PhD thesis, Department of Applied Mathematics, University of Washington, Seattle, WA, 1998.

[284] T.L. Jackson, S.R. Lubkin, and J.D. Murray. Theoretical analysis of conjugate localization in two-step cancer treatment. *J. Math. Biol.*, 39:335–376, 1999a.

[285] T.L. Jackson, S.R. Lubkin, S.R. Siemens, N.O. Kerr, P.D. Senter, and J.D. Murray. Mathematical and experimental analysis of localization of anti-tumor anti-body-enzyme conjugates. *Br. J. Cancer*, 80:1747–1753, 1999b.

[286] T.L. Jackson, P.D. Senter, and J.D. Murray. Development and validation of a mathematical model to describe antibody enzyme conjugates. *J. Theor. Medic.*, 2:93–111, 1999c.

[287] P.A. Janmey, S. Hvidt, J. Peetermans, J. Lamb, J.D. Ferry, and T.P. Stoggel. Viscoelasticity of F-actin and F-actin/gelsolin complexes. *Biochemistry*, 27:8218–27, 1988.

[288] R.W. Jennings and T.K. Hunt. Overview of postnatal wound healing. In N.S. Adzick and M.T. Longaker, editors, *Fetal Wound Healing*, pages 25–52. Elsevier, New York, 1991.

[289] J.V. Jester, W.M. Petroll, W. Feng, J. Essepian, and H.D. Cavanagh. Radial keratotomy. 1. The wound healing process and measurement of incisional gape in two animal models using in vivo confocal microscopy. *Investig. Opthal. and Visual Sci.*, 33:3255–3270, 1992.

[290] D.W. Jordan and P. Smith. *Nonlinear Ordinary Differential Equations*. Oxford University Press, Oxford, third edition, 1999.

[291] A.K. Jowett, S. Vainio, M.W.J. Ferguson, P.T. Sharpe, and I. Thesleff. Epithelial-mesenchymal interactions are required for msx1 and msx2 gene expression in the developing murine molar tooth. *Development*, 117:461–470, 1993.

[292] A. Källén, P. Arcuri, and J.D. Murray. A simple model for the spatial spread and control of rabies. *J. Theor. Biol.*, 116:377–393, 1985.

[293] C. Kaplan, editor. *Rabies: The Facts*. Oxford University Press, Oxford, 1977.

[294] P. Kareiva. Population dynamics in spatially complex environments—Theory and data. *Phil. Trans. R. Soc. Lond. B*, 330:175–190, 1990.

[295] G.B. Karev. Digital dermatoglyphics of Bulgarians from northeastern Bulgaria. *Amer. J. Phys. Anthrop.*, 69:37–50, 1986.

[296] W.L. Kath and J.D. Murray. Analysis of a model biological switch. *SIAM J. Appl. Math.*, 45:943–955, 1986.

[297] S.A. Kauffman, R. Shymko, and K. Trabert. Control of sequential compartment in *Drosophila*. *Science*, 199:259–270, 1978.

[298] K. Kawasaki, A. Mochizuki, M. Matsushita, T. Umeda, and N. Shigesada. Modeling spatio-temporal patterns generated by *Bacillus subtilis*. *J. Theor. Biol.*, 188:177–185, 1997.

[299] M.J. Keeling and C.A. Gilligan. Bubonic plague: a metapopulation model of a zoonosis. *Proc. R. Soc. Lond. B*, 267:2219–2230, 2000.

[300] J. Keener and J. Sneyd. *Mathematical Physiology*. Springer, New York, 1998.

[301] J.P. Keener. Waves in excitable media. *SIAM J. Appl. Math.*, 39:528–548, 1980.

[302] J.P. Keener. A geometrical theory for spiral waves in excitable media. *SIAM J. Appl. Math.*, 46:1039–1056, 1986.

[303] J.P. Keener and J.J. Tyson. Spiral waves in the Belousov–Zhabotinskii reaction. *Physica D*, 21:307–324, 1986.

[304] E.F. Keller and G.M. Odell. Necessary and sufficient conditions for chemotactic bands. *Math. Biosci.*, 27:309–317, 1975.

[305] E.F. Keller and L.A. Segel. Initiation of slime mold aggregation viewed as an instability. *J. Theor. Biol.*, 26:399–415, 1970.

[306] E.F. Keller and L.A. Segel. Travelling bands of chemotactic bacteria: a theoretical analysis. *J. Theor. Biol.*, 30:235–248, 1971.

[307] P. J. Kelley and C. Hunt. The limited value of cytoreductive surgery in elderly patients with malignant gliomas. *Neurosurgery*, 34:62–67, 1994.

[308] R. Kellogg, M. Knoll, and J. Kugler. Form-similarity between phosphenes of adults and pre-school children's scribblings. *Nature*, 208:1129–1130, 1965.

[309] C.R. Kennedy and R. Aris. Traveling waves in a simple population model involving growth and death. *Bull. Math. Biol.*, 42:397–429, 1980.

[310] R.S. Kerbel. A cancer therapy resistant to resistance. *Nature*, 390:335–336, 1997.

[311] L.D. Ketchum, I.K. Cohen, and F.W. Masters. Hypertrophic scars and keloids: A collective review. *Plast. Recon. Surg.*, 53:140–154, 1974.

[312] J. Kevorkian. *Partial Differential Equations: Analytical Solution Techniques (2nd edition)*. Springer-Verlag, New York, 1999.

[313] J. Kevorkian and J.D. Cole. *Multiple Scale and Singular Perturbation Methods*. Springer-Verlag, New York, 1996.

[314] J. Kingdon. *East African Mammals. An Atlas of Evolution in Africa. IIIA. Carnivores*. Academic, London, 1978.

[315] J. Kingdon. *East African Mammals. An Atlas of Evolution in Africa. IIIB. Large mammals*. Academic, London, 1979.

[316] C.W. Kischer, J. Pindur, P. Krasovitch, and E. Kischer. Characteristics of granulation tissue which promote hypertrophic scarring. *Scan. Microscopy*, 4:877–888, 1990.

[317] C.W. Kischer, M.R. Shetlar, and M. Chvapil. Hypertrophic scars and keloids: a review and new concept concerning their origin. *Scan. Electron Microscopy*, 4:1699–1713, 1982.

[318] L.M. Klauber. *Rattlesnakes: Their Habits, Life Histories, and Influence on Mankind*. University of California Press, Berkeley, CA, 1998.

[319] M.R. Klee, H.D. Lux, and E.-J. Speckmann, editors. *Physiology, Pharmacology and Development of Epileptogeneic Phenomena*. Springer-Verlag, Berlin, Heidelberg, New York, 1991.

[320] H. Klüver. *Mescal and Mechanisms of Hallucinations*. University of Chicago Press, Chicago, 1967.

[321] A.J. Koch and H. Meinhardt. Biological pattern formation: from basic mechanisms to complex structures. *Rev. of Modern Phys.*, 66:1481–1507, 1994.

[322] S. Koga. Rotating spiral waves in reaction-diffusion systems-phase singularities of multi-armed spirals. *Prog. Theor. Phys.*, 67:164–178, 1982.

[323] J. Kolega. Effects of mechanical tension on protrusive activity and microfilament and intermediate filament organization in an epidermal epithelium moving in culture. *J. Cell Biol.*, 102:1400–11, 1986.

[324] E.J. Kollar. The induction of hair follicles in embryonic dermal papillae. *J. Invest. Dermatol.*, 55:374–378, 1970.

[325] M.S. Kolodney and R.B. Wysolmerski. Isometric contraction by fibroblasts and endothelial cells in tissue culture: a quantitative study. *J. Cell Biol.*, 117:73–82, 1992.

[326] S. Kondo and R. Asai. A reaction-diffusion wave on the skin of the marine angelfish *Pomacanthus*. *Nature*, 376:765–768, 1995.

[327] N. Kopell and L.N. Howard. Plane wave solutions to reaction-diffusion equations. *Studies in Appl. Math.*, 42:291–328, 1973.

[328] N. Kopell and L.N. Howard. Target patterns and spiral solutions to reaction-diffusion equations with more than one space dimension. *Adv. Appl. Math.*, 2:417–449, 1981.

[329] F. W. Kreth, P. C. Warnke, R. Scheremet, and C. B. Ostertag. Surgical resection and radiation therapy versus biopsy and radiation therapy in the treatment of glioblastoma multiforme. *J. Neurosurg.*, 78:762–766, May 1993.

[330] V.I. Krinsky. Mathematical models of cardiac arrhythmias (spiral waves). *Pharmac. Ther. (B)*, 3:539–555, 1978.

[331] V.I. Krinsky, A.B. Medvinskii, and A.V. Parfilov. Evolutionary autonomous spiral waves (in the heart). *Mathematical Cybernetics. Popular Ser. (Life Sciences)*, 8:1–48, 1986. In Russian.

[332] J.E. Kronmiller, W.B. Upholt, and E.J. Kollar. EGF antisense oligodeoxynucleotides block murine odontogenesis *in vitro*. *Dev. Biol.*, 147:485–488, 1991.

[333] A. Kühn and A. von Engelhardt. Über die Determination des Symmetriesystems auf dem Vorderflügel von Ephestia kuehniella. *Z. Wilhelm Roux Arch. Entw. Mech. Org.*, 130:660–703, 1933.

[334] P.M. Kulesa. *A Model Mechanism for the Initiation and Spatial Patterning of Teeth Primordia in the Alligator*. PhD thesis, Department of Applied Mathematics, University of Washington, Seattle, WA, 1995.

[335] P.M. Kulesa and J.D. Murray. Modelling the wave-like initiation of teeth primordia in the alligator. *Forma*, 10:259–280, 1995.

[336] P.M. Kulesa, G.C. Cruywagen, S.R. Lubkin, M.W.J. Ferguson, and J.D. Murray. Modelling the spatial patterning of teeth primordia in the alligator. *Acta Biotheoretica*, 44:349–358, 1996a.

[337] P.M. Kulesa, G.C. Cruywagen, S.R. Lubkin, P.K. Maini, J. Sneyd, M.W.J. Ferguson, and J.D. Murray. On a model mechanism for the spatial patterning of teeth primordia in the alligator. *J. Theor. Biol.*, 180:287–296, 1996b.

[338] P.M. Kulesa, G.C. Cruywagen, S.R. Lubkin, P.K. Maini, J. Sneyd, and J.D. Murray. Modelling the spatial patterning of the teeth primordia in the lower jaw of *Alligator mississippiensis*. *J. Biol. Systems*, 3:975–985, 1993.

[339] K. Kuramoto. Instability and turbulence of wavefronts in reaction-diffusion systems. *Prog. Theor. Phys.*, 63:1885–1903, 1980.

[340] K. Kuramoto and S. Koga. Turbulized rotating chemical waves. *Prog. Theor. Phys.*, 66:1081–1085, 1981.

[341] L. Landau and E. Lifshitz. *Theory of Elasticity*. Pergamon, New York, second edition, 1970.

[342] D.C. Lane, J.D. Murray, and V.S. Manoranjan. Analysis of wave phenomena in a morphogenetic mechanochemical model and an application to post-fertilisation waves on eggs. *IMA J. Math. Applied Medic. and. Biol.*, 4:309–331, 1987.

[343] K. Langer. On the anatomy and physiology of the skin. I. the cleavability of cutis (original 1862, in German). *Br. J. Plast. Surg.*, 31:3–8, 1978a.

[344] K. Langer. On the anatomy and physiology of the skin. II. Skin tension (original 1862, in German). *Br. J. Plast. Surg.*, 31:93–106, 1978b.

[345] K. Langer. On the anatomy and physiology of the skin. III. The elasticity of the cutis (original 1862, in German). *Br. J. Plast. Surg.*, 31:185–199, 1978c.

[346] K. Langer. On the anatomy and physiology of the skin. IV. The swelling capabilities of the skin (original 1862, in German). *Br. J. Plast. Surg.*, 31:185–199, 1978d.

[347] W.L. Langer. The Black Death. *Sci. Amer.*, pages 114–121, February 1964.

[348] I.R. Lapidis and R. Schiller. Model for the chemotactic response of a bacterial population. *Biophys. J.*, 16:779–789, 1976.

[349] F. Lara-Ochoa. A generalized reaction diffusion model for spatial structureformed by mobile cells. *Biosystems*, 17:35–50, 1984.

[350] F. Lara-Ochoa and J.D. Murray. A nonlinear analysis for spatial structure in a reaction-diffusion model. *Bull. Math. Biol.*, 45:917–930, 1983.

[351] D.A. Lauffenburger and C.R. Kennedy. Localised bacterial infection in a distributed model for tissue inflammation. *J. Math. Biol.*, 16:141–163, 1983.

[352] N.M. Le Douarin. *The Neural Crest*. Cambridge University Press, Cambridge, UK, 1982.

[353] B. Lee, L. Mitchell, and G. Buchsbaum. Rheology of the vitreous body. Part 1: Viscoelasticity of human vitreous. *Biorheology*, 29:521–533, 1993.

[354] B. Lee, L. Mitchell, and G. Buchsbaum. Rheology of the vitreous body: Part 2. Viscoelasticity of bovine and porcine vitreous. *Biorheology*, 31:327–338, 1994a.

[355] B. Lee, L. Mitchell, and G. Buchsbaum. Rheology of the vitreous body: Part 3. Concentration of electrolytes, collagen and hyaluronic acid. *Biorheology*, 31:339–351, 1994b.

[356] R. Lefever and O. Lejeune. On the origin of tiger bush. *Bull. Math. Biol.*, 59:263–294, 1997.

[357] O. Lejeune and M. Tlidi. A model for the explanation of vegetation stripes (tiger bush). *J. Veg. Sci.*, 10:201–208, 1999.

[358] T. Lenoir. The eternal laws of form: morphotypes and the conditions of existence in Goethe's biological thought. *J. Social Biol. Struct.*, 7:317–324, 1984.

[359] S.A. Levin. Models of population dispersal. In S. Busenberg and K. Cooke, editors, *Differential Equations and Applications to Ecology, Epidemics and Population Problems*, pages 1–18. Academic, New York, 1981a.

[360] S.A. Levin. The role of theoretical ecology in the description and understanding of populations in heterogeneous environments. *Amer. Zool.*, 21:865–875, 1981b.

[361] J. Levinton. Developmental constraints and evolutionary saltations: a discussion and critique. In G. Stebbins and F. Ayala, editors, *Genetics and Evolution*. Plenum, New York, 1986.

[362] A.E. Leviton and S.C. Anderson. Description of a new species of *Cyrtodactylus* from Afghanistan with remarks on the status of *Gymnodactylus longpipes* and *Cyrtodactylus fedtschenkoi*. *J. Herpes*, 18:270–276, 1984.

[363] M.A. Lewis. Variability, patchiness, and jump dispersal in the spread of an invading population. In D. Tilman and P. Kareiva, editors, *Spatial Ecology. The Role of Space in Population Dynamics and Interspecific Interactions*, pages 46–69. Princeton University Press, Princeton, NJ, 1997.

[364] M.A. Lewis and P. Moorcroft. ESS analysis of mechanistic models for territoriality: The value of signals in spatial resource partitioning. *J. Theor. Biol.*, 210:449–461, 2001.

[365] M.A. Lewis and J.D. Murray. Analysis of stable two-dimensional patterns in contractile cytogel. *J. Nonlin. Sci.*, 1:289–311, 1991.

[366] M.A. Lewis and J.D. Murray. Modelling territoriality and wolf-deer interactions. *Nature*, 366:738–740, 1993.

[367] M.A. Lewis and G. Schmitz. Biological invasion of an organism with separate mobile and stationary states: modeling and anlaysis. *Forma*, 11:1–25, 1996.

[368] M.A. Lewis, G. Schmitz, P. Kareiva, and J.T. Trevors. Models to examine containment and spread of genetically engineered organisms. *J. Mol. Ecol.*, 5:165–175, 1996.

[369] M.A. Lewis, K.A.J. White, and J.D. Murray. Analysis of a model for wolf territories. *J. Math. Biol.*, 35:749–774, 1997.

[370] J.D. Lewis-Williams and T.A. Dowson. The signs of all times. Entopic phenomena in upper palaeolithic art. *Current Anthropol.*, 29:201–245, 1988.

[371] B. C. Liang and M. Weil. Locoregional approaches to therapy with gliomas as the paradigm. *Current Opinion in Oncology*, 10:201–206, 1998.

[372] S. Lindow. Competitive exclusion of epiphytic bacteria. *Appl. Envt. Microbiol.*, 53:2520–2527, 1987.

[373] G. Lindquist. The healing of skin defects. an experimental study of the white rat. *Acta Chirurgica Scandinavica*, 94:1–163, 1946. Supplement 107.

[374] P.L. Lions. On the existence of positive solutions of semilinear elliptic equations. *SIAM. Rev.*, 24:441–467, 1982.

[375] C.D. Little, V. Mironov, and E.H. Sage, editors. *Vascular Morphogenesis: In Vivo, In Vitro and In Mente*. Birkhaüser, Boston, 1998.

[376] H.G. Lloyd. Past and present distribution of red and grey squirrels. *Mamm. Res.*, 13:69–80, 1983.

[377] H.G. Lloyd, B. Jensen, J.L. Van Haaften, F.J.J. Niewold, A. Wandeler, K. Boegel, and A.A. Arata. Annual turnover of fox populations in Europe. *Zbl. Vet. Med.*, 23:580–589, 1976.

[378] D.Z. Loesch. *Quantitative Dermatoglyphics: Classification, Genetics, and Pathology*. Oxford University Press, Oxford, 1983.

[379] M.T. Longaker and N.S. Adzick. The biology of fetal wound healing: A review. *Plastic and Reconstructive Surg.*, 87:788–798, 1991.

[380] I. Loudon, editor. *Biomathematics and Cell Kinetics*. Oxford University Press, Oxford, 1997.

[381] S.R. Lubkin and J.D. Murray. A mechanism for early branching in lung morphogenesis. *J. Math. Biol.*, 34:77–94, 1995.

[382] D. Ludwig, D.G. Aronson, and H.F. Weinberger. Spatial patterning of the spruce budworm. *J. Math. Biol.*, 8:217–258, 1979.

[383] A.S. Lyons and R.J. Petrucelli. *Medicine: An Illustrated History*. Harry N. Abrams, New York, 1978.

[384] D.W. MacDonald. *Rabies and Wildlife: A Biologist's Perspective*. Oxford University Press, Oxford, 1980.

[385] A. MacKenzie, M.W.J. Ferguson, and P.T. Sharpe. Expression patterns of the homeobox gene, Hox-8, in the mouse embryo suggest a role in specifying tooth initiation and shape. *Development*, 115:403–420, 1992.

[386] A. MacKenzie, J.L. Leeming, A.K. Jowett, M.W.J. Ferguson, and P.T. Sharpe. The homeobox gene, Hox-7.1 has specific regional and temporal expression patterns during early murine craniofacial embryogenesis, especially tooth development *in vivo* and *in vitro*. *Development*, 111:269–285, 1991.

[387] K. MacKinnon. Competition between red and grey squirrels. *Mamm. Res.*, 8:185–190, 1978.

[388] M.R. Madden, E. Nolan, J.L. Finkelstein, R.W. Yurt, J. Smeland, C.W. Goodwin, J. Hefton, and L. Staiano-Coico. Comparison of an occlusive and a semi-occlusive dressing and the effect of the wound eudate upon keratinocyte proliferation. *J. Trauma*, 29:924–31, 1989.

[389] P.F.A. Maderson. Some developmental problems of the reptilian integument. In C. Gans, F. Billet, and P.F.A. Maderson, editors, *Biology of the Reptilia*, volume 14, pages 523–598. John Wiley, New York, 1985.

[390] J.B. Madison and R.R. Gronwall. Influence of wound shape on wound contraction in horses. *Am. J. Vet. Res.*, 53:1575–1577, 1992.

[391] P.K. Maini. Travelling waves in biology, chemistry, ecology and medicine. Part 1. *FORMA (Special Issue: P.K. Maini, editor)*, 10:145–280, 1995.

[392] P.K. Maini. Travelling waves in biology, chemistry, ecology and medicine. Part 2. *FORMA (Special Issue: P.K. Maini, editor)*, 11:1–80, 1996.

[393] P.K. Maini. Bones, feathers, teeth and coatmarkings: a unified model. *Science Progress*, 80:217–229, 1997.

[394] P.K. Maini. Some mathematical models for biological pattern formation. In M.A.J. Chaplain, G.D. Singh, and J.C. McLachlan, editors, *On Growth and Form. Spatio-Temporal Pattern Formation in Biology*, pages 111–128. John Wiley, New York, 1999.

[395] P.K. Maini and J.D. Murray. A nonlinear analysis of a mechanical model for biological pattern formation. *SIAM J. Appl. Math.*, 48:1064–1072, 1988.

[396] P.K. Maini and H.G. Othmer, editors. *Mathematical Models for Biological Pattern Formation*. Springer-Verlag, New York, 2000.

[397] P.K. Maini, M.R. Myerscough, K.H. Winters, and J.D. Murray. Bifurcating spatially heterogeneous solutions in a chemotaxis model for biological pattern formation. *Bull. Math. Biol.*, 53:701–719, 1991.

[398] G. Majno. *The Healing Hand. Man and Wound in the Ancient World*. Harvard University Press, Cambridge, 1975.

[399] V.S. Manoranjan and A.R. Mitchell. A numerical study of the Belousov–Zhabotinskii reaction using Galerkin finite element methods. *J. Math. Biol.*, 16:251–260, 1983.

[400] D. Manoussaki. *Modelling Formation of Planar Vascular Networks in vitro*. PhD thesis. Department of Applied Mathematics, University of Washington, Seattle, WA, 1996.

[401] D. Manoussaki, S.R. Lubkin, R.B. Vernon, and J.D. Murray. A mechanical model for the formation of vascular networks in vitro. *Acta Biotheoretica*, 44:271–282, 1996.

[402] E.L. Margetts. Trepanation of the skull by the medicine-men of primitive cultures, with particular reference to present-day native East African practice. In D. Brothwell and A.T. Sandison, editors, *Diseases in Antiquity*, pages 673–701. Charles C. Thomas, Springfield, IL, 1967.

[403] P. Martin. Wound healing—Aiming for perfect skin regeneration. *Science*, 276:75–81, 1997.

[404] P. Martin and J. Lewis. The mechanics of embryonic skin wound healing-limb bud lesions in mouse and chick embryos. In N.S. Adzick and M.T. Longaker, editors, *Fetal Wound Healing*, pages 265–279. Elsevier, New York, 1991.

[405] P. Martin and J. Lewis. Actin cables and epidermal movement in embryonic wound healing. *Nature*, 360:179–183, 1992.

[406] M. Marusic, Z. Bajzer, J.P. Freyer, and S. Vuk-Pavlovic. Analysis of growth of multicellular tumour spheroids by mathematical models. *Cell Prolif.*, 27:73–94, 1994.

[407] H. Matano. Asymptotic behaviour and stability of solutions of semilinear diffusion equations. *Publ. Res. Inst. Math. Sci. Kyoto*, 15:401–454, 1979.

[408] Y. Matsukado, C.S. McCarthy, and J.W. Kernohan. The growth of glioblastoma multiforme (asytrocytomas, grades 3 and 4) in neurosurgical practice. *J. Neurosurg.*, 18:636–644, 1961.

[409] M.M. Matsushita, J. Wakita, H. Itoh, T. Arai, T. Matsuyama, H. Sakaguchi, and M. Mimura. Formation of colony patterns by a bacterial population. *Physica A*, 274:190–199, 1999.

[410] M.M. Matsushita, J. Wakita, H. Itoh, I. Rifols, T. Matsuyama, H. Sakaguchi, and M. Mimura. Interface growth and pattern formation in bacterial colonies. *Physica A*, 249:517–524, 1998.

[411] T. Matsuyama and M. Matsushita. Fractal morphogenesis by a bacterial cell population. *Crit. Rev. Microbiol.*, 19:117–135, 1993.

[412] C. McEvedy. The bubonic plague. *Sci. Amer.*, pages 74–79, February 1988.

[413] M.H. McGrath and R.H. Simon. Wound geometry and the kinetics of wound contraction. *Plast. and Reconst. Surg.*, 72:66–73, 1983.

[414] H.P. McKean. Nagumo's equation. *Adv. in Math.*, 4:209–223, 1970.

[415] B.K. McNab. Bio-energetics and the determination of home range size. *Am. Nat.*, 97:133–140, 1963.

[416] L.D. Mech. *The Ecology and Behavior of an Endangered Species*. Natural History Press, Garden City, NY, 1970.

[417] L.D. Mech. Wolf numbers in the Superior National Forest of Minnesota. Technical Report, US Forest Service, 1973. Research Paper NC-97.

[418] L.D. Mech. *The Way of the Wolf*. Voyageur, Stillwater, MN, 1991.

[419] H. Meinhardt. *Models of Biological Pattern Formation*. Academic, London, 1982.

[420] H. Meinhardt. Hierarchical inductions of cell states: a model for segmentation of *Drosophila*. *J. Cell Sci.*, 4:357–381, 1986. (Suppl.).

[421] H. Meinhardt. *The Algorithmic Beauty of Sea Shells*. Springer-Verlag, Berlin, 1995.

[422] H. Meinhardt. On pattern and growth. In M.A.J. Chaplain, G.D. Singh, and J.C. McLachlan, editors, *On Growth and Form. Spatio-Temporal Pattern Formation in Biology*, pages 129–148. John Wiley, New York, 1999.

[423] H. Meinhardt. Beyond spots and stripes: generation of more complex patterns and modifications and additions of the basic reaction. In P.K. Maini and H.G. Othmer, editors, *Mathematical Models for Biological Pattern Formation*, pages 143–164. Springer-Verlag, New York, 2000.

[424] H. Meinhardt and M. Klingler. A model for pattern generation on the shells of molluscs. *J. Theor. Biol.*, 126:63–89, 1987.

[425] J.H. Merkin, V. Petrov, S.K. Scott, and K. Showalter. Wave-induced chemical chaos. *Phys. Rev. Letters*, 76:546–549, 1996.

[426] S. Michelson and J. Leith. Autocrine and paracrine growth factors in tumor growth: a mathematical model. *Bull. Math. Biol.*, 53:639–656, 1991.

[427] S. Michelson, B.E. Miller, A.S. Glicksman, and J. Leith. Tumor micro-ecology and competitive interactions. *J. Theor. Biol.*, 128:233–246, 1987.

[428] A.S. Mikhailov and V.I. Krinsky. Rotating spiral waves in excitable media: The analytical results. *Physica D*, 9:346–371, 1983.

[429] M. Mimura and T. Tsujikawa. Aggregating pattern dynamics in a chemotaxis model including growth. *Physica A*, 230:499–543, 1996.

[430] M. Mimura and M. Yamaguti. Pattern formation in interacting and diffusing systems in population biology. *Adv. Biophys.*, 15:19–65, 1982.

[431] M. Mimura, H. Sakaguchi, and M. Matsushita. Reaction-diffusion modelling of bacterial colony patterns. *Physica A*, 282:283–303, 2000.

[432] M. Mina and E.J. Kollar. The induction of odontogenesis in non-dental mesenchyme combined with early murine mandibular arch epithelium. *Archs. Oral Biol.*, 32(2):123–127, 1987.

[433] J.E. Mittenthal and R.M. Mazo. A model for shape generation by strain and cell-cell adhesion in the epithelium of an arthropod leg segment. *J. Theor. Biol.*, 100:443–483, 1983.

[434] A. Mogilner and L. Edelstein-Keshet. Spatio-angular order in populations of self-aligning objects: formation of oriented patches. *Physica D*, 89:346–367, 1996.

[435] A. Mogilner and G.F. Oster. Cell motility driven by actin polimerization. *Biophys. J.*, 71:3030–3045, 1996.

[436] D. Mollison. Dependence of epidemic and population velocities on basic parameters. *Math. Biosci.*, 107:255–287, 1991.

[437] P.R. Montague and M.J. Friedlander. Morphogenesis and territorial coverage by isolated mammalian retinal ganglion cells. *J. Neurosci.*, 11:1440–1457, 1991.

[438] P. Moorcroft. *Territoriality and Carnivore Home Ranges*. PhD thesis, Princeton University, Princeton, NJ, 1997.

[439] P. Moorcroft and M.A. Lewis. *Home Range Patterns: Mechanistic Approaches to the Analysis of Animal Movement*. Princeton University Press, Princeton, NJ, 2001.

[440] P. Moorcroft, M.A. Lewis, and R. Crabtree. Analysis of coyote home range using a mechanistic home range model. *Ecology*, 80:1656–1665, 1999.

[441] L.H. Morgan. *Ancient Society*. Charles H. Kerr, Chicago, 1877.

[442] S.C. Müller, T. Plesser, and B. Hess. The structure of the core of the spiral wave in the Belousov–Zhabotinskii reaction. *Science*, 230:661–663, 1985.

[443] S.C. Müller, T. Plesser, and B. Hess. Two-dimensional spectrophotometry and pseudo-color representation of chemical patterns. *Naturwiss.*, 73:165–179, 1986.

[444] S.C. Müller, T. Plesser, and B. Hess. Two-dimensional spectrophotometry of spiral wave propagation in the Belousov–Zhabotinskii reaction. I. Experiments and digital representation. II. Geometric and kinematic parameters. *Physica D*, 24:71–96, 1987.

[445] J.D. Murray. Singular perturbations of a class of nonlinear hyperbolic and parabolic equations. *J. Maths. and Physics*, 47:111–133, 1968.

[446] J.D. Murray. Perturbation effects on the decay of discontinuous solutions of nonlinear first order wave equations. *SIAM J. Appl. Math.*, 19:273–298, 1970a.

[447] J.D. Murray. On the Gunn effect and other physical examples of perturbed conservation equations. *J. Fluid Mech.*, 44:315–346, 1970b.

[448] J.D. Murray. On Burgers' model equations for turbulence. *J. Fluid Mech.*, 59:263–279, 1973.

[449] J.D. Murray. Non-existence of wave solutions for a class of reaction diffusion equations given by the Volterra interacting-population equations with diffusion. *J. Theor. Biol.*, 52:459–469, 1975.

[450] J.D. Murray. On travelling wave solutions in a model for the Belousov–Zhabotinskii reaction. *J. Theor. Biol.*, 52:329–353, 1976.

[451] J.D. Murray. *Nonlinear Differential Equation Models in Biology*. Clarendon, Oxford, 1977.

[452] J.D. Murray. A pattern formation mechanism and its application to mammalian coat markings. In *'Vito Volterra' Symposium on Mathematical Models in Biology. Accademia dei Lincei, Rome, Dec. 1979*, volume 39 of *Lect. Notes in Biomathematics*, pages 360–399. Springer-Verlag, Berlin-Heidelberg-New York, 1980.

[453] J.D. Murray. On pattern formation mechanisms for Lepidopteran wing patterns and mammalian coat markings. *Phil. Trans. R. Soc. Lond. B*, 295:473–496, 1981a.

[454] J.D. Murray. A pre-pattern formation mechanism for animal coat markings. *J. Theor. Biol.*, 88:161–199, 1981b.

[455] J.D. Murray. Parameter space for Turing instability in reaction diffusion mechanisms: a comparison of models. *J. Theor. Biol.*, 98:143–163, 1982.

[456] J.D. Murray. On a mechanical model for morphogenesis: Mesenchymal patterns. In W. Jäger and J.D. Murray, editors, *Conference on: Modelling of Patterns in Space and Time, Heidelberg 1983*. Lecture Notes in Biomathematics series, 55:279–291, Springer-Verlag, Berlin-Heidelberg-New York, 1983.

[457] J.D. Murray. *Asymptotic Analysis*. Springer-Verlag, Berlin-Heidelberg-New York, second edition, 1984.

[458] J.D. Murray. How the leopard gets its spots. *Sci. Amer.*, 258(3):80–87, 1988.

[459] J.D. Murray. Modelling the pattern generating mechanism in the formation of stripes on alligators. In B. Simon, A. Truman, and I.M. Davies, editors, *IXth Intern. Congr. Mathematical Physics 1988*, pages 208–213, 1989. Adam Hilger, Bristol.

[460] J.D. Murray. Complex pattern formation and tissue interaction. In J. Demongeot and V. Capasso, editors, *1st Europ. Confer. on Applics. Maths. to Medic. and Biol. 1990*, pages 495–505, Winnipeg, Canada, 1993. Wuerz Publishing.

[461] J.D. Murray and G.C. Cruywagen. Threshold bifurcation in tissue interaction models for spatial pattern formation. *Proc. R. Soc. Lond. A*, 443:1–16, 1994.

[462] J.D. Murray and C.L. Frenzen. A cell justification for Gompertz' equation. *SIAM J. Appl. Math.*, 46:614–629, 1986.

[463] J.D. Murray and P.M. Kulesa. On a dynamic reaction-diffusion mechanism: the spatial patterning of teeth primordia in the alligator. *J. Chem. Soc., Faraday Trans.*, 92:2927–2932, 1996.

[464] J.D. Murray and P.K. Maini. A new approach to the generation of pattern and form in embryology. *Sci. Prog. (Oxf.)*, 70:539–553, 1986.

[465] J.D. Murray and M.R. Myerscough. Pigmentation pattern formation on snakes. *J. Theor. Biol.*, 149:339–360, 1991.

[466] J.D. Murray and G.F. Oster. Cell traction models for generating pattern and form in morphogenesis. *J. Math. Biol.*, 19:265–279, 1984a.

[467] J.D. Murray and G.F. Oster. Generation of biological pattern and form. *IMA J. Math. Appl. in Medic. and Biol.*, 1:51–75, 1984b.

[468] J.D. Murray and W.L. Seward. On the spatial spread of rabies among foxes with immunity. *J. Theor. Biol.*, 156:327–348, 1992.

[469] J.D. Murray, D.C. Deeming, and M.W.J. Ferguson. Size-dependent pigmentation-pattern formation in embryos of *Alligator mississippiensis*: Time of initiation of pattern generation mechanism. *Proc. R. Soc. Lond. B*, 239:279–293, 1990.

[470] J.D. Murray, P.K. Maini, and R.T. Tranquillo. Mechanical models for generating biological pattern and form in development. *Physics Reports*, 171:60–84, 1988.

[471] J.D. Murray, D. Manoussaki, S.R. Lubkin, and R.B. Vernon. A mechanical theory of *in vitro* vascular network formation. In C.D. Little, V. Mironov, and E.H. Sage, editors, *Vascular Morphogenesis: In Vivo, In Vitro and In Mente*, pages 173–188, Birkhaüser, Boston, 1998.

[472] J.D. Murray, G.F. Oster, and A.K. Harris. A mechanical model for mesenchymal morphogenesis. *J. Math. Biol.*, 17:125–129, 1983.

[473] J.D. Murray, E.A. Stanley, and D.L. Brown. On the spatial spread of rabies among foxes. *Proc. R. Soc. Lond. B*, 229:111–150, 1986.

[474] J.D. Murray and J.E.R. Cohen. On nonlinear convection dispersal effects in an interacting population model. *SIAM J. Appl. Math.*, 43:66–78, 1983.

[475] J.D. Murray and R.P. Sperb. Minimum domains for spatial patterns in a class of reaction diffusion equations. *J. Math. Biol.*, 18:169–184, 1983.

[476] J.D. Murray and K.R. Swanson. On the mechanical theory of biological pattern formation with applications to wound healing and angiogenesis. In M.A.J. Chaplain, G.D. Singh, and J.C. McLachlan, editors, *On Growth and Form: Spatio-Temporal Pattern Formation in Biology*, pages 251–285, John Wiley, Chichester, UK, 1999.

[477] J.D. Murray, J. Cook, S.R. Lubkin, and R.C. Tyson. Spatial pattern formation in biology: I. Dermal wound healing. II. Bacterial patterns. *J. Franklin Inst.*, 335:303–332, 1998.

[478] M.R. Myerscough and J.D. Murray. Analysis of propagating pattern in a chemotaxis system. *Bull. Math. Biol.*, 54:77–94, 1992.

[479] M.R. Myerscough, P.K. Maini, J.D. Murray, and K.H. Winters. Two-dimensional pattern formation in a chemotactic system. In T.L. Vincent, A.I. Mees, and L.S. Jennings, editors, *Dynamics of Complex Interconnected Biological Systems*, pages 65–83. Birkhauser, Boston, 1990.

[480] H. Nagawa and Y. Nakanishi. Mechanical aspects of the mesenchymal influence on epithelial branching morphogenesis of mouse salivary gland. *Development*, 101:491–500, 1987.

[481] B.N. Nagorcka. The role of a reaction-diffusion system in the initiation of skin organ primordia. I. The first wave of initiation. *J. Theor. Biol.*, 121:449–475, 1986.

[482] B.N. Nagorcka. A pattern formation mechanism to control spatial organisation in the embryo of *Drosophila melanogaster*. *J. Theor. Biol.*, 132:277–306, 1988.

[483] B.N. Nagorcka and D.A. Adelson. Pattern formation mechanisms in skin and hair: Some experimental tests. In M.A.J. Chaplain, G.D. Singh, and J.C. McLachlan, editors, *On Growth and Form: Spatio-Temporal Pattern Formation in Biology*, pages 89–110, John Wiley, Chichester, UK, 1999.

[484] B.N. Nagorcka and J.R. Mooney. The role of a reaction-diffusion system in the formation of hair fibres. *J. Theor. Biol.*, 98:575–607, 1982.

[485] B.N. Nagorcka and J.R. Mooney. The role of a reaction-diffusion system in the initiation of primary hair follicles. *J. Theor. Biol.*, 114:243–272, 1985.

[486] B.N. Nagorcka and J.R. Mooney. From stripes to spots: prepatterns which can be produced in the skin by reaction-diffusion systems. *IMA J. Math. Appl. Med. and Biol.*, 9:249–267, 1992.

[487] B.N. Nagorcka, V.S. Manoranjan, and J.D. Murray. Complex spatial patterns from tissue interactions—An illustrative model. *J. Theor. Biol.*, 128:359–374, 1987.

[488] J. M . Nazzaro and E. A. Neuwelt. The role of surgery in the management of supranterorial intermediate and high-grade astrocytomas in adults. *J. Neurosurg.*, 73:331–344, 1990.

[489] M.E. Nelson and L.D. Mech. Wolf predation risk associated with white-tailed deer movements. *Can. J. Zool.*, 69:2696–2699, 1991.

[490] P.C. Newell. Attraction and adhesion in the slime mold *Dictyostelium*. In J.E. Smith, editor, *Fungal Differentiation: A Contemporary Synthesis*, pages 43–71. Marcel Dekker, New York, 1983.

[491] H.F. Nijhout. Wing pattern formation in Lepidoptera: a model. *J. Exp. Zool.*, 206:119–136, 1978.

[492] H.F. Nijhout. Pattern formation in Lepidopteran wings: determination of an eyespot. *Devl. Biol.*, 80:267–274, 1980a.

[493] H.F. Nijhout. Ontogeny of the color pattern formation on the wings of Precis coenia (Lepidoptera: Nymphalidae). *Devl. Biol.*, 80:275–288, 1980b.

[494] H.F. Nijhout. Colour pattern modification by coldshock in Lepidoptera. *J. Embryol. Exp. Morph.*, 81:287–305, 1984.

[495] H.F. Nijhout. The developmental physiology of colour patterns in Lepidoptera. *Adv. Insect Physiol.*, 18:181–247, 1985a.

[496] H.F. Nijhout. Cautery-induced colour patterns in *Precis coenia* (Lepidoptera: Zool. Nymphalidae). *J. Embryol. Exp. Morph.*, 86:191–302, 1985b.

[497] H.F. Nijhout. *The Development and Evolution of Butterfly Wing Patterns*. Smithsonian Institution Press, Washington, DC, 1991.

[498] J.V. Noble. Geographic and temporal development of plagues. *Nature*, 250:726–728, 1974.

[499] B. Obrink. Epithelial cell adhesion molecules. *Exp. Cell Res.*, 163:1–21, 1986.

[500] G. Odell, G.F. Oster, B. Burnside, and P. Alberch. The mechanical basis for morphogenesis. *Dev. Biol.*, 85:446–462, 1981.

[501] M. Ohgiwara, M. Matsushita, and T. Matsuyama. Morphological changes in growth phenomena of bacterial colony patterns. *J. Phys. Soc. Japan*, 61:816–822, 1992.

[502] M. Okajima. A methodological approach to the development of epidermal ridges. *Prog. in Dermatol. Res.*, 20:175–188, 1982.

[503] M. Okajima and L. Newell-Morris. Development of dermal ridges in volar skin of fetal pigtailed macaques *Macaca nemestrina*. *Amer. J. Anat.*, 183:323–327, 1988.

[504] A. Okubo. *Diffusion and Ecological Problems: Mathematical Models*. Springer-Verlag, Berlin-Heidelberg-New York, 1980.

[505] A. Okubo. Dynamical aspects of animal grouping: swarms, schools, flocks and herds. *Adv. Biophys.*, 22:1–94, 1986.

[506] A. Okubo, P.K. Maini, M.H. Williamson, and J.D. Murray. On the spatial spread of the grey squirrel in Britain. *Proc. R. Soc. Lond. B*, 238:113–125, 1989.

[507] L. Olsen, J.A. Sherratt, and P.K. Maini. A mechanochemical model for adult dermal wound contraction and the permanence of the contracted tissue displacement profile. *J. Theor. Biol.*, 177:113–128, 1995.

[508] L. Olsen, J.A. Sherratt, and P.K. Maini. A mathematical model for fibro-proliferative wound healing disorders. *Bull. Math. Biol.*, 58:787–808, 1996.

[509] M.S. O'Reilly, T. Boehm, Y. Shing, N. Fukai, G. Vasios, W.S. Lane, E. Flynn, J.R. Birkhead, B.R. Olsen, and J. Folkman. Endostatin: an endogenous inhibitor of angiogenesis and tumor growth. *Cell*, 88:277–285, 1997.

[510] M.S. O'Reilly, L. Holmgren, C.C. Chen, and J. Folkman. Angiostatin induces and sustains dormancy of human primary tumors in mice. *Nature Medicine*, 2:689–692, 1996.

[511] P.J. Ortoleva and S.L. Schmidt. The structure and variety of chemical waves. In R.J. Field and M. Burger, editors, *Oscillations and Travelling Waves in Chemical Systems*, pages 333–418. John Wiley, New York, 1985.

[512] J.W. Osborn. New approach to Zahnreihen. *Nature, Lond.*, 225:343–346, 1970.

[513] J.W. Osborn. The ontogeny of tooth succession in *Lacerta vivpara Jacquin*. *Proc. R. Soc. Lond.*, B179:261–289, 1971.

[514] J.W. Osborn. Morphogenetic gradients: fields versus clones. In P.M. Butler and K.A. Joysey, editors, *Development, Function and Evolution of Teeth*, pages 171–201. Academic, London and New York, 1978.

[515] J.W. Osborn. A model simulating tooth morphogenesis without morphogenes. *J. Theor. Biol.*, 165:429–445, 1993.

[516] Gerold F. Oster. 'Phosphenes'—The patterns we see when we close our eyes are clues to how the eye works. *Sci. Amer.*, pages 82–88, February, 1970.

[517] G. F. Oster and G.M. Odell. The mechanochemistry of cytogels. *Physica D*, 12:333–350, 1984.

[518] G.F. Oster. On the crawling of cells. *J. Embryol. Exp. Morphol.*, 83:329–364, 1984. (Suppl.).

[519] G.F. Oster and P. Alberch. Evolution and bifurcation of developmental programs. *Evolution*, 36:444–459, 1982.

[520] G.F. Oster and J.D. Murray. Pattern formation models and developmental constraints. *J. Exp. Zool.*, 251:186–202, 1989.

[521] G.F. Oster, J.D. Murray, and A.K. Harris. Mechanical aspects of mesenchymal morphogenesis. *J. Embryol. Exp. Morphol.*, 78:83–125, 1983.

[522] G.F. Oster, J.D. Murray, and P.K. Maini. A model for chondrogenic condensations in the developing limb: the role of extracellular matrix and cell tractions. *J. Embryol. Exp. Morphol.*, 89:93–112, 1985a.

[523] G.F. Oster, J.D. Murray, and G.M. Odell. The formation of microvilli. In *Molecular Determinants of Animal Form*, pages 365–384. Alan R. Liss, New York, 1985b.

[524] G.F. Oster, N. Shubin, J.D. Murray, and P. Alberch. Evolution and morphogenetic rules. The shape of the vertebrate limb in ontogeny and phylogeny. *Evolution*, 42:862–884, 1988.

[525] H. Othmer. *Interactions of Reaction and Diffusion in Open Systems*. PhD thesis, Chemical Engineering Department and University of Minnesota, 1969.

[526] H.G. Othmer. Current problems in pattern formation. *Amer. Math. Assoc. Lects. on Math. in the Life Sciences*, 9:57–85, 1977.

[527] H.G. Othmer, P.K. Maini, and J.D. Murray, editors. *Mathematical Models for Biological Pattern Formation*. Plenum, New York, 1993.

[528] J.H. Ottaway. Normalization in the fitting of data by iterative methods: application to tracer kinetics and enzyme kinetics. *Biochem. J.*, 134:729–736, 1973.

[529] H. Otto. Die Beschuppung der Brevilinguir und Ascaleten. *Jenaische Zeit. Wiss.*, 44:193–252, 1908.

[530] Q. Ouyang and H.L. Swinney. Transition from a uniform state to hexagonal and striped Turing patterns. *Nature*, 352:610–612, 1991.

[531] Q. Ouyang, V. Castets, J. Boissonade, J.C. Roux, P. De Kepper, and H.L. Swinney. Sustained patterns in chlorite-iodide reactions in a one-dimensional reactor. *J. Chem. Phys.*, 95:352–360, 1990.

[532] Q. Ouyang, G.H. Gunaratne, and H.L. Swinney. Rhombic patterns: broken hexagonal symmetry. *Chaos*, 3:707–711, 1993.

[533] M.R. Owen and J.A. Sherratt. Pattern formation and spatiotemporal irregularity in a model for macrophage-tumour interactions. *J. Theor. Biol.*, 189:63–80, 1997.

[534] K.J. Painter. Models for pigment pattern formation in the skin of fishes. In P.K. Maini and H.G. Othmer, editors, *Mathematical Models for Biological Pattern Formation*, pages 59–82. Springer, New York, 2000.

[535] K.J. Painter, P.K. Maini, and H.G. Othmer. Stripe formation in juvenile *Pomacanthus* explained by a generalised Turing mechanism with chemotaxis. *Proc. Nat. Acad. Sci. (U.S.)*, 96:5549–5554, 1999.

[536] J.-L. Pallister. *Introduction to "On Monsters and Marvels" by Ambroise Paré*. University of Chicago Press, Chicago, 1982.

[537] A.M. Partanen, P. Ekblom, and I. Thesleff. Epidermal growth factor inhibits morphogenesis and cell differentiation in cultured mouse embryonic teeth. *Dev. Biol.*, 111:84–94, 1985.

[538] M. Pascual. Diffusion-induced chaos in a spatial predator-prey system. *Proc. R. Soc. Lond. B*, 251:1–7, 1993.

[539] P.P. Pastoret. Evolution of fox rabies in Belgium and the European Union. *Bull. et Mem. Acad. Roy. Medicine de Belgique*, 153:93–98, 1998.

[540] S. Patan, L.L. Munn, and R.K. Jain. Intussusceptive microvascular growth in a human colon adenocarcinoma xenograft: a novel mechanism of tumor angiogenesis. *Microvascular Research*, 51:229–249, 1996.

[541] E. Pate and H.G. Othmer. Applications of a model for scale-invariant pattern formation. *Differentiation*, 28:1–8, 1984.

[542] M. Patou. Analyse de la morphogenèse du pied des oiseaux a l'aise de melanges cellulaires interspecifiques. I. Étude morphologique. *J. Embryol. Exp. Morphol.*, 29:175–196, 1973.

[543] E.E. Peacock. *Wound Repair*. W.B. Saunders, Philapdelphia, 1984.

[544] R. Penrose. The topology of ridge systems. *Ann. Hum. Genet. Lond.*, 42:435–444, 1979.

[545] A.S. Perelson, P.K. Maini, J.D. Murray, J.M. Hyman, and G.F. Oster. Nonlinear pattern selection in a mechanical model for morphogenesis. *J. Math. Biol.*, 24:525–541, 1986.

[546] A.J. Perumpanani, D.L. Simmons, A.J.H. Gearing, K.M. Miller, G. Ward, J. Norbury, M. Scheemann, and J.A. Sherratt. Extracellular matrix-mediated chemotaxis can impede cell migration. *Proc. R. Soc. Lond. B*, 265:2347–2352, 1998.

[547] R. Peters and L.D. Mech. Scent-marking in wolves. *Am. Nat.*, 63:628–637, 1975.

[548] R.O. Peterson. Ecological studies of wolves on Isle Royale. Technical Report, School of Forestry, Michigan Technical University, 1999.

[549] W.M. Petroll, H.D. Cavanagh, P. Barry, P. Andrews, and J.V. Jester. Quantitative analysis of stress fibre orientation during corneal wound contraction. *J. Cell Sci.*, 104:353–363, 1993.

[550] V. Petrov, S.K. Scott, and K. Showalter. Excitability, wave reflection, and wave splitting in a cubic autocatalysis reaction-diffusion system. *Phil. Trans. R. Soc. A*, 347:631–642, 1994.

[551] B.R. Phillips, J.A. Quinn, and H. Goldfine. Random motility of swimming bacteria: Single cells compared to cell populations. *AIChE J.*, 40:334–348, 1994.

[552] G. J. Pilkington. Glioma heterogeneity *in vitro*: the significance of growth factors and gangliosides. *Neuropathol. Appl. Neurobiol.*, 18:434–442, 1992.

[553] G. J. Pilkington. The paradox of neoplastic glial cell invasion of the brain and apparent metastatic failure. *Anticancer Res.*, 17:4103–4106, 1997a.

[554] G. J. Pilkington. In vitro and in vivo models for the study of brain tumor invasion. *Anticancer Res.*, 17:4107–4110, 1997b.

[555] R.I. Pocock. Description of a new species of cheetah (*Acinonyx*). *Proc. R. Soc. Lond.*, 1927:245–252, 1927.

[556] T.D. Pollard. Actin. *Curr. Op. Cell Biol.*, 2:33–40, 1990.

[557] A. Portmann. *Animal Forms and Patterns. A Study of the Appearance of Animals. (English translation)*. Faber and Faber, London, 1952.

[558] C.S. Potten, W.J. Hume, and E.K. Parkinson. Migration and mitosis in the epidermis. *Br. J. Dermatol.*, 111:695–699, 1984.

[559] R.J. Price and R. Skalak. Circumferential wall stress as a mechanism for arteriolar rarefaction and proliferation in a network model. *Microvascular Research*, 47:188–202, 1994.

[560] T. Price and M. Pavelka. Evolution of a colour pattern: history, development, and selection. *J. Evol. Biol.*, 9:451–470, 1996.

[561] G. Prota. *Melanins and Melanogenesis*. Academic, London, 1992.

[562] E. Purcell. Life at low Reynolds number. *Amer. J. Phys.*, 45:1–11, 1977.

[563] G. Radice. The spreading of epithelial cells during wound closure in *Xenopus* larvae. *Dev. Biol.*, 76:26–46, 1980.

[564] La Rage. *Centre Nationale d'Études sur la Rage*. CERN, Paris, 1977.

[565] G.F. Raggett. Modelling the Eyam plague. *Bull. Inst. Math. and its Applic.*, 18:221–226, 1982.

[566] R. Ramina, M. C. Neto, M. Meneses, W. O. Arruda, S. C. Hunhevicz, and A. A. Pedrozo. Management of deep-seated gliomas. *Critical Rev. Neurosurg.*, 9:34–40, 1999.

[567] M. Rawles. Tissue interactions in scale and feather development as studied in dermal-epidermal recombinations. *J. Embryol. Exp. Morph.*, 11:765–789, 1963.

[568] J.C. Reynolds. Details of the geographic replacement of the red squirrel (Sciurus vulgaris) by the grey squirrel (Sciurus carolinensis) in Eastern England. *J. Animal Ecology*, 54:149–162, 1985.

[569] M.K. Richardson, A. Hornbruch, and L. Wolpert. Pigment patterns in neural crest chimeras constructed from quail and guinea fowl embryos. *Dev. Biol.*, 143:309–319, 1991.

[570] M.K. Richardson and G. Keuck. A question of intent: when is a 'schematic' illustration or fraud? *Nature*, 410:144, 2001.

[571] R.D. Riddle and C.J. Tabin. How limbs develop. *Scientific American*, pages 54–59, February 1999.

[572] J. Rinzel. Models in neurobiology. In R.H. Enns, B.L. Jones, R.M. Miura, and S.S. Rangnekar, editors, *Nonlinear Phenomena in Physics and Biology*, pages 345–367. Plenum, New York, 1981.

[573] J. Rinzel and J.B. Keller. Traveling wave solutions of a nerve conduction equation. *Biophys. J.*, 13:1313–1337, 1973.

[574] J. Rinzel and D. Terman. Propagation phenomena in a bistable reaction-diffusion system. *SIAM J. Appl. Math.*, 42:1111–1137, 1982.

[575] G.B. Risse. A long pull, a strong pull and all together—San Francisco and bubonic plague 1907-1908. *Bull.Hist. Med.*, 66:260–286, 1992.

[576] H. Ritvo. *The Animal Estate. The English and Other Creatures in the Victorian Age*. Harvard University Press, Cambridge, 1987.

[577] E.K. Rodriguez, A. Hoger, and A.D. McCulloch. Stress-dependent finite growth in soft elastic tissues. *J. Biomech.*, 27:455–467, 1994.

[578] A.S. Romer. *Vertebrate Palaeontology*. University of Chicago Press, Chicago, 1977.

[579] E. Röse. Ueber die Zahnentwicklung der Crocodile. *Morph. Arbeit.*, 3:195–228, 1894.

[580] T. Rytömaa and K. Kiviniemi. Chloroma repression induced by the granulocytic chalone. *Nature*, 222:995–996, 1969.

[581] T. Rytömaa and K. Kiviniemi. Regression of generalised leukemia in rat induced by the granulocytic chalone. *Eur. J. Cancer*, 6:401–410, 1970.

[582] E.H. Sage. Pieces of eight: bioactive fragments of extracellular proteins as regulators of angiogenesis. *Trends in Cell Biol.*, 7:182–186, 1997a.

[583] E.H. Sage. Terms of attachment: SPARC and tumorigenesis. *Nature Medicine*, 3:171–176, 1997b.

[584] D. Savic. Models of pattern formation in animal coatings. *J. Theor. Biol.*, 172:299–303, 1995.

[585] B. Schaumann and M. Alter. *Dermatoglyphics in Medical Disorders*. Springer-Verlag, New York, 1976.

[586] G.W. Scherer, H. Hdach, and J. Phalippou. Thermal expansion of gels: A novel method for measuring permeability. *J. of Non-Crystalline Solids*, 130:157–170, 1991.

[587] S. Schmidt and P. Ortoleva. Asymptotic solutions of the FKN chemical wave equation. *J. Chem. Phys.*, 72:2733–2736, 1980.

[588] J. Schnackenberg. Simple chemical reaction systems with limit cycle behaviour. *J. Theor. Biol.*, 81:389–400, 1979.

[589] A.M. Schor, S.L. Schor, and R. Baillie. Angiogenesis: experimental data relevant to theoretical analysis. In M.A.J. Chaplain, G.D. Singh, and J.C. McLachlan, editors, *On Growth and Form. Spatio-Temporal Pattern Formation in Biology*, pages 201–224. John Wiley, New York, 1999.

[590] B.N. Schwanwitsch. On the ground-plan of wing-pattern in nymphalids and other families of rhopalocerous Lepidoptera. *Proc. Zool. Soc. (Lond.)*, 34:509–528, 1924.

[591] V. Schwartz. Neue Versuche zur Determination des zentralen Symmetriesystems bei Plodia interpunctella. *Biol. Zentr.*, 81:19–44, 1962.

[592] A.G. Searle. *Comparative Genetics of Coat Colour in Mammals*. Academic, London, 1968.

[593] L.A. Segel, editor. *Mathematics Applied to Continuum Mechanics*. Macmillan, New York, 1977.

[594] T. Sekimura, P.K. Maini, J.B. Nardi, M. Zhu, and J.D. Murray. Pattern formation in lepidopteran wings. *Comments in Theor. Biol.*, 5:69–87, 1998.

[595] T. Sekimura, M. Zhu, J. Cook, P.K. Maini, and J.D. Murray. Pattern formation of scale cells in lepidoptera differential origin-dependent cell adhesion. *Bull. Math. Biol.*, 61:807–827, 1999.

[596] P. Sengel. *Morphogenesis of Skin*. Cambridge University Press, Cambridge, UK, 1976.

[597] L.J. Shaw and J.D. Murray. Analysis of a model for complex skin patterns. *SIAM J. Appl. Math.*, 50:279–293, 1990.

[598] P.R. Sheldon. Parallel gradualistic evolution of Ordovician trilobites. *Nature*, 330:561–563, 1987.

[599] J.A. Sherratt. *Mathematical Models of Wound Healing*. PhD thesis, University of Oxford, 1991.

[600] J.A. Sherratt. Actin aggregation and embryonic epidermal wound healing. *J. Math. Biol.*, 31:703–716, 1993.

[601] J.A. Sherratt. Chemotaxis and chemokinesis in eukaryotic cells: the Keller–Segel equations as an approximation to a detailed model. *Bull. Math. Biol.*, 56:129–146, 1994.

[602] J.A. Sherratt and J. Lewis. Stress-induced alignment of actin filaments and the mechanics of cytogel. *Bull. Math. Biol.*, 55:637–654, 1993.

[603] J.A. Sherratt and J.D. Murray. Models of epidermal wound healing. *Proc. R. Soc. Lond. B*, 241:29–36, 1990.

[604] J.A. Sherratt and J.D. Murray. Mathematical analysis of a basic model for epidermal wound healing. *J. Math. Biol.*, 29:389–404, 1991.

[605] J.A. Sherratt and J.D. Murray. Epidermal wound healing: A theoretical approach. *Comm. Theor. Biol.*, 2:315–333, 1992a.

[606] J.A. Sherratt and J.D. Murray. Epidermal wound healing: the clinical implications of a simple mathematical model. *Cell Transplant*, 1:365–371, 1992b.

[607] J.A. Sherratt, M.A. Lewis, and A.C. Fowler. Ecological chaos in the wake of invasion. *Proc. Nat. Acad. Sci. USA*, 92:2524–2528, 1995.

[608] J.A. Sherratt, P. Martin, J.D. Murray, and J. Lewis. Mathematical models of wound healing in embryonic and adult epidermis. *IMA J. Math. Appl. Med. & Biol.*, 9:177–196, 1992.

[609] J.A. Sherratt, E.H. Sage, and J.D. Murray. Chemical control of eukaryotic cell movement: a new model. *J. Theor. Biol.*, 162:23–44, 1993b.

[610] M. Shibata and J. Bureš. Reverberation of cortical spreading depression along closed pathways in rat cerebral cortex. *J. Neurophysiol.*, 35:381–388, 1972.

[611] M. Shibata and J. Bureš. Optimum topographical conditions for reverberating cortical spreading depression in rats. *J. Neurobiol.*, 5:107–118, 1974.

[612] N. Shigesada and K. Kawasaki. *Biological Invasions: Theory and Practice*. Oxford University Press, Oxford, 1997.

[613] N. Shigesada, K. Kawasaki, and E. Teramoto. Travelling periodic waves in heterogeneous environments. *Theor. Popul. Biol.*, 30:143–160, 1986.

[614] E. Shochat, D. Hart, and Z. Agur. Using computer simulation for evaluating the efficacy of breast cancer chemotherapy protocols. *Math. Models and Methods in Appl. Sciences*, 9:599–615, 1999.

[615] N. Shubin and P. Alberch. A morphogenetic appraoch to the origin and basic organisation of the tetrapod limb. In M. Hecht, B. Wallace, and W. Steere, editors, *Evolutionary Biology*, volume 20, pages 319–387. Plenum, New York, 1986.

[616] S. Shuster. The cause of striae distensae. *Acta Dermato-Venereologica*, 59:161–169, 1979. (Supplement 85).

[617] A. Sibatani. Wing homeosis in Lepidoptera: a survey. *Devl. Biol.*, 79:1–18, 1981.

[618] D.L. Silbergeld and M.R. Chicoine. Isolation and characterization of human malignant glioma cells from histologically normal brain. *J. Neurosurg.*, 86:525–531, March 1997.

[619] D.L. Silbergeld, R.C. Rostomily, and E.C. Alvord, Jr. The cause of death in patients with glioblastoma is multifactorial: Clinical factors and autopsy findings in 117 cases of supratentorial glioblastoma in adults. *J. Neuro-Oncol.*, 10:179–185, 1991.

[620] R. Skalak and R.J. Price. The role of mechanical stresses in microvascular remodeling. *Microcirculation*, 3:143–165, 1996.

[621] R. Skalak, G. Dasgupta, M. Moss, E. Otten, P. Dullemeijer, and H. Vilmann. Analytical description of growth. *J. Theor. Biol.*, 94:555–577, 1982.

[622] J.M.W. Slack. *From Egg to Embryo. Determinative Events in Early Development*. Cambridge University Press, Cambridge, UK, 1983.

[623] J.L.R.M. Smeets, M.A. Allessie, W.J.E.P. Lammers, F.I.M. Bonke, and J. Hollen. The wavelength of the cardiac impulse and the reentrant arrhythmias in isolated rabbit atrium. The role of heart rate, autonomic transmitters, temperature and potassium. *Circ. Res.*, 73:96–108, 1986.

[624] J.C. Smith and L. Wolpert. Pattern formation along the anterioposterior axis of the chick wing: the increase in width following a polarizing region graft and the effect of X-irradiation. *J. Embryol. Exp. Morph.*, 63:127–144, 1981.

[625] J. Smoller. *Shock Waves and Reaction-Diffusion Equations*. Springer-Verlag, Berlin-Heidelberg-New York, 1983.

[626] J. Sneyd, A. Atri, M.W.J. Ferguson, M.A. Lewis, W. Seward, and J.D. Murray. A model for the spatial patterning of teeth primordia in the Alligator: Initiation of the dental determinant. *J. Theor. Biol.*, 165:633–658, 1993.

[627] J.M. Snowden. Wound closure: an analysis of the relative contributions of contraction and epithelialization. *J. Surg. Res.*, 37:453–463, 1984.

[628] M.K. Sparrow and P.J. Sparrow. *Topological Approach to the Matching of Single Fingerprints: Development of Algorithms for Use on Rolled Impressions*. US Govt. Printing Office (NBS/SP-50/124), Washington, DC, 1985.

[629] A. Spiros and L. Edelstein-Keshet. Testing a model for the dynamics of actin structures with biological parameter values. *Bull. Math. Biol.*, 60:275–305, 1998.

[630] F. Steck and A. Wandeler. The epidemiology of fox rabies in Europe. *Epidem. Rev.*, 2:71–96, 1980.

[631] O. Steinbock, P. Kuttunen, and K. Showalter. Chemical wave logic gates. *J. Chem. Phys.*, 100:18970–18975, 1996.

[632] M.G. Stern, M.T. Longaker, and R. Stern. Hyaluronic acid and its modulation in fetal and adult wound. In N.S. Adzick and M.T. Longaker, editors, *Fetal Wound Healing*, pages 189–198. Elsevier, New York, 1992.

[633] C.R. Stockard. The artificial production of one-eyed monsters and other defects, which occur in nature, by the use of chemicals. *Proc. Assoc. of Amer. Anatomists*, III(4):167–173, 1909.

[634] C.R. Stockard. Development rate and structural expression: an experimental study of twins, "double monsters" and single deformities, and the interaction among embryonic organs during their origin and development. *Amer. J. Anatomy*, 28:115–266, 1921.

[635] S.H. Strogatz. *Nonlinear Dynamics and Chaos: with Applications in Physics, Biology, Chemistry, and Engineering*. Addison-Wesley, Reading, MA, 1994.

[636] F.A. Stuart, K.H. Mahmood, J.L. Stanford, and D.G. Pritchard. Development of diagnostic test for, and vaccination against, tuberculosis in badgers. *Mammal Review*, 18:74–75, 1988.

[637] F. Suffert. Zur vergleichenden Analyse der Schmetterlingszeichnung. *Bull. Zentr.*, 47:385–413, 1927.

[638] G.W. Swan. Tumour growth models and cancer therapy. In J.R. Thomson and B.W. Brown, editors, *Cancer Modeling*, pages 91–104. Marcel Dekker, New York, 1987.

[639] K.R. Swanson. *Mathematical Modeling of the Growth and Control of Tumors*. PhD thesis, University of Washington, Seattle, WA, 1999.

[640] K.R. Swanson, E.C. Alvord, Jr, and J.D. Murray. A quantitative model for differential motility of gliomas in grey and white matter. *Cell Prolif.*, 33:317–329, 2000.

[641] N.V. Swindale. A model for the formation of ocular dominance stripes. *Proc. R. Soc. Lond. B*, 208:243–264, 1980.

[642] L.A. Taber. Biomechanics of growth, remodeling, and morphogenesis. *Appl. Mech. Rev.*, 48:487–545, 1995.

[643] P. Tass. Cortical pattern formation during visual hallucinations. *J. Biol. Phys.*, 21:177–210, 1995.

[644] O.R. Taylor. The past and possible future spread of Africanized honeybees in the Americas. *Bee World*, 58:19–30, 1977.

[645] L. Teulières and P. Saliou. Rabies in France, 100 years after Pasteur. *Presse Medicale*, 24:134–135, 1995.

[646] I. Thesleff and A.M. Partanen. Localization and quantitation of 125I-epidermal growth factor binding in mouse embryonic tooth and other embryonic tissues at different developmental stages. *Dev. Biol.*, 120:186–197, 1987.

[647] R. Thoma. *Untersuchungen ber die Histogenese und Histomechanik*. Enkeverlag, Stuttgart, 1893.

[648] D. Thomas. Artificial enzyme membranes, transport, memory, and oscillatory phenomena. In D. Thomas and J.-P. Kernevez, editors, *Analysis and Control of Immobilized Enzyme Systems*, pages 115–150. Springer-Verlag, Berlin-Heidelberg-New York, 1975.

[649] D'Arcy W. Thompson. *On Growth and Form*. Cambridge University Press, Cambridge, UK, 1917.

[650] P. Thorogood. Morphogenesis of cartilage. In B.K. Hall, editor, *Cartilage: Development, Differentiation and Growth*, volume 2. Academic, New York, 1983.

[651] C. Tickle. Development of the vertebrate limb: a model for growth and patterning. In M.A.J. Chaplain, G.D. Singh, and J.C McLachlan, editors, *On Growth and Form. Spatio-Temporal Pattern Formation in Biology*, pages 13–29. John Wiley, New York, 1999.

[652] C. Tickle, J. Lee, and G. Eichele. A quantitative analysis of the effect of all-trans-retinoic acid on the pattern of chick wing development. *Dev. Biol.*, 109:82–95, 1985.

[653] D. Tilman and P. Kareiva, editors. *Spatial Ecology. The Role of Space in Population Dynamics and Interspecific Interactions*. Princeton University Press, Princeton, NJ, 1997.

[654] E.J.F. Timmenga, T.T. Andreassen, H.J. Houthoff, and P.J. Klopper. The effect of mechanical stress on healing skin wounds: an experimental study in rabbits using tissue expansion. *Brit. J. Plastic Surg.*, 44:514–519, 1991.

[655] E.C. Titchmarsh. *Eigenfunctions Expansions Associated with Second-Order Differential Equations*. Clarendon, Oxford, 1964.

[656] A.W. Toga, E.M. Santori, R. Hazani, and K. Ambach. A 3D digital map of the rat brain. *Brain Res. Bull.*, 38:77–85, 1995.

[657] B. Toma and L. Andral. Epidemiology of fox rabies. *Adv. Vir. Res.*, 21:15, 1977.

[658] A. Tozeren and R. Skalak. Interaction of stress and growth in a fibrous tissue. *J. Theor. Biol.*, 130:337–350, 1988.

[659] P. Tracqui. From passive diffusion to active cellular migration in mathematical models of tumour invasion. *Acta Biotheoretica*, 43:443–464, 1995.

[660] P. Tracqui, G.C. Cruywagen, D.E. Woodward, G.T. Bartoo, J.D. Murray, and E.C. Alvord, Jr. A mathematical model of glioma growth: the effect of chemotherapy on spatio-temporal growth. *Cell Proliferation*, 28:17–31, 1995.

[661] P. Tracqui, D.E. Woodward, G.C. Cruywagen, and J.D. Murray. A mechanical model for fibroblast-driven wound healing. *J. Biol. Syst.*, 3:1075–1085, 1993.

[662] L. Tranqui and P. Tracqui. Mechanical signalling and angiogenesis. the integration of cell-extracellular matrix couplings. *C.R. Acad. Sci. Paris, Science de la Vie*, 323:31–47, 2000.

[663] R.T. Tranquillo and D.A. Lauffenburger. Stochastic model of leukocyte chemosensory movement. *J. Math. Biol.*, 25:229–262, 1987.

[664] R.T. Tranquillo and J.D. Murray. Continuum model of fibroblast-driven wound contraction: inflammation mediation. *J. Theor. Biol.*, 158:135–172, 1992.

[665] R.T. Tranquillo and J.D. Murray. Mechanistic model of wound contraction. *J. Surg. Research*, 55:233–247, 1993.

[666] R.W. Treadwell. Time and sequence of appearance of certain gross structures in *Pituophis melanoleucus sayi* embryos. *Herpetologica*, 18:120–124, 1962.

[667] J.P. Trinkaus. Formation of protrusions of the cell surface during tissue cell movement. In R.D. Hynes and C.E. Fox, editors, *Tumor Cell Surfaces and Malignancy*, pages 887–906. Alan R. Liss, New York, 1980.

[668] J.P. Trinkaus. *Cells into Organs. The Forces that Shape the Embryo*. Prentice-Hall, Englewood Cliffs, NJ, 1984.

[669] T. Tsujikawa, T. Nagai, M. Mimura, R. Kobayashi, and H. Ikeda. Stability properties of traveling pulse solutions of the higher dimensional FitzHugh–Nagumo equations. *Japan J. Appl. Math.*, 6:341–366, 1989.

[670] A.M. Turing. The chemical basis of morphogenesis. *Phil. Trans. R. Soc. Lond. B*, 237:37–72, 1952.

[671] W. Turner. *A Compleat History Of the Most Remarkable Providence, both of Judgement and Mercy, Which have hapened in this Present Age*. John Duynton, Raven, Jewet Street, London, 1697.

[672] J.J. Tyson and P.C. Fife. Target patterns in a realistic model of the Belousov–Zhabotinskii reaction. *J. Chem. Phys.*, 75:2224–2237, 1980.

[673] J.J. Tyson and J.P. Keener. Singular perturbation theory of travelling waves in excitable media (a review). *Physica D*, 32:327–361, 1988.

[674] J.J. Tyson, K.A. Alexander, V.S. Manoranjan, and J.D. Murray. Cyclic-AMP waves during aggregation of *Dictyostelium* amoebae. *Development*, 106:421–426, 1989a.

[675] J.J. Tyson, K.A. Alexander, V.S. Manoranjan, and J.D. Murray. Spiral waves of cyclic-AMP in a model of slime mold aggregation. *Physica D*, 34:193–207, 1989b.

[676] R.C. Tyson. *Pattern Formation by E. coli—Mathematical and Numerical Investigation of a Biological Phenomenon*. PhD thesis, Department of Applied Mathematics, University of Washington, Seattle, WA, 1996.

[677] R.C. Tyson, S.R. Lubkin, and J.D. Murray. A minimal mechanism for bacterial pattern formation. *Proc. R. Soc. Lond. B*, 266:299–304, 1998.

[678] R.C. Tyson, S.R. Lubkin, and J.D. Murray. Model and analysis of chemotactic bacterial patterns in liquid medium. *J. Math. Biol.*, 38:359–375, 1999.

[679] S. Vainio, I. Karanvanova, A. Jowett, and I. Thesleff. Identification of BMP-4 as a signal mediating secondary induction between epithelial and mesenchymal tissues during early tooth development. *Cell*, 75:45–58, 1993.

[680] E.S. Valenstein. History of psychosurgery. In S.H. Greenblatt, editor, *A History of Neurosurgery*, pages 499–516. American Society of Neurological Surgeons, Park Ridge, IL, 1997.

[681] V. van Ballenberghe, A.W. Erickson, and D. Byman. Ecology of the timber wolf in Northeastern Minnesota. *Wildl. Monogr.*, 43:1–43, 1975.

[682] H.A.S. Van den Brenk. Studies in restorative growth processes in mammalian wound healing. *Br. J. Surg.*, 43:525–550, 1956.

[683] J.W. Verano, L.S. Anderson, and R. Franco. Foot amputation by the Moche of ancient Peru: osteological evidence and archaeological context. *Int. J. Osteoarchaeol.*, 10:177–188, 2000.

[684] J.W. Verano, S. Uceda, C. Chapdelaine, R. Tello, M.I. Paredes, and V. Pimentel. Modified human skulls from the urban sector of the pyramids of Moche, northern Peru. *Latin American Antiquity*, 10:59–70, 1999.

[685] R.B. Vernon and E.H. Sage. Between molecules and morphology. extracellular matrix and creation of vascular form. *Amer. J. of Pathol.*, 147:873–883, 1995.

[686] R.B. Vernon, J.C. Angello, M.L. Iruela-Arispe, T.F. Lane, and E.H. Sage. Reorganization of basement membrane matrices by cellular traction promotes the formation of cellular networks *in vitro*. *Laboratory Investigation*, 66:536–547, 1992.

[687] R.B. Vernon, S.L. Lara, M.L. Drake, M.L. Iruela-Arispe, J.C. Angello, C.D. Little, T.N. Wight, and E.H. Sage. Organized type I collagen influences endothelial patterns during "spontaneous" angiogenesis *in vitro*: Planar cultures as models of vascular development. *In Vitro Vascular and Dev. Biol.*, 31:120–131, 1995.

[688] C.H. Waddington and J. Cowe. Computer simulations of a molluscan pigmentation pattern. *J. Theor. Biol.*, 25:219–225, 1969.

[689] V. Walbot and N. Holder. *Developmental Biology*. Random House, New York, 1987.

[690] H. Walker, editor. *A History of Neurological Surgery*. Williams and Wilkins, Baltimore, 1951.

[691] J. Walker. About phosphenes: luminous patterns that appear when the eyes are closed. *Scientific American*, 244:174–184, 1981.

[692] M. Walter, A. Fournier, and M. Reimers. Clonal mosaic model for the synthesis of mammalian coat patterns. *Graphics Interface '98 (Intern. Computer Graphics Conf. Vancouver)*, pages 82–91, 1998.

[693] A. Wandeler. Rabies virus. In M.J. Appel, editor, *Virus Infections of Carnivores*, pages 449–461. Elsevier Science, Amsterdam, 1987.

[694] D.A. Warrell. Rabies in man. In C. Kapalan, editor, *Rabies: the Facts*, pages 32–52. Oxford University Press, Oxford, 1977.

[695] F.M. Watt. The extracellular matrix and cell shape. *Trends in Biochem. Sci.*, 11:482–485, 1986.

[696] F.M. Watt. Proliferation and terminal differentiation of human epidermal keratinocytes in culture. *Biochem. Soc. Trans.*, 16:666–668, 1988a.

[697] F.M. Watt. The epidermal keratinocyte. *Bioessays*, 8:163–167, 1988b.

[698] G.T. Watt. Wound shape and tissue tension in healing. *Brit. J. Surg.*, 47:555–561, 1959.

[699] M.P. Welch, G.F. Odland, and A.F. Clark. Temporal relationships of F-actin bundle formation, collagen and fibronectin matrix assembly, and fibronectin receptor expression to wound contraction. *J. Cell Biol.*, 110:133–145, 1990.

[700] K.F. Wellmann. North American Indian rock art and hallucinogenic drugs. *J. Amer. Medical Assoc.*, 239:1524–1527, 1978.

[701] B.J. Welsh, J. Gomatam, and A.E. Burgess. Three-dimensional chemical waves in the Belousov–Zhabotinskii reaction. *Nature*, 304:611–614, 1983.

[702] S. Werner, H. Smola, X. Liao, M.T. Longaker, T. Krieg, P.H. Hofschneider, and L.T. Williams. The function of KGF in epithelial morphogenesis and wound reepithelialization. *Science*, 266:819–822, 1994.

[703] N. Wessells. *Tissue Interaction in Development*. W. A. Benjamin, Menlo Park, CA, 1977.

[704] B. Westergaard and M.W.J. Ferguson. Development of the dentition in *Alligator mississippiensis*. early embryonic development in the lower jaw. *J. Zool. Lond.*, 210:575–597, 1986.

[705] B. Westergaard and M.W.J. Ferguson. Development of the dentition in *Alligator mississippiensis*. later development in the lower jaws of embryos, hatchlings and young juveniles. *J. Zool. Lond.*, 212:191–222, 1987.

[706] B. Westergaard and M.W.J. Ferguson. Development of the dentition in *Alligator mississippiensis*. upper jaw dental and craniofacial development in embryos, hatchlings, and young juveniles. with a comparison to lower jaw development. *Amer. J. Anatomy*, 187:393–421, 1990.

[707] J.M. Westergaard. Measures applied in Denmark to control the rabies epizootic in 1977–1980. *Comp. Immunol. Microbiol. Infect. Dis.*, 5:383–387, 1982.

[708] D.J. Whitby and M.W.J. Ferguson. The extracellular matrix of lip wounds in fetal, neonatal and adult mice. *Development*, 112:651–668, 1991.

[709] K.A.J. White. *Territoriality and Survival in Wolf-Deer Interactions*. PhD thesis, Department of Applied Mathematics, University of Washington, Seattle, WA, 1995.

[710] K.A.J. White, M.A. Lewis, and J.D. Murray. A model for wolf-pack territory formation and maintenance. *J. Theor. Biol.*, 178:29–43, 1996a.

[711] K.A.J. White, M.A. Lewis, and J.D. Murray. Wolf-deer interactions: a mathematical model. *Proc. R. Soc. Lond. B*, 263:299–305, 1996b.

[712] K.A.J. White, M.A. Lewis, and J.D. Murray. On wolf territoriality and deer survival. In J. Bascompte and R.V. Sole, editors, *Modeling Spatiotemporal Dynamics in Ecology*, pages 105–126. Springer-Verlag, New York, 1998.

[713] M.H. Williamson. *Biological Invasions*. Chapman and Hall, London, 1996.

[714] M.H. Williamson and K.C. Brown. The analysis and modelling of British invasions. *Phil. Trans. R. Soc. Lond. B*, 314:505–522, 1986.

[715] P.G. Williamson. Palaeontological documentation of speciation in Cenozoic molluscs from Turkana Basan. *Nature*, 293:437–443, 1981a.

[716] P.G. Williamson. Morphological stasis and developmental constraints: real problems for neo-Darwinism. *Nature*, 294:214–215, 1981b.

[717] A.T. Winfree. Spiral waves of chemical activity. *Science*, 175:634–636, 1972.

[718] A.T. Winfree. Rotating chemical reactions. *Sci. Amer.*, 230(6):82–95, 1974.

[719] A.T. Winfree. The rotor in reaction-diffusion problems and in sudden cardiac death. In M. Cosnard and J. Demongeot, editors, *Lect. Notes in Biomathematics (Luminy Symposium on Oscillations, 1981)*, volume 49, pages 201–207, Berlin-Heidelberg-New York, 1983a. Springer-Verlag.

[720] A.T. Winfree. Sudden cardiac death: a problem in topology. *Sci. Amer.*, 248(5):144–161, 1983b.

[721] A.T. Winfree. *The Timing of Biological Clocks*. Scientific American Books, New York, 1987a.

[722] A.T. Winfree. *When Time Breaks Down: The Three-Dimensional Dynamics of Electrochemical Waves and Cardiac Arrhythmias*. Princeton University Press, Princeton, NJ, 1987b.

[723] A.T. Winfree. Electrical turbulence in three-dimensional heart muscle. *Science*, 266:1003–1006, 1994a.

[724] A.T. Winfree. Persistent tangled vortex rings in generic excitable media. *Nature*, 371:233–236, 1994b.

[725] A.T. Winfree. Mechanisms of cardiac fibrillation. *Science*, 270:1222–1225, 1995.

[726] A.T. Winfree. Heart muscle as a reaction diffusion medium: the roles of electrical potential diffusion, activation front curvature, and anisotropy. *Internat. J. Bifurc. and Chaos Appl. Sci. Engrg.*, 7:487–526, 1997.

[727] A.T. Winfree. *The Geometry of Biological Time*. Springer-Verlag, Berlin-Heidelberg-New York, 2nd edition, 2000.

[728] A.T. Winfree and S.H. Strogatz. Organising centres for three-dimensional chemical waves. *Nature*, 311:611–615, 1984.

[729] A.T. Winfree, G. Caudle, P. McGuire, and Z. Szilagyi. Quantitative optical tomography of chemical waves and their organising centers. *Chaos*, 6:617–626, 1996.

[730] K.H. Winters, M.R. Myerscough, P.K. Maini, and J.D. Murray. Tracking bifurcating solutions of a model biological pattern generator. *IMPACT of Computing in Sci. and Eng.*, 2:355–371, 1990.

[731] R. Wittenberg. *Models of Self-Organisation in Biological Development*. Master's thesis, University of Cape Town, 1993.

[732] M.W. Woerdeman. Beitrage zur Entwicklungsgeschichte von Zahnen und Gebiss der Reptilien. Beitrag I. Die Anlage und Entwicklung des embryonalen Gebisses als Ganzes. *Arch. mikrosk. Anat.*, 92:104–192, 1919.

[733] M.W. Woerdeman. Beitrage zur Entwicklungsgeschichte von Zahnen und Gebiss der Reptilien. Beitrag IV. Uber die Anlage und Entwicklung der Zahne. *Arch. mikrosk. Anat.*, 95:265–395, 1921.

[734] S. Wolfram. Cellular automata as models of complexity. *Nature*, 311:419–424, 1984.

[735] D.J. Wollkind and L.E. Stephenson. Chemical Turing pattern formation analyses: Comparison of theory and experiment. *SIAM J. Appl. Math.*, 61:387–431, 2000a.

[736] D.J. Wollkind and L.E. Stephenson. Chemical Turing patterns: a model system of a paradigm for morphogenesis. In P.K. Maini and H.G. Othmer, editors, *Mathematical Models for Biological Pattern Formation*, pages 113–142. Springer-Verlag, New York, 2000b.

[737] D.J. Wollkind, V.S. Manoranjan, and L. Zhang. Weakly nonlinear stability analyses of prototype reaction-diffusion model equations. *SIAM Rev.*, 36:176–214, 1994.

[738] L. Wolpert. Positional information and the spatial pattern of cellular differentiation. *J. Theor. Biol.*, 25:1–47, 1969.

[739] L. Wolpert. Positional information and pattern formation. *Curr. Top. Dev. Biol.*, 6:183–224, 1971.

[740] L. Wolpert. The development of pattern and form in animals. *Carolina Biol. Readers*, 1(5):1–16, 1977.

[741] L. Wolpert. Positional information and pattern formation. *Phil. Trans. R. Soc. Lond. B*, 295:441–450, 1981.

[742] L. Wolpert and A. Hornbruch. Positional signalling and the development of the humerus in the chick limb bud. *Development*, 100:333–338, 1987.

[743] L. Wolpert and W.D. Stein. Molecular aspects of early development. In G.M. Malacinski and S.V. Bryant, editors, *Proc. Symp. on Molecular Aspects of Early Development (Annual Meeting Amer. Soc. Zoologists, Louisville, 1982)*, pages 2–21, MacMillan, New York, 1984.

[744] D. E. Woodward, J. Cook, P. Tracqui, G.C. Cruywagen, J.D. Murray, and E.C. Alvord, Jr. A mathematical model of glioma growth: the effect of extent of surgical resection. *Cell Proliferation*, 29:269–288, 1996.

[745] D.E. Woodward, R.C. Tyson, J.D. Murray, E.O. Budrene, and H. Berg. Spatio-temporal patterns generated by *Salmonella typhimurium*. *Biophysical J.*, 68:2181–2189, 1995.

[746] N.A. Wright. Cell proliferation kinetics of the epidermis. In L.A. Goldsmith, editor, *Biochemistry and Physiology of the Skin*, pages 203–229. Oxford University Press, Oxford, 1983.

[747] N.A. Wright and M. Alison. *Biology of Epithelial Cell Populations*. Clarendon, Oxford, 1984.

[748] T. Wyatt. The biology of *Oikopleara dioica* and *Fritillaria borealis* in the Southern Bight. *Mar. Biol.*, 22:137–158, 1973.

[749] Y. Xu, C.M. Vest, and J.D. Murray. Holographic interferometry used to demonstrate a theory of pattern formation in animal coats. *Appl. Optics.*, 22:3479–3483, 1983.

[750] S. Yachi, K. Kawasaki, N. Shigesada, and E. Teramoto. Spatial patterns of propagating waves of fox rabies. *Forma*, 4:3–12, 1989.

[751] H. Yagisita, M. Mimura, and M. Yamada. Spiral wave behaviors in an excitable reaction-diffusion system on a sphere. *Physica D*, 124:126–136, 1998.

[752] T. Yamaguchi, T. Hirobe, Y. Kinjo, and K. Manaka. The effect of chalone on the cell cycle in the epidermis during wound healing. *Exp. Cell Res.*, 89:247–254, 1974.

[753] A. Yoshikawa and M. Yamaguti. On some further properties of solutions to a certain semi-linear system of partial differential equations. *Publ. RIMS, Kyoto Univ.*, 9:577–595, 1974.

[754] D.A. Young. A local activator-inhibitor model of vertebrate skin patterns. *Math. Biosciences*, 72:51–58, 1984.

[755] G.L. Yount, D.A. Haas-Kogan, K.S. Levine, K.D. Aldape, and M.A. Israel. Ionizing radiation inhibits chemotherapy-induced apoptosis in cultured glioma cells: implications for combined modality therapy. *Cancer Res.*, 58:3819–3825, 1998.

[756] A.N. Zaikin and A.M. Zhabotinskii. Concentration wave propagation in two-dimensional liquid-phase self-organising system. *Nature*, 225:535–537, 1970.

[757] L.R. Zehr. Stages in the development of the common garter snake *Thamnophis sirtalis sirtalis*. *Copeia*, 1962:322–329, 1962.

[758] M. Zhu and J.D. Murray. Parameter domains for generating spatial pattern: a comparison of reaction-diffusion and cell-chemotaxis models. *Intern. J. Bifurcation & Chaos*, 5:1503–1524, 1995.

[759] J.D. Zieske, S.C. Higashij, S.J. Spurrmic, and I.K. Gipson. Biosynthetic response of the rabbit cornea to a keratectomy wound. *Invest. Ophthalmol. Vis. Sci.*, 28:1668–1677, 1987.

[760] R.G. Zweifel. Genetics of color pattern polymorphism in the California king snake. *J. Heredity*, 72:238–244, 1981.

[761] V.S. Zykov. *Modelling of Wave Processes in Excitable Media*. Manchester University Press, Manchester, 1988.